PREPARATION, STRUCTURAL CHARACTERIZATION AND ELECTRICAL PROPERTIES OF SOME POLYATOMIC CATIONS OF MERCURY

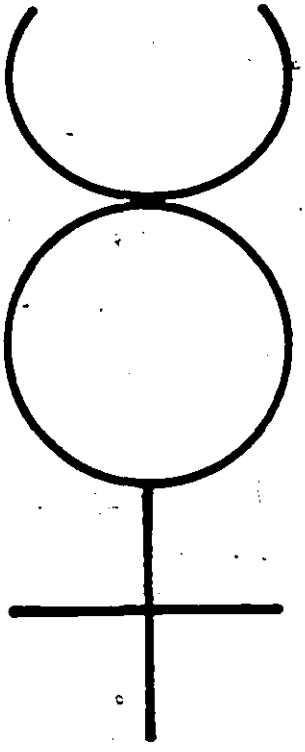

PREPARATION, STRUCTURAL CHARACTERIZATION AND ELECTRICAL PROPERTIES OF SOME POLYATOMIC CATIONS OF MERCURY

by

BRENT D. CUTFORTH

A Thesis
Submitted to the Faculty of Graduate Studies
in Partial Fulfilment of the Requirements
for the Degree
Doctor of Philosophy

McMaster University

October 1975

© BRENT D. CUTFORTH 1977

DOCTOR OF PHILOSOPHY (1975)
(Chemistry)

MCMASTER UNIVERSITY
Hamilton, Ontario

TITLE: Preparation, Structural Characterization and Electrical Properties of Some Polyatomic Cations of Mercury

AUTHOR: Brent D. Cutforth B.Sc. (University of Victoria)

SUPERVISOR: Professor R.J. Gillespie

NUMBER OF PAGES: xii, 134

ABSTRACT

The preparation of a number of new compounds containing mercury in formally low oxidation states is reported. The preparations are described and Raman spectra are reported for $Hg_2(AsF_6)_2 \cdot SO_2$, $Hg_2(AsF_6)_2$, $Hg_2(Sb_2F_{11})_2 \cdot SO_2$, $Hg_2(SbF_6)_2 \cdot SO_2$, $Hg_2(SbF_6)_2$, and $Hg_2(SO_3F)_2$. All of the mercurous salts have been prepared for the first time. The preparations of $Hg_3(AsF_6)_2$ and $Hg_3(Sb_2F_{11})_2$, both of which contain the Hg_3^{2+} cation, are presented. The Hg_4^{2+} cation, which has not been identified previously, is present in $Hg_4(AsF_6)_2$. The preparation of this compound and its Raman and UV-visible spectra are discussed. Raman spectroscopic and x-ray crystallographic studies show that the ions are linear, and that the bond lengths increase in the order $Hg_2^{2+} < Hg_3^{2+} < Hg_4^{2+}$.

Two new compounds containing infinite, linear, non-intersecting chains of mercury atoms in two mutually perpendicular directions have been prepared. The bonding in the metal atoms chains can be described as metallic, with the charge delocalized over the mercury atom chains.

An experimental technique for measuring the electrical conductivity of these extremely hygroscopic compounds is described, and conductivity and optical studies show that the compounds are anisotropic, metallic conductors. They constitute a new class of anisotropic materials.

ACKNOWLEDGEMENTS

I wish to thank Professor R.J. Gillespie, my research supervisor, for his advice, enthusiasm and insight during the course of this work.

The help and friendship of the members of the Chemistry Department have made my stay at McMaster rewarding and enjoyable.

I wish to thank Professor W.R. Datars of the Physics Department for his assistance and also Mr. A. van Schyndel for designing the electronics, without which many of the results included in this thesis could not have been completed.

I also thank Malerie Feldman for typing this thesis and Dave Hodgson for drawing the figures.

The financial assistance of the National Research Council, who provided a Scholarship, and McMaster University and the Chemistry Department, who provided an Assistantship, is gratefully acknowledged.

TABLE OF CONTENTS

LIST OF TABLES

LIST OF FIGURES

CHAPTER I

INTRODUCTION

Mercury was one of the first metals known to man, having been discovered at least as early as the fifteenth or sixteenth century B.C. Its liquid state and shiny metallic appearance fascinated early chemists and it played a central role in the Age of Alchemy, which reached its zenith in seventeenth century Europe. Mercury, symbolizing the mineral spirit of metals, and sulphur, symbolizing combustibility or the spirit of fire, were considered to contain the essence of all metals. If the two "spirits" or principles were joined whilst in an impure state they gave rise to base metals, such as tin and lead; when they were of high purity they gave silver and gold; but when each of the two principles was of superfine purity they yielded the "Philosopher's Stone". One of the favourite metals for multiplying an initial small quantity of ultrapure gold by means of the Philosopher's Stone was quicksilver, or mercury.

1.1 POLYATOMIC CATIONS OF THE NON-METALS

Polyatomic cation formation by the non-metals has been an active research area in the last several years. Cation formation is usually associated with the metals, but under suitable conditions the elements of Groups VI and VII form cationic clusters. The I^+ cation has long been proposed as an intermediate in electrophilic substitution

reactions, and although no evidence has yet been presented to support the existence of the simple I^+ cation, it has been shown that the intense blue colour of iodine in 65% oleum is due to the I_2^+ cation (1). Halogen cations, which may be homonuclear (I_3^+) or heteronuclear (ClF_2^+), have been discussed in a recent review article(2). Such species are highly electrophilic, and consequently exist only in media of very low basicity.

Shortly after the discovery of the O_2^+ cation by Bartlett (3) in the compound $O_2^+ PtF_6^-$ it was shown that the highly coloured solutions of sulphur in oleum, which have been known for well over 150 years, are due to the S_{16}^{2+}, S_8^{2+} and S_4^{2+} cations (4,5). Oxidation of sulphur by Lewis acids such as arsenic pentafluoride and antimony pentafluoride forms solid compounds containing the same cations. Selenium and tellurium form analogous cations. The polycations of Group VI have been discussed in detail in a review article (6). Again, cation formation by the non-metals is only possible in very weakly basic media. Stabilization of solid derivatives of polycations is achieved by using anions such as AsF_6^-, SbF_6^-, SO_3F^-, etc., and the development of superacid media has greatly facilitated their study.

1.2 POLYATOMIC CATION FORMATION BY THE METALS

Metal-metal bonded systems involving the transition metals (in particular Nb, Ta, Cr, Mo, W, Tc and Re) have received a great deal of attention lately and have been the subject of several review articles (7,8). Magnetic and structural data have demonstrated the

existence of a direct metal-metal interaction in such cations as $Mo_6Cl_8^{2+}$ and $Ta_6Cl_{12}^{2+}$. Although it is sometimes convenient to depict the bonding between metal atoms by a simple 2 centre-2 electron model, Molecular Orbital Theory is generally favoured. Transition metal clusters are invariably heteropolyatomic; the stability of a cation such as $Mo_6Cl_8^{2+}$ is due in no small part to the presence of the external ligands. As this thesis is concerned with homopolyatomic cations of metals, it is perhaps worthwhile to briefly discuss the cationic clusters of bismuth, which are the only other examples of metallic homopolyatomic cations.

Bismuth metal is appreciably soluble in molten bismuth trichloride, and it was thought for a long time that this was due to the formation of a subhalide of bismuth, formulated as "BiCl". An x-ray structural analysis by Corbett and co-workers (9) established the correct stoichiometry as $Bi_{12}Cl_{14}$, and showed, in addition to the $BiCl_5^{2-}$ and $Bi_2Cl_8^{2-}$ anions, the presence of the Bi_9^{5+} cation. The geometry of the cation is that of a trigonal prism with a bismuth atom capping each of the rectangular faces. Other polycations may be formed in the melt system as well. Spectroscopic measurements have shown (10,11) that a solution of bismuth and $BiCl_3$ in molten $AlCl_3$-NaCl contains Bi_5^{3+} and Bi_8^{2+} ions. These cations can also be isolated as the compounds $Bi_5(AlCl_4)_3$ and $Bi_8(AlCl_4)_2$ (12). Clearly, the bonding in the bismuth polycations is of considerable interest. Although the structures are not known, models have been proposed using Molecular Orbital Theory (13) and VSEPR Theory (14), and are amenable to simple interpretation by both methods.

Mercury (I), which has been known to exist as the dimer Hg_2^{2+} for over fifty years, provided the first example of a metal-metal bond. It remains today as the only homonuclear metallic cation stable in aqueous media. Although chemical evidence had suggested the dimeric nature of Hg(I) for some time, it was not until 1934 that Woodward (15) confirmed this spectroscopically by means of the solution Raman spectrum of $Hg_2(NO_3)_2.2H_2O$, which showed a strong line at 169 cm^{-1}. This could only be assigned as ν_1 arising from the mercury-mercury stretch. Woodward's observation was one of the first applications of Raman spectroscopy, which was to become in later years such an important tool for the study of metal-metal bonds. Krishnamurty had noticed the same strong low frequency peak several years earlier in the Raman spectrum of solid $Hg_2(NO_3)_2.2H_2O$ (16) and calomel (17), which he had mistakenly assigned to lattice modes. The initial observation (18) of the similarity of the $Cd/CdCl_2$ melt with that of $Hg/HgCl_2$ suggested the possible formation of Cd_2Cl_2. Many explanations were proposed to explain the solubility of metals such as zinc, cadmium, gallium, and bismuth in their respective halide melts, but the most convincing was the formation of the relatively unstable subhalides (19). Corbett stabilized the cadmium subhalide by the addition of the strong chloride acceptor (Lewis acid) $AlCl_3$ to the $Cd/CdCl_2$ melt (20) and succeeded in isolating $Cd_2(AlCl_4)_2$. The dimeric nature of the Cd(I) species was again confirmed by the Raman spectrum (21). Although zinc is only sparingly soluble in molten $ZnCl_2$, rapid freezing of the saturated melt resulted in the isolation of a yellow glass which was shown (22) by a combination

of chemical and spectroscopic means to contain Zn_2Cl_2. Thus all cations of the type M_2^{2+} of Group IIB exist; however, Hg_2^{2+} is unique in that it has by far the strongest bond and is the only one stable in aqueous media.

1.3 PURPOSE OF THIS RESEARCH

An initial observation by Dr. P. Ummat of this laboratory that arsenic pentafluoride reacted with mercury to yield highly coloured solutions in liquid sulphur dioxide, led to the preparation and preliminary structural elucidation of the Hg_3^{2+}(23)cation. The purpose of the present research was twofold: firstly, to prepare and identify polyatomic cations of mercury in formally low oxidation states employing suitable oxidizing agents such as arsenic pentafluoride, antimony pentafluoride, peroxydisulphuryldiflouride and others; and secondly, to determine the structures of the polycations by x-ray crystallography.

During the course of the research a most interesting compound was prepared which had a distinct metallic lustre. Crystallography revealed that the compound contained infinite chains of mercury atoms in two of three dimensions, and it seemed desirable, therefore, to determine the electrical conductivity along these chains and to measure the anisotropy suggested by the structure. The preparation of other compounds with the same structural characteristics, i.e. infinite chains of metal atoms, was also of immediate concern.

CHAPTER II

EXPERIMENTAL

2.1 PREPARATION AND PURIFICATION OF MATERIALS

Mercury

Triply distilled mercury (Shawingigan) was used directly.

Sulphur dioxide

Sulphur dioxide (Matheson) was stored as a liquid over P_2O_5 prior to use.

Fluorosulphuric acid

Fluorosulphuric acid (Allied) was doubly distilled in moisture-free glass apparatus.

Arsenic pentafluoride

Arsenic pentafluoride (Ozark Mahoning) was used directly.

Antimony pentafluoride

Antimony pentafluoride (Ozark Mahoning) was distilled at least twice in moisture-free glass apparatus.

Tantalum pentafluoride

Tantalum pentafluoride (Alpha) was purified by sublimation onto a water-cooled cold finger in glass apparatus.

Antimony pentachloride

Antimony pentachloride (BDH) was vacuum distilled prior to use.

Mercurous fluoride

Mercurous fluoride (Alpha) was used directly. Because of its photosensitivity it was handled with the room lights out and the reaction vessel was wrapped with black tape.

Peroxydisulphuryl difluoride

$S_2O_6F_2$ was kindly supplied by Dr. G.J. Schrobilgen, formerly of this laboratory, who prepared it by the decomposition of $Xe(OSO_2F)_2$.

Mercurous chloride

Mercurous chloride (Alpha) was used directly.

2.2 MANIPULATION OF MATERIALS

2.2.1 DRY BOX

Because of the extremely hygroscopic nature of all of the compounds studied, manual operations were carried out in a very good dry box (S. Blickman) equipped with an external circulating system and an evacuable ante-chamber. The dry box was equipped with a quantitative balance.

2.2.2 HANDLING OF CHEMICALS

Antimony pentafluoride was handled in the dry box using an all-glass syringe.

Gases were handled on a calibrated Pyrex vacuum line fitted with high vacuum stopcocks lubricated with Fluorolube grease (Hooker Chemical Co.) and a mercury manometer. Gas cylinders were connected to the line via a Swagelok Teflon union. $S_2O_6F_2$ and other liquids with a reasonable vapour pressure were tranferred on the vacuum line.

All other chemicals were transferred in the dry box.

2.2.3 CRYSTAL MOUNTING

Crystals for x-ray crystallography were handled in a dry box equipped with a microscope. The crystals were viewed through the microscope and cut to a suitable shape and size with a razor blade. The optimum size was generally about 0.1 mm. Each crystal was transferred to a thin-walled quartz capillary tube which was sealed with Halocarbon grease and Teflon tape. The capillary was flame scaled with a micro-burner outside the dry box.

2.3 EXPERIMENTAL TECHNIQUES

2.3.1 LASER RAMAN SPECTROSCOPY

The Raman instrument (Spex Industries Model 1400) has been described in detail elsewhere (24). Excitation was achieved with either a Spectra-Physics Model 125 He-Ne laser, operating at 6328Å, or a Spectra-Physics Model 265 Ar ion laser, operating at 5145Å. Samples were sealed in 2 mm o.d. glass capillary tubes and mounted horizontally with the scattered light collected at right angles to the incident beam. Low temperature spectra were recorded by mounting the capillary tube in an evacuated Dewar, silvered except for a one centimetre band around the centre. Liquid nitrogen was boiled off through the Dewar at a variable rate. The temperature was monitored with a thermocouple. Toward the end of this research the sample position was modified so the sample was mounted vertically and the scattered light was collected at 45° to the incident beam.

A rotating Raman cell was developed based on that used by Bernstein (25). The cell was constructed from a Vycor UV cell that was capable of holding SO_2 pressures, and was rotated with an electric motor at approximately 1000 rpm. This virtually eliminated local heating of the sample, which is a common problem when studying deeply coloured solutions. The scattered light was collected at 90° to the incident beam.

The vertical sample position that was adopted in the latter part of the research enabled rotating Raman spectra to be run in virtually any size tubing. Because the scattered light was collected at 45° to the incident beam, the scattering was primarily from the surface of the solution and absorption of the beam was minimal.

2.3.2 X-RAY CRYSTALLOGRAPHY

The theory of x-ray crystallography is covered in many standard reference books (26) and will not be discussed here. The crystal was wedged in a sealed quartz capillary, and mounted on a standard goniometer head. Preliminary crystal alignment was achieved with a Beurger precession camera using a low precession angle (μ= 10°) and unfiltered Mo radiation. The space group was determined from the systematic absences characteristic of the space group by examination of the zero, first and second layer precession photographs obtained using Mo K_α (λ=0.71069Å) radiation and the appropriate screen. In no case was the experimental density measured as no satisfactory procedure was found for these very hygroscopic materials. Intensity data were collected on a Syntex P1 four-circle auto-diffractometer. Unit cell parameters were found by least squares refinement of the Bragg

angle and crystal orientation for 15 reflections in the region $5° < 2\theta < 25°$. The θ-2θ scan technique was used with scan rates varying from 2 to 24°/min (in 2θ)so that the weaker reflections were counted most slowly to minimize counting errors. Stationary background counts with a time equal to half the scan time for each reflection were made at the end of the scan range. Two standard reflections were recorded every 100 measurements to monitor the stability of the crystal and its alignment and in no case was any time dependent trend observed with the maximum intensity variation being of the order of 3%. The recorded intensities were corrected for background, Lorentz and polarization factors. Absorption corrections were made assuming spherical geometry. Although a more accurate absorption correction would have been desirable, it was not possible because of the generally poor crystal shapes and lack of suitable programs. The atomic scattering factors were taken from reference (27). All calculations were performed on a CDC 6400 computer using the x-ray 71 system (28) and local programs.

2.3.3 UV-VISIBLE SPECTROSCOPY

Absorption spectra were recorded from 220 to 700 nm on a Cary 14 spectrophotometer. One centimetre path length quartz cells (Hellma Ltd.) with Teflon covers were used for spectra with fluorosulphuric acid as a solvent. The cells were filled in a dry box using a syringe equipped with a platinum needle and the cover was bound tightly with Teflon tape. Absorption spectra with SO_2 as solvent were run in one centimetre path length quartz cells with a graded seal to 1/4" o.d. Pyrex tubing. The solid was transferred in the dry box

and the SO_2 was transferred on the vacuum line. Low temperature spectra were recorded by mounting the cell in an evacuated Dewar with optical flats and cooling by cold nitrogen gas. The nitrogen was obtained by boiling liquid N_2 with an electric heater controlled by a Variac to give the required flow rate.

2.3.4 NMR SPECTROSCOPY

^{19}F nmr spectra were recorded on a Varian DP-60 spectrometer operating at 58.3 MHz. Low temperature spectra were obtained using a Varian V-4540 temperature controller with a variable temperature probe.

2.4 CONDUCTIVITY STUDIES

2.4.1 ELECTRONICS

A block diagram of the experimental set-up is shown in Figure 2.1. The electronics were designed by Mr. A. van Schyndel. An alternating current method was used to eliminate thermocouple voltages because of the small size of the crystals studied. AC current, which was typically 3 ma, was supplied by the output of a phase sensitive detector (P.S.D.) which was isolated electrically from the sample by a transformer. The frequency was 9.8 Hz, low enough to minimize inductive and capacitive coupling and sufficiently far removed from sub-harmonics of the line frequency (60 Hz). The voltage drop across the potential probes on the sample was amplified by the P.S.D. and the phase of the reference signal in the P.S.D. was set to measure the resistive component of the ac signal. This component was changed to a dc signal which was recorded on a strip charge recorder. Any

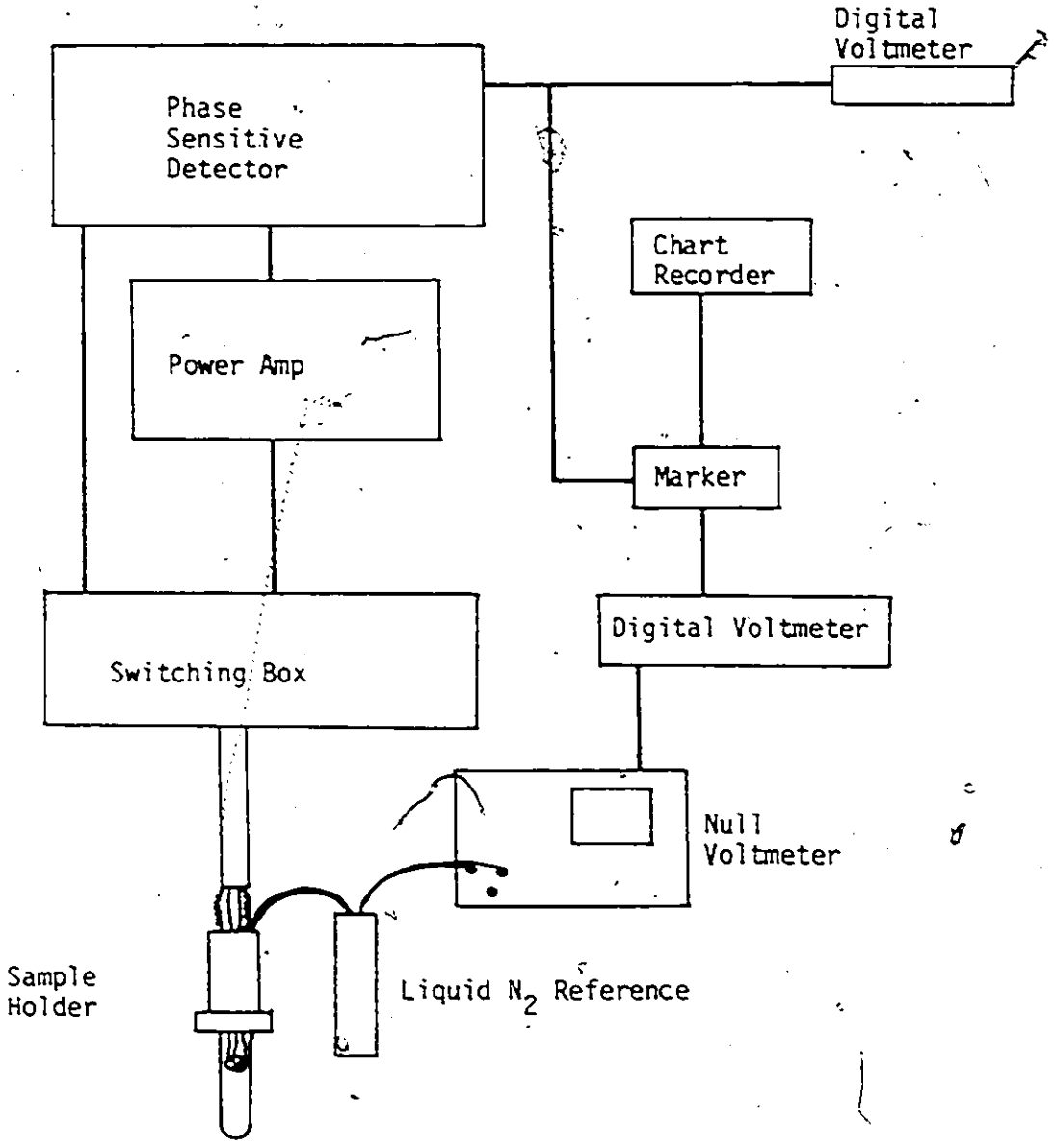

Figure 2.1 Block Diagram of Electronics for Conductivity Experiments

inductive or capacitive coupling which had a phase difference of 90° from the resistive component was eliminated by proper adjustment of the reference phase.

The resistivities of anisotropic materials were measured by means of the Montgomery technique(29). For a tetragonal system, there are two components of resistivity: ρ_1 and ρ_2 (= ρ_3). These can be calculated by measuring the voltages obtained when leads are placed on an anisotropic crystal face in a square or rectangular configuration. (The optimum contact position depends on the electrical anisotropy of the crystal). This is shown schematically in the following diagram:

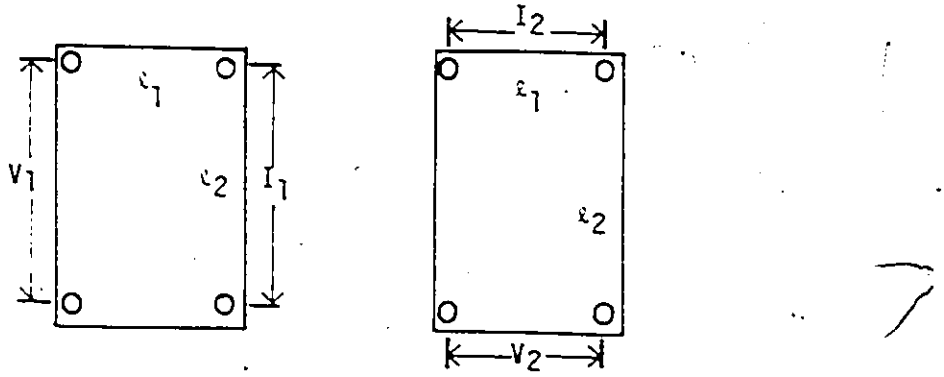

By means of a simple switching device, V_2 and V_1 were measured on the same sample face without altering the contact configuration. To reduce inductive and capacitive coupling, twisted lead pairs were used to and from the sample. Four twisted pairs were used so a voltage and current lead would not be paired at any one time, which would lead to a very high background signal.

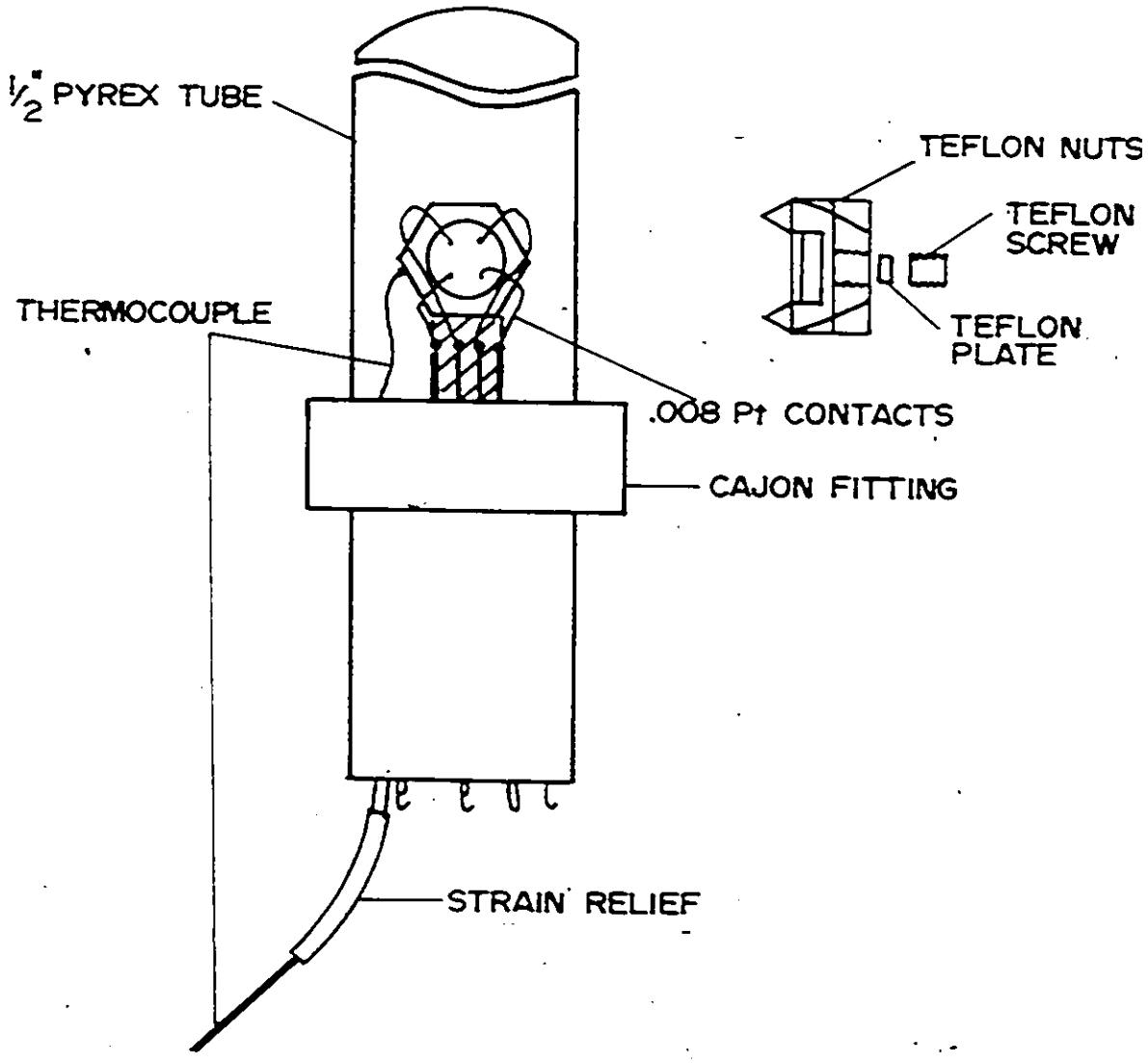

Figure 2.2 Sample Holder for Conductivity Experiments

2.4.2 SAMPLE HOLDER AND HANDLING

The sample holder is shown in Figure 2.2. Because of the extremely hygroscopic nature of the compounds studied, all manipulations with the sample had to be carried out in a very good dry box. The sample holder consisted of a Cajon vacuum connector with a 7-pin feedthrough soldered to one end. Contact was made by four .008 inch platinum wires, bent 90° at the ends to insure good point contact, in a square configuration. The wires were melted into two Nylon nuts, and the sample was held in place with a flat Teflon plug which was pressed against the sample by a Teflon screw. The pressure of the screw was adjusted until good point contact was made. The contacts were checked with an ohmmeter, and contact resistances of less than 1 Ω were considered satisfactory. The contact separations were measured using a microscope.

The sample holder was evacuated at 10^{-6} torr for several days before using to ensure complete dryness. Room temperature measurements were carried out directly in the dry box using an electrical feedthrough into the box. For low temperature measurements the sample holder was sealed with a Pyrex tube and removed from the dry box. It was put in a stainless steel Dewar where temperatures ranging from ~ 296° K to 4.2 K were possible. The temperature was monitored with a copper - constantan thermocouple placed next to the crystal.

2.5 PREPARATIVE REACTIONS

The reaction vessels that were generally used have been described in detail previously (30). A diagram is shown on the following page.

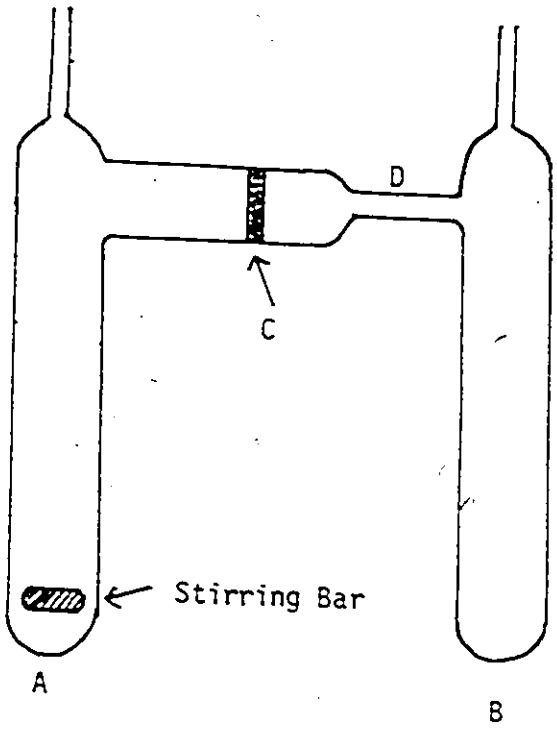

The reaction vessel was flame-sealed after addition of the sulphur dioxide. If there was an insoluble product after the reaction had taken place inside (A), the solution could be filtered through the glass sinter (C). The SO_2 was conveniently transferred from one side to the other by cooling the appropriate side-arm, and the desired product was isolated by flame-sealing at (D).

2.5.1 THE REACTION OF Hg WITH AsF_5

The reaction of mercury with AsF_5 in the mole ratio 2:3 will be described. The preparation of the individual polyatomic cations will then be described separately.

In a typical experiment arsenic pentafluoride (3.42g, 20.1 mmole) was condensed onto elemental mercury (2.69g, 13.4 mmole) in SO_2 at -196°C, and then allowed to warm to room temperature. The mixture was stirred

and the reaction proceeded quickly to give initially a yellow solution. The remaining elemental mercury solidified suddenly to give a golden crystalline mass. The solution gradually became deep red. After approximately one-half hour the golden crystals and red solution reacted further to yield a yellow solution which became colourless after an additional fifteen minutes.

2.5.2 $Hg_2(AsF_6)_2.SO_2$

Arsenic pentafluoride (3.42g, 20.1 mmole) was condensed onto elemental mercury (2.69g, 13.4 mmole) in sulphur dioxide at -196°C and the mixture was allowed to warm to room temperature. After the reaction was complete the clear solution yielded a white compound on removal of volatiles, which was identified by the Raman spectrum.

2.5.3 $Hg_2(AsF_6)_2$

$Hg_2(AsF_6)_2.SO_2$ was pumped at 50°C under dynamic vacuum for one hour. The resulting white solid showed the absence of SO_2 in the Raman spectrum.

2.5.4 $Hg_3(AsF_6)_2$

In a typical experiment arsenic pentafluoride (2.78g, 16.4 mmole) was condensed onto elemental mercury (3.29g, 16.4 mmole) in sulphur dioxide at -196°C and the mixture was allowed to warm to room temperature and then stirred for a few hours. All the mercury reacted to give a light yellow solution, which yielded a light yellow crystalline solid

upon removal of volatiles

Analysis: Calculated for $Hg_3(AsF_6)_2$: Hg, 61.43; As, 15.30; F, 23.27

found : Hg, 61.39; As, 15.28; F, 22.92

2.5.5 $Hg_4(AsF_6)_2$

When elemental mercury (2.47g, 12.3 mmole) was reacted with arsenic pentafluoride (1.56g, 9.2 mmole) in liquid sulphur dioxide, a deep red solution was obtained in addition to insoluble golden crystals. The red solution was filtered and the solvent was slowly removed over a period of a few days. Two distinct types of crystals were formed: yellow crystals which were identified as $Hg_3(AsF_6)_2$ by the Raman spectra; and red-black needle shaped crystals. The latter were hand-picked under a microscope in a dry box.

Analysis: Calculated for $Hg_4(AsF_6)_2$: Hg, 67.9; As, 12.7; F, 19.3

found : Hg, 67.77;As, 12.65;F, 19.47

2.5.6 $Hg_{2.86}AsF_6$

In a typical experiment, arsenic pentafluoride was condensed onto elemental mercury in liquid SO_2 at -196°C and the mixture was allowed to warm to room temperature and slowly stirred. A slight excess of AsF_5 than that required by the stoichiometry was used to ensure that no unreacted mercury contaminated the surface of the crystals. After the reaction was complete golden metallic crystals were present with a

slightly yellow solution. The crystals were filtered, washed with SO_2 and pumped dry. Care was taken not to cool the crystals in SO_2 when washing because of the disproportionation discussed in Section 7.3.1.

Analysis: Calculated for $Hg_{2.86}AsF_6$: Hg, 75.23; As, 9.82; F, 14.95
found: Hg, 75.83; As, 9.52; F, 14.61

Although the analysis is closer to Hg_3AsF_6, crystallographic arguments (Chapter VI) show that the empirical formula must be $Hg_{2.86}AsF_6$.

2.5.7 Hg WITH SbF_5

Antimony pentafluoride (0.96g, 4.4 mmole) was added to one side of a reaction vessel while elemental mercury (0.36g, 1.8 mmole) was added to the other. Sulphur dioxide was condensed onto the SbF_5 at -196°C and the mixture was warmed to room temperature. When the SbF_5 had dissolved in the SO_2, the solution was transferred onto the Hg and allowed to react. The mercury reacted within 10 min. to yield a light yellow solution in equilibrium with unreacted mercury. The colour of the solution became orange within one-half hour with very little solid left. Very suddenly an orange solid precipitated which gradually became yellow with a light yellow solution. After one week the solution was colourless with a slightly yellow solid. The solution yielded an off-white solid when the volatiles were removed which was tentatively identified by the Raman spectrum as $Hg_2(Sb_2F_{11})_2.SO_2$.

2.5.8 $Hg_2(SbF_6).SO_2$

Sulphur dioxide was condensed onto antimony pentafluoride

(0.35g, 1.6 mmole) at -196°C and allowed to warm to room temperature. After dissolution it was transferred onto mercurous flouride (0.34g, 0.8 mmole) and stirred. After one-half hour a clear solution was obtained in addition to a small amount of insoluble white solid. The volatiles were removed from the solution yielding a white solid, which was identified as $Hg_2(SbF_6)_2.SO_2$ by the Raman spectrum.

2.5.9 $Hg_2(SbF_6)_2$

$Hg_2(SbF_6)_2.SO_2$ was pumped at 50°C under dynamic vacuum for one hour to remove the SO_2. Alternatively, the SO_2 soluble product from 2.5.6 could be pumped at 50°C for one hour. The Raman spectra of the two compounds were identical.

2.5.10 $Hg_3(Sb_2F_{11})_2$

Elemental mercury (2.74g, 13.7 mmole) was stirred at room temperature with antimony pentafluoride (4.94g, 22.8 mmole) in liquid SO_2. After 48 hours a very light yellow solution containing a yellow solid was obtained. The yellow solid was extracted with SO_2 until the remaining solid was white. The white solid was identified as SbF_3. The sulphur dioxide was removed from the yellow solution yielding a light yellow crystalline solid.

Analysis: Calculated for $Hg_3(Sb_2F_{11})_2$: Hg, 39.94; Sb, 32.32; F, 27.74

found : Hg, 39.80; Sb, 32.23; F, 27.92

2.5.11 $Hg_{2.91}SbF_6$

In a typical experimental a large excess of $Hg_3(Sb_2F_{11})_2$ was dissolved in SO_2 and stirred with elemental mercury at -10°C. The mercury reacted quickly to give finely divided insoluble golden crystals. When all the mercury had reacted the crystals were quickly filtered and washed several times with SO_2. A method was developed for growing large crystals (2-3 mm) of $Hg_{2.91}SbF_6$ which is described in Section 7.4.1.

2.5.12 $Hg_2(SO_3F)_2$

In a typical experiment peroxydisulphuryl difluoride (0.60g, 3.0 mmole) was condensed onto elemental mercury (1.20g, 6.0 mmoles) in liquid SO_2 at -196°C. The reaction mixture was allowed to warm to room temperature and stirred. After one week all the mercury had reacted to yield a white, insoluble solid. The solid was filtered and pumped to constant weight. The compound was identified by the Raman spectrum.

2.5.13 ELEMENTAL ANALYSES

All analyses were performed by Alfred Bernhardt Microanalytical Laboratories, 5251 Elbach uber Engelskirchen, Fritz-Pregl-Strasse 14-16, West Germany.

CHAPTER III

THE MERCUROUS CATION

3.1 INTRODUCTION

Mercury (I) has been known to exist for many years as the dimercury dication, Hg_2^{2+}. This was demonstrated as early as 1898 by Ogg (31) who studied the reaction between Ag^+ and elemental mercury and concluded that the equilibrium constant could only be expressed in terms of $[Hg_2^{2+}]$. Abel (32) reached the same conclusion by studying the reduction of mercuric nitrate with elemental mercury. Although Hg_2^{2+} has been known for a long time, the ion is much less stable than is generally assumed, its stability being confined to relatively few anions and solvents. The stability of the mercurous ion will be discussed.

This chapter reports the preparation of several new mercurous compounds with very weakly basic anions in non-aqueous media. The Raman spectra of the compounds are presented and discussed.

3.2 COMPOUNDS OF THE Hg_2^{2+} CATION

3.2.1 PREPARATION AND IDENTIFICATION

When mercury was treated with a solution of AsF_5 in liquid SO_2 in the mole ratio 2:3 the reaction proceeded according to the equation:

$$2Hg + 3AsF_5 \rightarrow Hg_2(AsF_6)_2 + AsF_3$$

The product is exceedingly soluble in liquid SO_2 and exists as the sulphur dioxide adduct, $Hg_2(AsF_6)_2.SO_2$, when the volatiles are removed under vacuum. The solution Raman spectrum in SO_2 shows, in addition to the anion frequencies, a single strong polarized band at 160 cm^{-1} which may be assigned to ν_1, the Hg-Hg stretch, of the Hg_2^{2+} ion. This value is considerably lower than those found for the aqueous solutions of mercurous nitrate and mercurous perchlorate (33). The possible reasons for this will be discussed in Section 3.2.2. The UV-visible spectrum of $Hg_2(AsF_6)_2$ exhibits a single absorption at 248 nm in HSO_3F with an approximate extinction coefficient of 10^4. This may be compared with the peak at 237 nm obtained for aqueous solutions of mercurous compounds (34). The anion was identified by the characteristic ν_1, ν_2 and ν_5 modes of AsF_6^- in the solution Raman spectrum and by the characteristic 1:1:1:1 quartet in the ^{19}F nmr when the compound was dissolved in acetone, with which some reaction occurred. When the compound is added to water, an exothermic disproportionation takes place with the deposition of finely divided elemental mercury.

Sulphur dioxide is a much stronger donor towards the Hg_2^{2+} ion than has previously been realized. The Raman spectrum of the white powder obtained when the volatiles were removed under vacuum showed peaks at 1108 cm^{-1} and 1305 cm^{-1}, which can be assigned to the ν_1 and ν_3 modes of SO_2 respectively. It is noteworthy that these modes, which occur at 1147 cm^{-1} and 1362 cm^{-1} in free SO_2 (35), have been lowered considerably in the compound $Hg_2(AsF_6)_2.SO_2$. Very slow removal of the solvent from a

sulphur dioxide solution of $Hg_2(AsF_6)_2$ yielded crystals which exhibited a Raman spectrum which was identical with that of the powder. Prelimina crystallographic information on $Hg_2(AsF_6)_2.SO_2$ is presented in Section 3 together with a discussion on adducts of the mercurous ion.

The sulphur dioxide could be removed from $Hg_2(AsF_6)_2.SO_2$ by heating the compound to 50°C under a dynamic vacuum for 1 hr. The resulting white powder showed a single strong peak at 188 cm^{-1} with a shoulder at 197 cm^{-1}, which can be assigned to ν_1 (Hg-Hg), along with an absence of bands due to SO_2. The Raman spectra of both $Hg_2(AsF_6)_2.SO_2$ and $Hg_2(AsF_6)_2$ are reported in Section 3.2.2, as well as the results of a Raman spectral study of the thermal decomposition of $Hg_2(AsF_6)_2$.

Oxidation of mercury with peroxydisulphuryldifluoride, ($S_2O_6F_2$), in the mole ratio 2:1 proceeded rapidly to give a white, SO_2 insoluble compound which had the characteristic 248 nm peak in the UV-visible spectrum with HSO_3F as a solvent and a Raman spectrum, reported in Section 3.2.2, consistent with the composition $Hg_2(SO_3F)_2$. The reaction may be described by the equation:

$$2Hg + S_2O_6F_2 \xrightarrow{SO_2} Hg_2(SO_3F)_2$$

$S_2O_6F_2$ is a particularly convenient oxidizing agent because the only reaction product is mercurous fluorosulphate. In contrast with the coloured solutions that were initially observed when Hg was oxidized by AsF_5, no intermediate colours were observed. In addition, it was impossible to reduce the product by the addition of excess mercury. This

is in marked contrast with $Hg_2(AsF_6)_2$, which is readily reduced by mercury in sulphur dioxide to yield $Hg_3(AsF_6)_2$. The inability to reduce $Hg_2(SO_3F)_2$ is due to its insolubility in SO_2, which shifts the equilibrium in favour of Hg_2^{2+}.

$$Hg_3^{2+} \rightarrow Hg + Hg_2^{2+}$$

However, the Hg_3^{2+} ion is formed when mercury is dissolved in fluorosulphuric acid (Section 4.2.1).

When mercury was treated with antimony pentafluoride in the mole ratio 2:5 the reaction proceeded very slowly over a period of a few weeks to give a clear solution which yielded a creamy white solid when the volatiles were removed. The white solid was identified as $Hg_2(Sb_2F_{11})$ xSO_2 by the Raman spectrum, which is discussed in Section 3.2.2. The reaction proceeds according to the equation:

$$2Hg + 5SbF_5 \rightarrow Hg_2(Sb_2F_{11})_2 + SbF_3$$

The addition of excess SbF_5 to a solution of the solid in SO_2 resulted in the formation of $SbF_5.SO_2$, which indicates that the mercurous ion is only slowly oxidized to Hg^{+2} in this system. The $SbF_5.SO_2$ was identified by the ^{19}F nmr spectrum of a solution of the white solid with excess SbF_5 in SO_2. The spectrum showed, in addition to the characteristic spectrum of $Sb_2F_{11}^-$ (36), a doublet at 103 ppm upfield from $CFCl_3$. This may be assigned to the equatorial fluorines in the $SbF_5.SO_2$ adduct (I), previousl reported at 102 ppm (37).

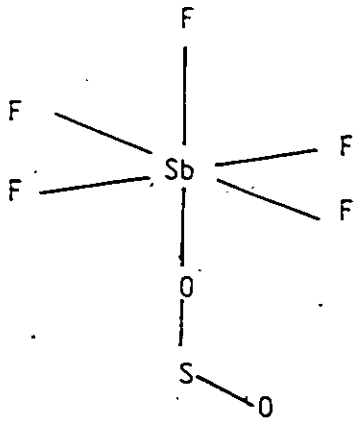

(I)

The expected weak quintet due to the axial fluorine reported at 137 ppm would be obscured by the quintet of the $Sb_2F_{11}^-$ ion which occurs at 134 ppm.

If $Hg_2(Sb_2F_{11})_2.SO_2$ was pumped for 24 hours at 70°C the compound was converted to $Hg_2(SbF_6)_2$, which had an identical Raman spectrum to that of another sample of $Hg_2(SbF_6)_2$ prepared by a different method which is described below.

The reaction of Hg_2F_2 with SbF_5 in the mole ratio 1:2 proceeded within minutes to give a white, SO_2 soluble product whose Raman spectrum was consistent with the composition $Hg_2(SbF_6)_2.SO_2$. When the compound was pumped at 70°C for 24 hours the SO_2 was removed to yield $Hg_2(SbF_6)_2$. The equation for the reaction can be written as follows:

$$Hg_2F_2 + 2SbF_5 \xrightarrow{SO_2} Hg_2(SbF_6)_2.SO_2$$

$$Hg_2(SbF_6)_2.SO_2 \xrightarrow{\Delta} Hg_2(SbF_6)_2 + SO_2$$

When Hg was oxidized by SbF_5 there was a small amount of insoluble white solid which was identified by the Raman spectrum as an $SbF_3.SbF_5$

adduct. In the reaction of Hg_2F_2 with SbF_5 there was also a small amount of insoluble material which was not identified.

Attempts to prepare $Hg_2(SbCl_6)_2$ by the reaction of Hg_2Cl_2 with $SbCl_5$ according to the equation

$$Hg_2Cl_2 + 2SbCl_5 \rightarrow Hg_2(SbCl_6)_2$$

were unsuccessful. The reaction was carried out in sulphur dioxide and in neat $SbCl_5$, both at room temperature and at 80°C in a sealed tube. The products were invariably $HgCl_2$ and $SbCl_3$, which were identified by their characteristic Raman spectra. The reaction may be described by the equation:

$$Hg_2Cl_2 + SbCl_5 \rightarrow 2HgCl_2 + SbCl_3$$

It appears that $SbCl_5$ is a comparitively good oxidizing agent but a relatively poor Lewis acid. When using Lewis acids such as AsF_5, the oxidation of mercury proceeds quantitatively to Hg_2^{2+} because of the facile formation of AsF_6^-. It is interesting to note that $AsCl_5$ is unknown, and although $AsCl_4^+$ has been identified (38), the stable chloride is $AsCl_3$. Although the instability of the pentachloride is not as pronounced with antimony, the most stable chloride appears to be $SbCl_3$.

The reaction between Hg_2F_2 and TaF_5 proceeds according to the equation:

$$Hg_2F_2 + 2TaF_5 \rightarrow Hg_2(TaF_6)_2$$

The product is a white, SO_2 insoluble solid. The compound was identified by the Raman spectrum.

3.2.2 RAMAN SPECTRA

The Raman spectra of $Hg_2(AsF_6)_2$ in solution in liquid sulphur dioxide, solid $Hg_2(AsF_6)_2.SO_2$ and solid $Hg_2(AsF_6)_2$ are shown in Figure 3.1. The mercury-mercury stretching vibration, ν_1, has a frequency of 160 cm^{-1} in SO_2, a value considerably lower than those found for aqueous solutions of mercurous nitrate (172 cm^{-1}) and mercurous perchlorate (173 cm^{-1}) (33). The spectrum of solid $Hg_2(AsF_6)_2.SO_2$ shows that the Hg-Hg stretching frequency shifts to 180 cm^{-1} from the value of 160 cm^{-1} in SO_2 solution. In addition, a broad weak band appears at 109 cm^{-1} in the spectrum of $Hg_2(AsF_6)_2.SO_2$. The large frequency shift in the Hg-Hg stretch is attributed to solvation of the Hg_2^{2+} ion by SO_2, probably by donation through the lone pairs on oxygen. A reduction of the positive charge on the mercury atoms would tend to expand the outer filled d-electron clouds, causing greater electronic repulsions and thus weakening the metal-metal bond. The Hg-Hg stretching frequency in solid $Hg_2(AsF_6)_2$ is centered at 192 cm^{-1}. This is one of the highest that has been observed for mercurous compounds, and is consistent with the very low basicity of AsF_6^-.

The bands due to the SO_2 molecule in $Hg_2(AsF_6)_2.SO_2$ can be assigned by comparing the spectra of $Hg_2(AsF_6)_2.SO_2$ and $Hg_2(AsF_6)_2$, which is prepared by simply heating the former to 50°C under vacuum. Those bands which disappear upon heating and pumping $Hg_2(AsF_6)_2.SO_2$ include,

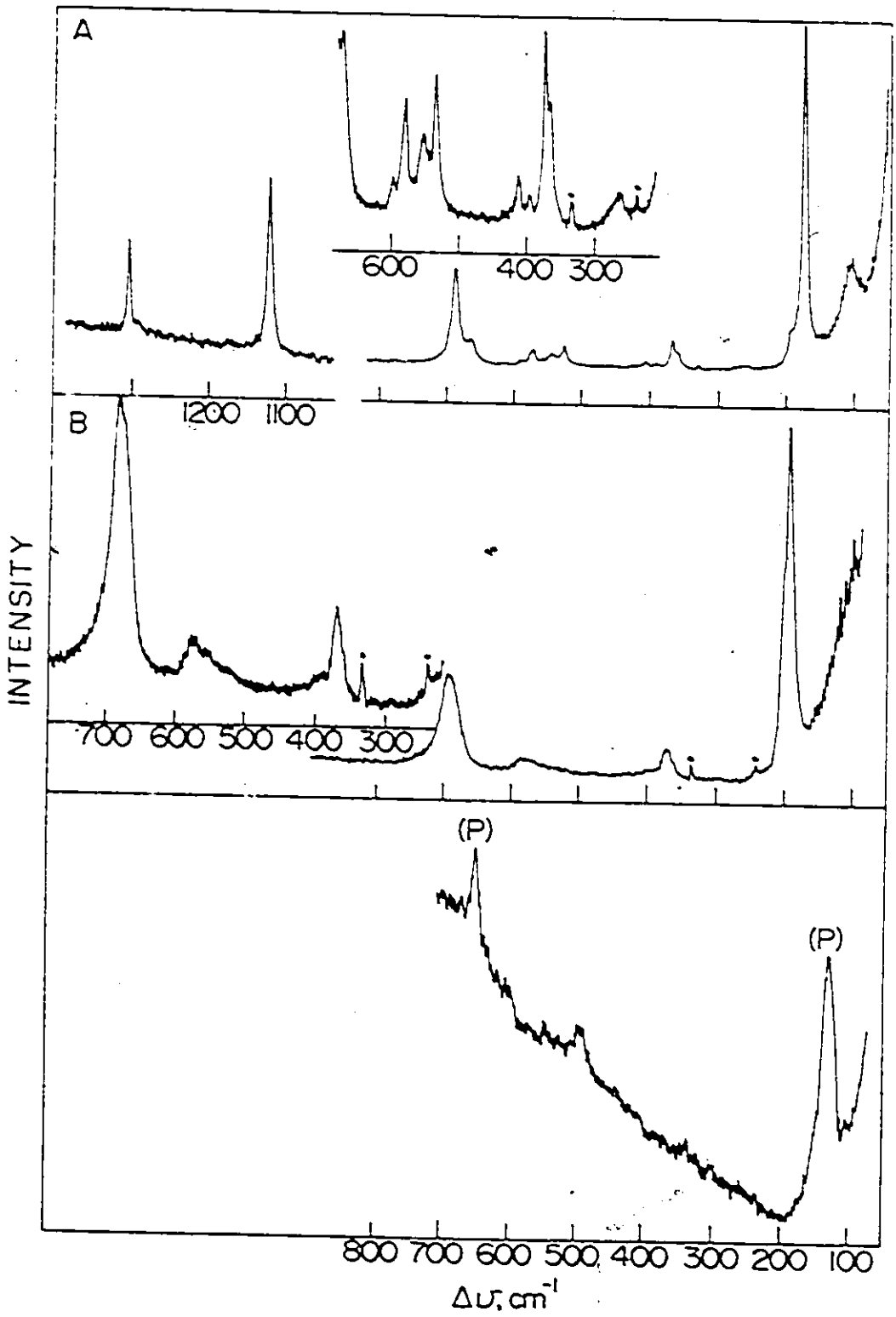

Figure 3.1 Raman Spectra of (A) $Hg_2(AsF_6)_2.SO_2$
(B) $Hg_2(AsF_6)_2$ and $Hg_2(AsF_6)_2$(SO_2 solution)
asterisk denotes glass

TABLE 3.1

Raman Frequencies and Assignments for $Hg_2(AsF_6)_2.SO_2$ and $Hg_2(AsF_6)_2$

$Hg_2(AsF_6)_2.SO_2$	$Hg_2(AsF_6)_2$		Assignment
	Solution	Solid	
109 (14)			δ(Hg-O-S)
180 (100)	160(p)vs	188 (100) 197 (sh)	$\nu_1(\sigma_g^+)$ Hg_2^{2+}
266 (1)			Hg-O stretch?
367 (5) 376 (8) 396 (1)	369 m	371(8)	$\nu_5(t_{2g})AsF_6^-$
413 (1)			Hg-O stretch?
533 (6)			ν_2 SO_2
549 (4) 576 (4) 595 (1)	526 w	574(3) br.	$\nu_2(e_g)AsF_6^-$
670 (7) 690 (28)	677 s	679(sh) 687(28)	$\nu_1(a_{1g})AsF_6^-$
1118			ν_1 SO_2
1305			ν_3 SO_2

in addition to those at 1118 cm^{-1} and 1305 cm^{-1} due to ν_1 and ν_3 of SO_2 respectively, bands at 533 cm^{-1}, 413 cm^{-1}, 266 cm^{-1} and 109 cm^{-1}. The band at 533 cm^{-1} is probably due to ν_2 of the SO_2 molecule. The decrease in the ν_1 and ν_3 modes of SO_2 is consistent with coordination of SO_2. The frequency shift of 12 cm^{-1} in the Hg-Hg stretching frequency between $Hg_2(AsF_6)_2$ and $Hg_2(AsF_6)_2 \cdot SO_2$ is also consistent with coordination of the mercurous ion with the SO_2 molecule, although admittedly the frequency shift is small. Therefore, it seems reasonable to assign either the band at 413 cm^{-1} or the band at 266 cm^{-1} to the Raman active Hg-O stretching frequency. The band at 109 cm^{-1} may then be due to δ(Hg-O-S), although this peak seems somewhat intense for a bending mode. The tentative assignments are given in Table 3.1.

In addition to the bands due to the SO_2 molecule and its interaction with the mercurous ion, the AsF_6^- region contains considerably more bands than would be expected for O_h symmetry. Gillespie and Schrobilgen (39) have suggested that a highly polarizing cation can perturb the O_h symmetry of MF_6^- anions to pseudo C_{4v} symmetry. They have interpreted the anion spectra of such specieis as $NgF^+MF_6^-$ (Ng = Xe,Kr; M = As,Sb) in terms of pseudo C_{4v} symmetry. The three Raman active modes (a_{1g}, e_g, t_{2g}) of an octahedral anion observed in the Raman spectrum of a wholly ionic hexafluoroarsenate such as $K^+AsF_6^-$ (40) are replaced by 11 Raman active bands under C_{4v} symmetry, excluding those associated with the cation. This explanation seems unlikely for $Hg_2(AsF_6)_2 \cdot SO_2$ because the relatively intense ν_8 mode in the C_{4v} approximation, which invariably occurs at 710-730 cm^{-1}, is not observed. Also, the Hg_2^{2+} cation would not be expected to be as polarizing as a noble

gas fluoro-cation and hence the observation of additional bands arising from an anion of pseudo C_{4v} symmetry caused by fluorine bridging would seem improbable. Therefore the spectrum of $Hg_2(AsF_6)_2.SO_2$ is assigned (Table 3.1) on the basis of an octahedral anion. The observation of additional bands may well be caused by site symmetry or factor group splitting. In principle, all 15 modes of the AsF_6^- ion would be Raman active under the site symmetry C_1. (The space group of $Hg_2(AsF_6)_2.SO_2$ is $P2_1/c$ and Z=4). The 15 modes would be further split to give 30 bands under the factor group symmetry of C_{2h}. Although it is unlikely that all bands would be resolved, it may be seen that a complicated spectrum is expected for AsF_6^- in $Hg_2(AsF_6)_2.SO_2$.

Raman spectral assignments for $Hg_2(AsF_6)_2$ are given in Table 3.1. The peak due to ν_1(Hg-Hg) centered at 192 cm^{-1} is actually composed of two peaks, one at 188 cm^{-1} and the other at 197 cm^{-1}. The appearance of a doublet may well be due to factor group splitting, although in the absence of structural information this must remain speculative. Although the spectrum is not particularly well resolved, the bands due to AsF_6^- are broad and may well be split. Again, it seems unlikely that this is due to an interaction between the AsF_6^- anion and the Hg_2^{2+} cation. The occurrence of split bands arising from the $\nu_1(a_{1g})$, $\nu_2(e_g)$ and $\nu_5(t_{2g})$ modes of AsF_6^- does not necessarily mean that the symmetry of the anion has been lowered by fluorine bridging; lowering of the site symmetry or factor group splitting might also account for this.

It is interesting to examine the spectra following the decomposition of $Hg_2(AsF_6)_2$ as it is heated under vacuum. The compound, initially

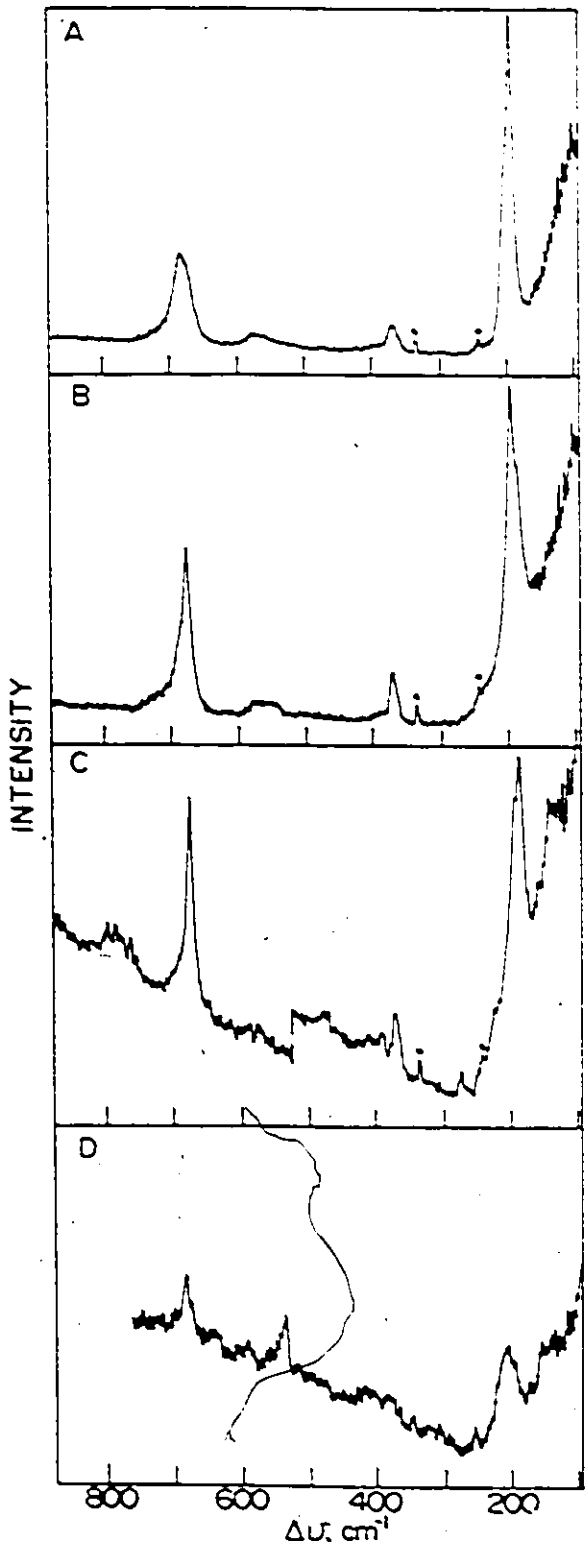

Figure 3.2 Thermal Decomposition of $Hg_2(AsF_6)_2$
(A) $Hg_2(AsF_6)_2$
(B) 1 hour at 50°C
(C) 3 hours at 70°C
(D) 24 hours at 80°C
All samples were pumped under vacuum

prepared by heating $Hg_2(AsF_6)_2.SO_2$ to 50°C while pumping to drive of the sulphur dioxide, apparently loses AsF_5 to yield Hg_2F_2 as it is heated further. The stepwise decomposition, which can be represented by the equations

$$Hg_2(AsF_6)_2.SO_2 \xrightarrow{\Delta} Hg_2(AsF_6)_2 + SO_2$$

$$Hg_2(AsF_6)_2 \xrightarrow{\Delta} Hg_2F_2 + 2AsF_5$$

is shown by the Raman spectra in Figure 3.2. The peaks at 188 cm^{-1} and 197 cm^{-1}, due to ν_1(Hg-Hg) in $Hg_2(AsF_6)_2$, as well as those due to the AsF_6^- ion, diminish in intensity. Concurrently, a new peak appears at 180 cm^{-1} which is presumably due to ν_1(Hg-Hg) in Hg_2F_2. This has been previously reported at 182 cm^{-1} (33). After leaving the compound for 24 hours at 80°C the spectrum shows little evidence for $Hg_2(AsF_6)_2$, and the disappearance of the peak at 180 cm^{-1} suggests that Hg_2F_2 has decomposed as well.

A reasonable assignment for the spectrum of $Hg_2(SO_3F)_2$, shown in Figure 3.3 and Table 3.2, can be made by analogy with the spectra of $ClOSO_2F$ (41) and $Xe(OSO_2F)_2$ (42). Although the symmetry of the molecule is not known, an approximate assignment can be made in terms of the modes of a single fluorosulphate group. Landa (24) has observed that the Raman active symmetric and asymmetric modes that would be expected for a bis-fluorosulphate of C_1 symmetry are generally not resolved. The modes assigned to the SO_2 and S-F stretching frequencies in $Hg_2(OSO_2F)_2$ are intermediate between those arising from a covalent fluorosulphate, such as $ClOSO_2F$ (41), and the ionic fluorosulphate anion in KSO_3F (43).

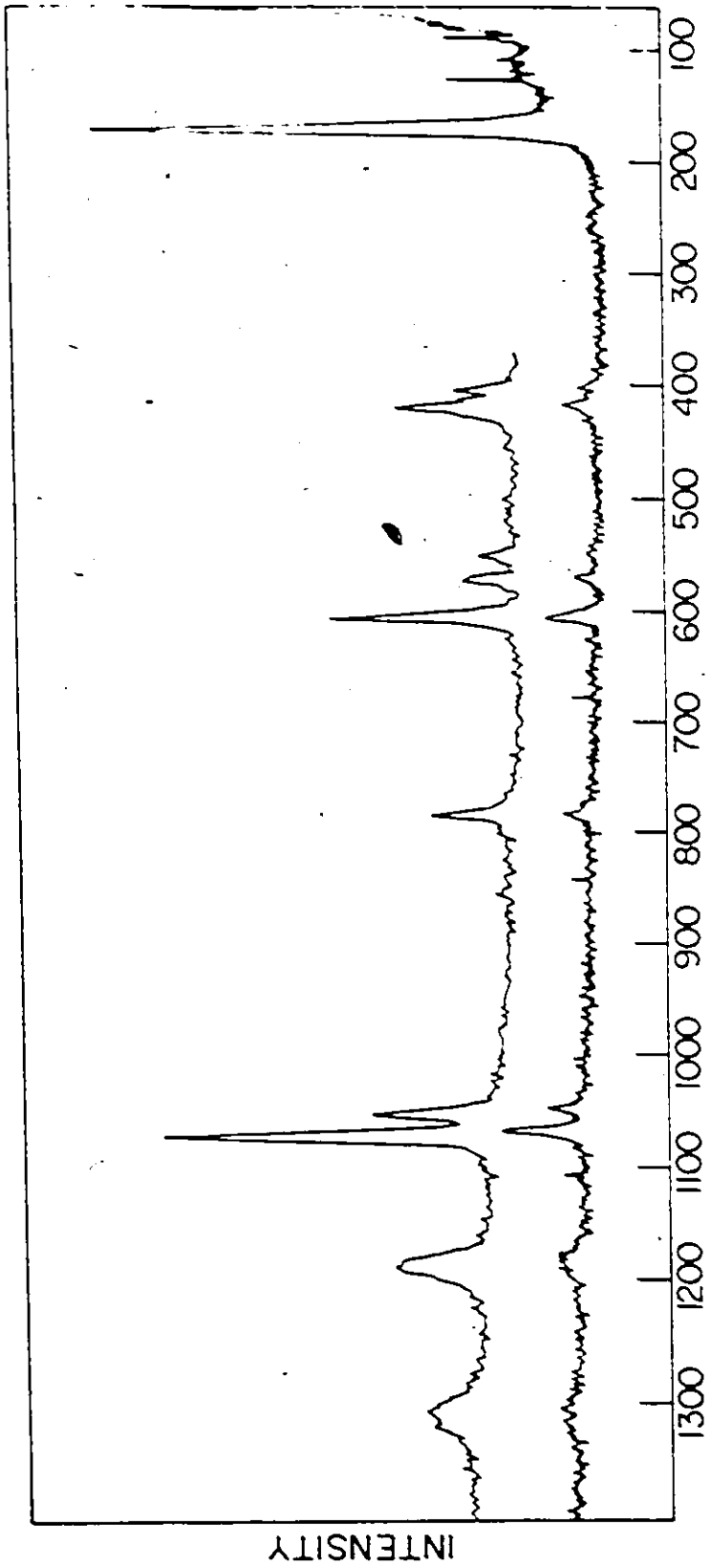

Figure 3.3 Raman Spectrum of $Hg_2(OSO_2F)_2$

TABLE 3.2

Raman Frequencies for $Hg_2(OSO_2F)_2$ and Related Molecules

$ClOSO_2F$ [b]	SO_3F^- [c]	$Xe(OSO_2F)_2$ [d]	$Hg_2(OSO_2F)_2$	Assignment [a]
		1420 (1)		
1478 (1)	1285	1416 (1)	1310 (4)	SO_2 asym.stretch (a"
		1388 (1)		
1225 (5)	1084 vs	1238 (1)	1184 (5)	SO_2 sym. stretch (a'
		1214 (2)		
856 (1.5)		954 (4)	1056 (17)	S-OX stretch (a')
		940	1072 (7)	
830 (1.5)	741 m	818 (<1)	791 (5)	S-F stretch (a')
706 (10)		436 (5)	420 (8) 413 (sh)	O-X stretch (a')
573 (< 1)	586 m	610 (7)	613 (8)	SO_2 bend (a')
		599 (< 1)		
534 (1)	570 m	570-584 (< 1)	579 (4)	SO_2 rock (a")
486 (4.5)	405 s	539 (< 1)	555 (2)	SF wag (a')
389 (< 1)		385 (1)	404 (5)	SO_2 twist (a")
363 (8)		256 (9)	252 (3)	S-OX bend
		253 (10)		
			162(100)	Hg-Hg stretch
			100 (3)	Hg-Hg-O bend ?

a. assigned on basis of C_s symmetry

b. ref. (41)

c. ref. (43)

d. ref. (42)

Therefore it seems reasonable to suppose that the Hg-O band has a considerable covalent character resulting from resonance form (b).

$$Hg_2^{2+}(OSO_2F^-)_2 \longleftrightarrow FSO_2O\text{-}Hg\text{-}Hg\text{-}OSO_2F$$

(a) (b)

This is in accord with the observation that ν_1 (Hg-Hg) occurs at 162 cm^{-1}, a value considerably lower than that arising from ν_1 (Hg-Hg) in $Hg_2(AsF_6)_2.SO_2$ or $Hg_2(AsF_6)_2$. It is concluded that $Hg_2(OSO_2F)_2$ is more covalent than either of the mercurous hexafluoroarsenates. The very weak, broad band observed at 252 cm^{-1} can reasonably be assigned to the mercury-oxygen interaction. It is probable that this is the bending mode δ(Hg-O-S), and if so the Raman active stretching frequency may be at 420 cm^{-1} or 413 cm^{-1}. These values may be compared with δ(Hg-O-S) observed at 108 cm^{-1} and ν(Hg-O) observed at 266 cm^{-1} or 413 cm^{-1} in $Hg_2(AsF_6)_2.SO_2$. The band at 100 cm^{-1} in $Hg_2(OSO_2F)_2$ may be due to δ(Hg-Hg-O).

The Raman spectrum of the sulphur dioxide soluble product obtained from the oxidation of Hg by SbF_5 in the mole ratio 2:5 is shown in Figure 3.4. The presence of SO_2 is indicated by bands at 1323 cm^{-1} and 1140 cm^{-1}. The Hg-Hg stretching frequency at 160 cm^{-1} seems unusually low, particularly in view of the fact that the modes due to ν_1 and ν_3 of SO_2 are much closer to their values in free SO_2 than is the case in $Hg_2(AsF_6)_2.SO_2$, which would seem to indicate that the mercurous cation is less strongly assocated with SO_2 in $Hg_2(Sb_2F_{11})_2.SO_2$ than in $Hg_2(AsF_6)_2.SO_2$. The peak at 107 cm^{-1} is probably a lattice mode, while the shoulder at 193 cm^{-1} is not assigned. When $Hg_2(Sb_2F_{11})_2.SO_2$ is pumped at 70°C for 24 hours the

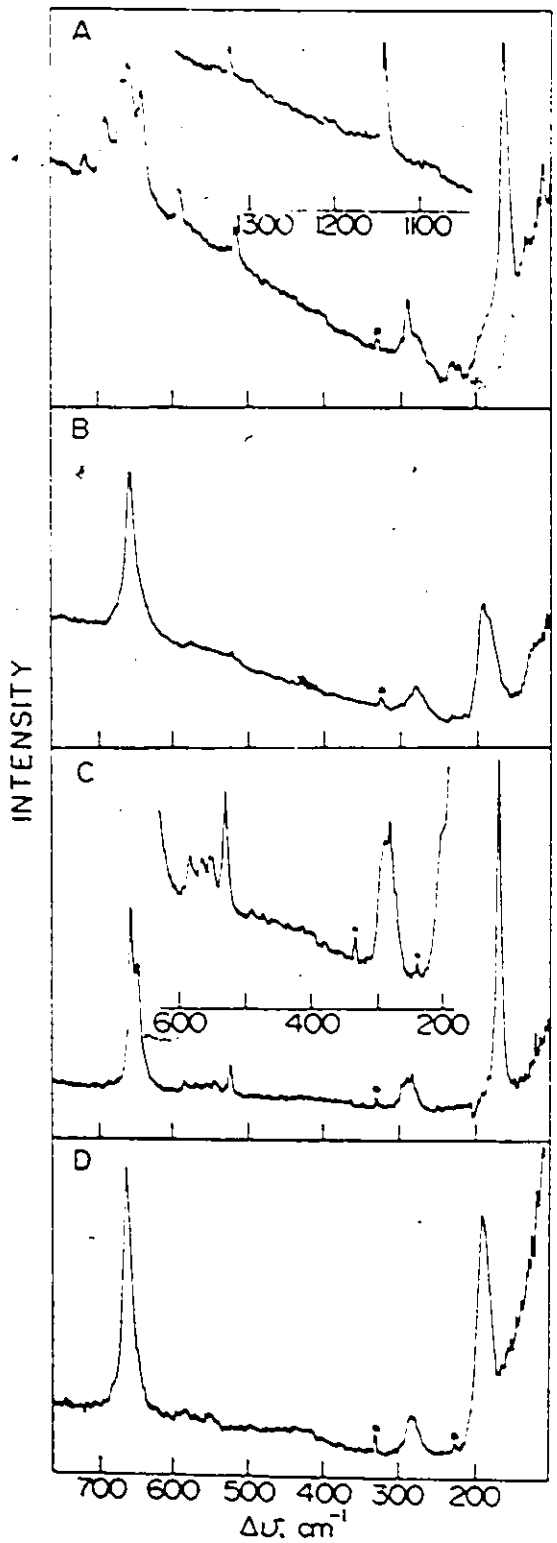

Figure 3.4 Raman Spectra of (A) $Hg_2(Sb_2F_{11})_2.SO_2$
(B) $Hg_2(SbF_6)_2$ obtained by heating (A) to 70°C and pumping
(C) $Hg_2(SbF_6)_2.SO_2$ from reaction $Hg_2F_2 + 2SbF_5$
(D) $Hg_2(SbF_6)_2$ obtained by heating (C) to 70°C and pumping
asterisk denotes glass

TABLE 3.3

Raman Frequencies and Assignments for $Hg_2(SbF_6)_2.SO_2$ and $Hg_2(SbF_6)_2$

$Hg_2(SbF_6)_2.SO_2$ [a]	$Hg_2(SbF_6)_2$ [b]	$Hg_2(SbF_6)_2$ [c]	Assignment
		125 (9)	
172 (100)	194 (78)	195 (66)	$\nu_1(\sigma_g^+)$ Hg-Hg
280 (10)	286 (16)	286 (20)	$\nu_5(t_{2g})$ SbF_6^-
288			
529 (9)			ν_2 SO_2
554 (2)	531 (3)	533 (3)	
565 (2)	566 (3)	570 (3)	ν_2 (e_g) SbF_6^-
584 (2)			
645 (36)	657 (100)	661 (100)	ν_1 (a_{1g}) SbF_6^-
654 (54)			
1112 (27)			ν_1 SO_2
1312 (13)			ν_3 SO_2

a. from the SO_2 soluble product from $Hg_2F_2 + 2SbF_5$

b. Above pumped at 70°C for 24 hours

c. reaction product from $2Hg + 5SbF_5$ pumped at 70°C for 24 hours

Raman spectrum of the product is consistent with the composition $Hg_2(SbF_6)_2$ (Figure 3.4). The decomposition can be written as:

$$Hg_2(Sb_2F_{11})_2.SO_2 \xrightarrow{\Delta} Hg_2(SbF_6)_2 + 2SbF_5 + SO_2$$

When Hg_2F_2 is reacted with SbF_5 in the mole ratio 1:2 the white, SO_2 insoluble compound obtained upon the removal of volatiles exhibits a Raman spectrum consistent with the composition $Hg_2(SbF_6)_2.SO_2$, shown in Figure 3.4. Spectral frequencies and assignments are listed in Table 3.3. When the adduct is pumped and heated at 70°C for 24 hours, the Raman spectrum of the product can be assigned to $Hg_2(SbF_6)_2$. There is a considerable frequency shift in ν_1(Hg-Hg) upon going from $Hg_2(SbF_6)_2.SO_2$ to $Hg_2(SbF_6)$. This indicates that the sulphur dioxide molecule is associated rather strongly with the mercurous cation. The Hg-Hg stretching frequency in $Hg_2(SbF_6)_2$ is the highest that has been observed for a mercurous salt; this is reasonable because SbF_6^- is less basic than AsF_6^-, SO_3F^- etc.

3.3 MERCURY (I) COMPLEXES

3.3.1 DISCUSSION

The complex chemistry of Hg(I) is restricted to those ligands which are not strongly bound to the Hg^{+2} ion, and which cause the disproportionation of Hg(I) to Hg^{+2} and elemental mercury. Until very recently, mercury (I) complexes were known only with oxygen and nitrogen donor ligands. Mercurous nitrate dihydrate, $Hg_2(NO_3)_2.2H_2O$, has a linear coordination of two water molecules around the mercurous ion (44,45) with a mercury-oxygen distance of 2.15Å. It has been

suggested that the mercurous ions in other soluble Hg (I) compounds are present in aqueous solution as the linear aquo complex $[H_2O\text{-}Hg\text{-}Hg\text{-}OH_2]^{2+}$. Evidence has also been presented (46,47) for weak mercurous complexes with the nitrate, sulphate and perchlorate anions. Hg(I) complexes have been reported for phenanthroline (48) and aniline (49).

Potts and Allred (50) have prepared and characterized a large series of mercurous complexes with oxygen donor atoms. These include the complexes $Hg_2[(C_6H_5)_3PO]_4(ClO_4)_2$, $Hg_2(C_5H_5NO)_4(ClO_4)_2$, $Hg_2SiF_6.5(C_5H_5NO)$ and others. These complexes are interesting because there appears to be four-coordination around the mercurous ion. This is in marked contrast with the normal linear two coordination around Hg(I) found in mercurous compounds. The authors suggest that four is the common coordination number for the Hg_2^{2+} ion. An attempt to prepare mercurous complexes with ligands having donor atoms other than oxygen such as triphenylphosphine, triphenylstibine and triphenylphosphine sulphide resulted in the disproportionation of Hg(I). It seems that polarizable ligands with phosphorous or sulphur donor atoms preferentially complex Hg^{+2} and cause disproportionation.

Recently Dean and Ibott (51,52) have prepared a number of complexes of the mercurous ion in sulphur dioxide with the heavier GpV and GpVI elements as donor atoms. They have shown by ^{19}F nmr, ^{13}C nmr and Raman spectroscopy that the mercurous ion is complexed by CF_3PPh_2 and PF_3, while PPh_3 causes disproportionation of the Hg_2^{2+} cation to Hg^{+2} and Hg(0). No complex is formed with $P(PF_3)_3$, which is presumably too weak a base. Adducts of Ph_3PS, $(p\text{-}FC_6H_4)_3PS$, Ph_3PSe, Ph_3As, and Ph_3Sb with

$Hg_2(AsF_6)_2$ were formed when the ratio L: $Hg_2(AsF_6)_2$ was < 1. The composition of all adducts was $Hg_2(AsF_6)_2.L$ and they were insoluble in sulphur dioxide. It is not clear whether the complexes are stable simply because of their insolubility in SO_2. A marked decrease of ν_1(Hg-Hg) in the Raman spectrum of the complexes indicated that the mercurous ion is directly coordinated.

During the course of the present work it has been shown that sulphur dioxide is a much stronger base towards the Hg_2^{2+} ion than had previously been supposed. $Hg_2(AsF_6)_2$, $Hg_2(Sb_2F_{11})_2$ and $Hg_2(SbF_6)_2$ are extremely soluble in SO_2. Removal of the solvent under vacuum resulted in the isolation of the complexes $Hg_2(AsF_6)_2.SO_2$, $Hg_2(Sb_2F_{11}).SO_2$ and $Hg_2(SbF_6)_2.SO_2$. In order to remove the SO_2 molecule it was necessary to heat the complexes to ~50°C under dynamic vacuum. The Raman stretching frequency of the Hg-Hg bond in a sulphur dioxide solution of $Hg_2(AsF_6)_2$ was found to be 160 cm^{-1}, which is considerably lower than aqueous solutions of other soluble mercurous salts. This indicates that the Hg_2^{2+} ion is strongly solvated in SO_2. Both solid $Hg_2(AsF_6)_2.SO_2$ and $Hg_2(SbF_6)_2.SO_2$ exhibit Hg-Hg stretching frequencies lower than the uncoordinated compound.

Compound	ν_1(Hg-Hg), cm^{-1}	$\Delta\nu_1$, cm^{-1}
$Hg_2(AsF_6)_2.SO_2$	180	
		12
$Hg_2(AsF_6)_2$	188 197	
$Hg_2(SbF_6)_2.SO_2$	172	
		22
$Hg_2(SbF_6)_2$	194	

3.3.2 PRELIMINARY CRYSTAL STRUCTURE OF $Hg_2(AsF_6)_2.SO_2$

It was of interest to determine the crystal structure of the compound $Hg_2(AsF_6)_2.SO_2$ for two reasons: firstly, to determine the length of the Hg-Hg bond for comparison with the bond lengths in other mercurous compounds; and secondly,to determine the position of the SO_2 molecule and thus ascertain whether it is simply present as a molecule of solvation or whether it is actually coordinated to the mercurous ion, either via the oxygen atom or the sulphur atom.

Intensity data were collected in the usual manner after initially examining the crystal on a precession camera. The crystal data are given in Table 3.4. The mercury and arsenic atoms were located by inspection of the three-dimensional Patterson. A subsequent three-dimensional Fourier map revealed the positions of the fluorine and sulphur atoms. Unfortunately, the structure is poorly refined (R_1 = 0.20) due to an inadequate absorption correction, and it was not possible to refine the positions of the oxygen atoms. However, it is clear that the SO_2 molecule is not coordinated to the mercurous ion through a sulphur atom. Although the position of the oxygen was not properly refined, the preliminary structure indicates a nearly linear Hg-Hg-O bond angle, which would be expected if the mercurous ion is coordinated by oxygen. The adduct appears to be similar to the 1:1 adducts discussed in the previous section. The Hg-Hg bond length in $Hg_2(AsF_6)_2.SO_2$ is 2.45(1) Å, which is equal to the Hg-Hg bond lengths in other mercurous compounds.

TABLE 3.4

Crystal Data For $Hg_2(AsF_6)_2.SO_2$

Formula weight	843.1
System	monoclinic
Conditions limiting possible reflections	hoℓ: ℓ=2n oko: k=2n
Space Group	$P2_1/c$ (no. 14, C_{2n}^5)
Cell Constants	
a	12.347 (9) Å
b	10.615 (12) Å
c	9.985 (6) Å
β	112.82 (5)°
number of formula units/unit cell	4
Cell Volume	1206.3 $Å^3$
Linear absorption coefficient	322.2 cm^{-1}

3.4 THE STABILITY OF THE MERCUROUS ION

One of the reasons for the existence of the rather unique Hg_2^{2+} ion, and to a lesser extent its GpIIB counterparts Zn_2^{2+} and Cd_2^{2+}, can be seen by examination of the electronic configurations, shown in Table 3.5. The ionization potentialsof all three elements, and mercury in particular, are very high. In fact the 1st I.P. of mercury is slightly greater than the 2nd I.P. of barium. The high ionization potentials are due to the poor screening of the valence electrons by the inner electrons, particularly the weakly penetrating 4f electrons of mercury. The effect manifests itself in tighter binding of the outer electrons and smaller atomic and ionic radii for the B group metals than for the A group metals, commonly referred to as the "Lanthanide contraction". The high ionization potentials make mercury one of the least electropositive of all metals. The particularly high electron affinity of the hypothetical Hg^{+1} ion leads to dimerization and formation of the Hg_2^{2+} ion. These ideas are discussed in more detail in reference books (53,54,55).

It is instructive to examine the stability of the Hg_2^{2+} ion with respect to disproportionation to elemental mercury and the Hg^{+2} ion. The standard potentials are listed in Table 3.5 along with the equilibrium constant for the disproportionation. The potentials for Hg_2^{2+} and Hg^{+2} are very similar, and common oxidants will oxidize Hg to Hg^{+2}. However, the equilibrium constant shows that in the presence of excess Hg metal Hg^{+2} will be readily reduced. Therefore, Hg_2^{2+} will be formed providing

TABLE 3.5

Electronic Configurations and Ionization Potentials for GpIIB Metals

	Zn	Cd	Hg
electronic configuration	$[Ar]3d^{10}4s^2$	$[Kr]4d^{10}5s^2$	$[Xe]4f^{14}5d^{10}6s^2$
1st I.P., $M \rightarrow M^+$ (eV)	9.4	9.0	10.4
2nd I.P., $M^+ \rightarrow M^{++}$ (eV)	18.0	16.9	18.7

Electrode Potentials for Mercury (Aqueous)

$$Hg_2^{2+} + 2e \rightleftharpoons 2Hg(\ell) \qquad E^o = 0.789\ V$$

$$2Hg^{2+} + 2e = Hg_2^{2+} \qquad E^o = 0.920\ V$$

$$Hg^{+2} + 2e = Hg(\ell) \qquad E^o = 0.854\ V$$

and $$Hg_2^{2+} = Hg(\ell) + Hg^{2+} \qquad E^o = -0.131\ V$$

$$K = \frac{[Hg^{2+}]}{[Hg_2^{2+}]} = 6.0 \times 10^{-3}$$

there is an excess of elemental mercury. It should be noted that these data are for aqueous solution. The Hg^{+2} is a highly polarizing cation; indeed, all Hg^{+2} compounds, except perhaps the fluoride, are molecular, covalent compounds. Any ligand that strongly complexes the Hg^{+2} ion will lead to the disproportionation of the Hg_2^{2+} cation according to the equation:

$$Hg_2^{2+}\ (aq) \rightarrow Hg\ (\ell) + Hg^{+2}\ (aq)$$

Except for the very insoluble halides, only oxygen and fluorine ligands stabilize the Hg_2^{2+} cation.

The stabilization of low oxidation states by large weakly basic anions has been discussed in detail by Corbett (20) for the Cd_2^{2+} system and may be applied equally well to the mercury system. The reduction of Cd^{+2} by Cd metal in the $CdCl_2$ melt was increased four-fold by the addition of sufficient $AlCl_3$ to quantitatively convert all Cl^- to $AlCl_4^-$. Because the highly polarizing Cd^{+2} ion is less strongly complexed to the weakly basic $AlCl_4^-$ ion than to the Cl^- ion, the addition of $AlCl_3$ to the melt greatly reduces the disproportionation of Cd_2^{2+}. In the solid state the stability of $Cd_2(AlCl_4)_2$, although moisture sensitive, is due to the lowering of the lattice energies between the two oxidation states by substitution of a large, weakly basic anion in place of Cl^-. This has been discussed by Van Arkel (56).

This chapter has shown that mercurous salts can be readily prepared in solution and the solid state by using large, weakly basic anions such as AsF_6^-, SbF_6^- and SO_3F^-. They are stable in a weakly basic

solvent such as SO_2 because the Hg^{+2} ion is not strongly complexed. It is interesting to note here that although the same anions that stabilize the mercurous ion also stabilize the polyatomic cations of the non-metals, they do so for a different reason. Whereas the latter are highly electrophilic and extremely unstable in the presence of any base, the existence of formally low positive oxidation states of metals is inherently reasonable. Therefore, disproportionation is due not to the instability of the low oxidation state of the metal, but rather to complexation of the higher oxidation state, thereby shifting the equilibrium in its favour.

Many workers have speculated on the effect of ligand electronegativity on the mercury-mercury bond length in mercurous compounds. Early structural studies (57,45) were from powder data and quite unreliable. Table 3.6 shows that the bond lengths seemed to show a marked increase with decreasing electronegativity of the anion. Various reasons were proposed for this supposed trend (58,59,33). A recent structural study (60) has shown that the Hg-Hg distances are independent of ligand electronegativity (Table 3.6). Even though there is little difference in bond length, there is a wide variation in ν_1 (Hg-Hg), particularly among the halides (Table 3.6). The vibrational frequency is not indicative of the bond strength, as the frequency would not be expected to be a "pure" Hg-Hg stretching frequency, but rather would manifest the mass effect. Durig et al (61), in a study of the vibrational spectra and molecular potential force fields of the mercurous halides, concluded that there is considerable coupling between the Hg-Hg and Hg-X stretching modes.

TABLE 3.6

Structural and Vibrational Data for Mercurous Compounds

Compound	Hg-Hg(old), Å	Hg-Hg(new), Å	ν_1(Hg-Hg), cm^{-1}
Hg_2F_2	2.43	2.507 (1)	186[c]
Hg_2Cl_2	2.53	2.526 (6)	169[d]
Hg_2Br_2	2.58	2.49 (1)[b]	136[d]
Hg_2I_2	2.69		113[d]
$Hg_2(NO_3)_2.2H_2O$[a]	2.54		

a. the structural unit is $[H_2O\text{-}Hg\text{-}Hg\text{-}OH_2]^{2+}$

b. from photographic data

c. reference (33)

d. reference (61)

CHAPTER IV

THE Hg_3^{2+} CATION

4.1 INTRODUCTION

Meyer and Schram reported in 1932 (62) that mercury reacts with fluorosulphuric acid to give a yellow solution. They appear to have assumed that the colour was due to the mercurous ion even though it normally gives colourless compounds and solutions. Thus it was not until 1960 that Gut's polarographic measurements on mercury (63) in the ternary eutectic $AlCl_3$-NaCl-KCl (6:20:14 moles %) suggested the possible existence of an oxidation state of mercury lower than +1. In the 1966 edition of a popular Inorganic Chemistry textbook, the authors view Hg_2^{2+} as a complex of Hg^{+2} with a mercury atom. In this context they state that "there would seem to be no good theoretical reason why a second Hg atom should not be bound to give $[Hg_3]^{2+}$" (64). This species has been prepared in the present study and it has been found that the only limitation to its stability is the basicity of the solvent and counterion. If the solvent or counterion are too basic, solvation of the highly polarizing Hg^{+2} cation causes the disproportionation of the Hg_3^{2+} cation.

$$Hg_3^{2+} \rightarrow Hg^{2+}\ (\text{solvated}) + 2Hg$$

The existence of the Hg_3^{2+} cation was first claimed in two preliminary communications. Torsi and Mamintov (65) reported the preparation of the compound $Hg_3(AlCl_4)_2$ from the reaction of mercury with

a molten mixture of $HgCl_2$ and $AlCl_3$, and this was followed by a report from this laboratory (23)of the preparation of $Hg_3(AsF_6)_2$ by the oxidation of mercury with arsenic pentafluoride in liquid sulphur dioxide.

This chapter reports the preparation of the compounds $Hg_3(AsF_6)_2$ and $Hg_3(Sb_2F_{11})_2$. The Raman spectra of both compounds will be discussed. The crystal structure of $Hg_3(AsF_6)_2$, which shows the Hg_3^{2+} ion to be linear and centrosymmetric, is presented and compared with the structure of $Hg_3(AlCl_4)_2$, determined by Ellison et al (66). It is also shown that the Hg_3^{2+} ion is formed when mercury is dissolved in HSO_3F.

4.2 COMPOUNDS OF THE Hg_3^{2+} CATION

4.2.1 PREPARATION AND IDENTIFICATION

When mercury is treated with AsF_5 in the mole ratio 1:1 the reaction proceeds according to the equation:

$$3Hg + 3AsF_5 \rightarrow Hg_3(AsF_6)_2 + AsF_3$$

The compound is light yellow and exceedingly soluble in sulphur dioxide. $Hg_3(AsF_6)_2$ is diamagnetic. The analysis was consistent with the composition $Hg_3(AsF_6)_2$. The solution Raman spectrum shows a single polarized peak (113 cm^{-1}) in the mercury-mercury region, as expected for a linear centrosymmetric ion of $D_{\infty h}$ symmetry. The AsF_6^-

ion in $Hg_3(AsF_6)_2$ was characterized by the 1:1:1:1 quartet of the AsF_6^- ion in the ^{19}F nmr spectrum of a solution of the salt in acetone, with which some reaction occurs, and by the observation of its characteristic bands in the Raman spectrum of the solid and the solution in sulphur dioxide. The compound can also be prepared by adding an equimolar amount of mercury to a solution of $Hg_2(AsF_6)_2$ in SO_2.

$$Hg + Hg_2(AsF_6)_2 \xrightarrow{SO_2} Hg_3(AsF_6)_2$$

This demonstrates the reversibility of the oxidation of mercury to mercury polyatomic cations which will be discussed in more detail later.

The reaction of mercury with antimony pentafluoride in the mole ration 3:5 proceeds according to the equation:

$$3Hg + 5SbF_5 \rightarrow Hg_3(Sb_2F_{11})_2 + SbF_3$$

The compound is light yellow and considerably less soluble then the hexafluoroarsenate analogue. It can be separated from the insoluble antimony triflouride by repeated extraction with sulphur dioxide. The elemental analysis of the pale yellow crystalline solid was in excellent agreement with the composition $Hg_3(Sb_2F_{11})_2$. The solution Raman spectrum exhibited the single polarized band at 113 cm^{-1} in addition to the characteristic frequencies for $Sb_2F_{11}^-$.

The use of SbF_5 as an oxidizing agent in the mercury system poses several problems, the most important of which is the possibility

of obtaining either SbF_6^-, or the complex anion $Sb_2F_{11}^-$, or both. (There are still higher complex anions such as $Sb_3F_{16}^-$ but these are present only in very low concentrations in the SO_2 solvent system). This is well illustrated by the behaviour of $Hg_3(Sb_2F_{11})_2$. When the solid is redissolved in sulphur dioxide, there is always a small amount of white material which remains undissolved. This may be explained by proposing an equilibrium such as:

$$Hg_3(Sb_2F_{11})_2 \rightleftharpoons Hg_3(SbF_6)_2 + 2SbF_5$$

The equilibrium lies well to the left but the liberated SbF_5 would immediately oxidize the $Hg_3(SbF_6)_2$ according to the equation:

$$2Hg_3(SbF_6)_2 + 3SbF_5 \rightarrow 3Hg_2(SbF_6)_2 + SbF_3$$

The cloudiness observed when $Hg_3(Sb_2F_{11})_2$ is redissolved in SO_2 is presumably due to SbF_3. Spectral evidence for the proposed equilibrium has been obtained. The ^{19}F nmr spectrum of $Hg_3(Sb_2F_{11})_2$ in SO_2 shows, in addition to the characteristic spectrum of $Sb_2F_{11}^-$, previously reported by Gillespie and Moss (36), a small peak at 56.3 ppm upfield from $CFCl_3$ which may be assigned to SbF_6^-. When the same solution is crystallized very slowly a small amount of white solid is obtained which is considerably more soluble in SO_2 than is $Hg_3(Sb_2F_{11})_2$. The Raman spectrum of the white solid is identical with that of $Hg_2(SbF_6)_2$, discussed in Chapter III. It is somewhat surprising that $Hg_3(Sb_2F_{11})_2$

is formed at all; in solution it would be expected that the Hg_3^{2+} cation would be oxidized much more readily than it actually is by the SbF_5 present in the $Sb_2F_{11}^-$ anion. Another problem associated with the use of SbF_5 is the insolubility of the reduced product, SbF_3, in sulphur dioxide. This presents no problem if the reaction product is itself soluble, but if it is insoluble separation from SbF_3 is impracticable.

The yellow colour reported by Meyer and Schram (62) when Hg is dissolved in HSO_3F is due to the Hg_3^{2+} ion. The Raman spectrum of the solution shows the characteristic polarized peak at 113 cm^{-1}.

4.2.2 UV-VISIBLE SPECTRA

The UV-visible spectrum of a solution of Hg in HSO_3F shows a peak at 325 nm with an approximate extinction coefficient of 10^4, consistent with the absorption at 325 nm ascribed to Hg_3^{2+} in $Hg_3(AlCl_4)_2$ (67). The 325 nm peak in HSO_3F, however, disappears fairly quickly to be replaced by two peaks at 248 nm and 280 nm. The peak at 248 nm is due to the Hg_2^{2+} cation, while the peak at 280 nm is due to the reduction product of HSO_3F, sulphur dioxide. Clearly, the oxidation of Hg in HSO_3F proceeds according to the equations:

$$3Hg + 4HSO_3F \rightarrow Hg_3^{2+} + SO_2 + HF + H_3O^+ + 3SO_3F^-$$

$$2Hg_3^{2+} + 4HSO_3F \rightarrow 3Hg_2^{2+} + SO_2 + H_3O^+ + 3SO_3F^- + HF$$

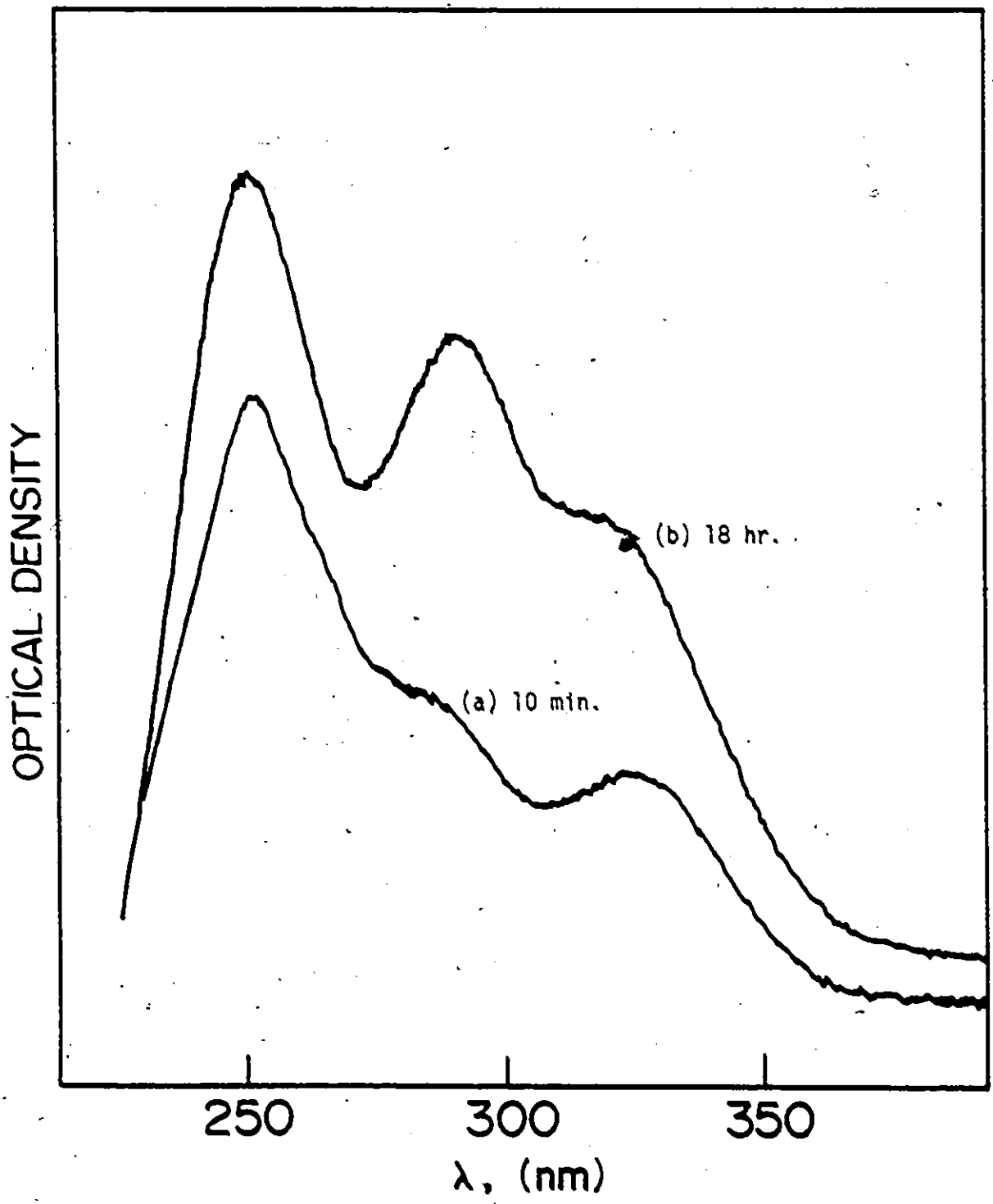

Figure 4.1 Time Dependent UV-Visible Spectrum of $Hg_3(Sb_2F_{11})_2$ in HSO_3F.

The absorption spectra of $Hg_3(AsF_6)_2$ and $Hg_3(Sb_2F_{11})_2$ in HSO_3F show an initial peak at 325 nm which quickly diminishes as the cations are oxidized to Hg_2^{2+}, to yield peaks at 248 nm and 280 nm, shown in Figure 4.1 for $Hg_3(Sb_2F_{11})_2$ in HSO_3F. The absorption spectra of the compounds in SO_2 is complicated by the fact that the very strong absorption of SO_2 at 280 nm tails into the visible and tends to obscure the peak at 325 nm. It is possible, however, to detect the peak before the sulphur dioxide absorption dominates the spectrum.

4.2.3 RAMAN SPECTRA

The Raman frequencies, with assignments, are listed in Table 4.1. In solution in liquid SO_2 or HSO_3F all the compounds gave, in addition to the solvent lines and expected anion frequencies, a single strong polarized band at 113 cm^{-1}. This is in accord with the single peak ($\nu_1(\sigma_g^+)$) that would be expected for a linear centrosymmetric ion of $D_{\infty h}$ symmetry. This band is at a much lower frequency than that observed for mercurous hexafluoroarsenate, but this is not surprising as the bond is expected to be weaker since each mercury atom in the Hg_3^{2+} ion has a lower formal positve charge (+2/3). In the limiting case of elemental mercury (zero charge) the bond length is 3.005Å (68).

The Raman spectra of the solid compounds are surprisingly different from the spectra of their solutions. Rather than the single line attributed to the Hg_3^{2+} symmetrical stretching mode, they show bands at 79 cm^{-1} and 140 cm^{-1} for $Hg_3(AsF_6)_2$, and at 83 cm^{-1} and 133 cm^{-1} for $Hg_3(Sb_2F_{11})_2$. These spectra are reproduced in Figure 4.2. The

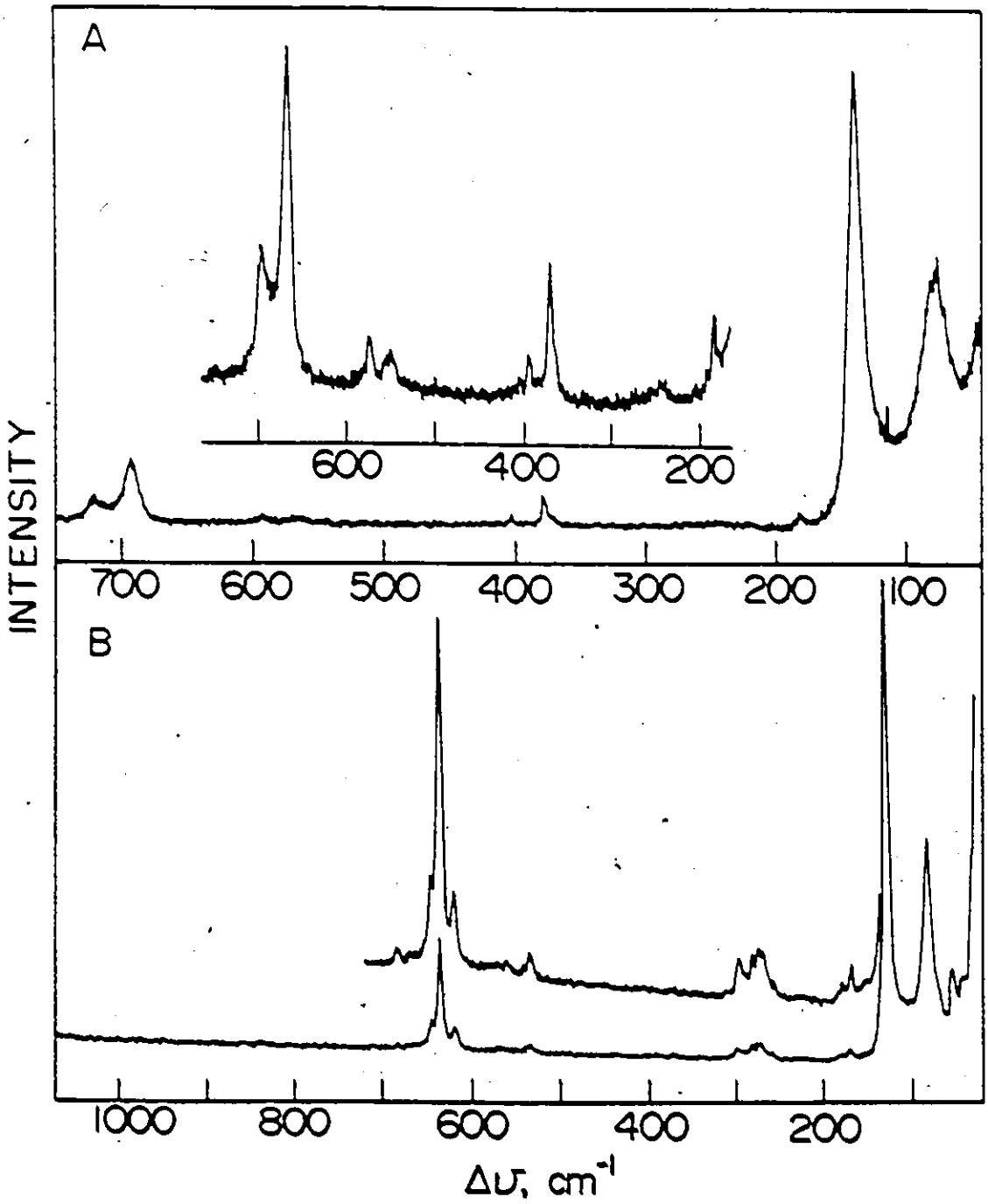

Figure 4.2 Raman Spectra of (A) $Hg_3(AsF_6)_2$ and (B) $Hg_3(Sb_2F_{11})_2$

TABLE 4.1

RAMAN SPECTRA OF Hg_3^{2+} COMPOUNDS

$Hg_3(AsF_6)_2$			Assignment
Solution	Solid		
	76 (37)		Hg...F-As
113 vs(p)	140(100)		$\nu_1(\sigma_g^+)$ Hg_3^{2+}
	179 (2)		(Hg_2^{2+} impurity?)
	241 (4)		
371w	372(7)		ν_5 (t_{2g})
	390(2)		
	554(1)		ν_2 (e_g) AsF_6^-
	577(1)		
675s	672(15)		ν_1 (a_{1g})
	698(7)		
$Hg_3(Sb_2F_{11})_2$		$Hg_3(SO_3F)_2$[a]	
Solution[b]	Solid		Assignment
	53(8)		
	83(40)		Hg...F-Sb
113(p)	133(100)	113(p)	$\nu_1(\sigma_g^+)$ Hg_3^{2+}
	171(1)		(Hg_2^{2+} impurity?)
	183(<1)		
	263(<1)		
	275(3)		
	279(3)		
	286(3)		$Sb_2F_{11}^-$
	301(2)		
	538(1)		
	622(4)		
	637(24)		
	647(5)		
	683(<1)		

(a) a concentrated solution of Hg in HSO_3F
(b) plus bands due to $Sb_2F_{11}^-$.

spectrum of $Hg_3(Sb_2F_{11})_2$ shows in addition a small peak at 53 cm^{-1} which must be assigned to a lattice mode. The bands at 140 cm^{-1} and 133 cm^{-1} in $Hg_3(AsF_6)_2$ and $Hg_3(Sb_2F_{11})_2$ respectively are assigned to ν_1, the symmetric Hg-Hg stretching mode. The spectra of both compounds may be compared with those of the mercurous analogues, in which the symmetric vibration for the Hg_2 groups is also shifted considerably upon going from a sulphur dioxide solution to the solid compound. Again it seems reasonable to suppose that the Hg_3^{2+} ion is solvated by the SO_2 molecule, probably by donation through oxygen. The fact that the solid compounds do not contain an SO_2 adduct molecule when the volatiles are removed under vacuum is understandable in view of the fact that Hg_3^{2+} would be expected to be less polarizing than Hg_2^{2+}.

Although the crystal structure of $Hg_3(AsF_6)_2$ shows some evidence for weak fluorine bridging (Section 4.3.2), it seems unlikely that the symmetry has been lowered sufficiently to allow interpretation of the AsF_6^- spectrum on the basis of pseudo C_{4v} symmetry. The characteristic ν_8 vibration arising from an AsF_6^- anion of pseudo C_{4v} symmetry is absent in the Raman spectrum. This frequency is also absent in the spectrum of $Hg_2(AsF_6)_2.SO_2$ (Section 3.2.2). A more reasonable explanation for the observation of six bands in the AsF_6^- region, rather than the three (a_{1g}, e_g, t_{2g}) that would be expected for an ionic hexafluoroarsenate, is factor group splitting. Each Raman active band of an octahedral anion in a site of symmetry C_1 would be split into two bands, one A_g and one B_g, in the space group $P2_1/c(C_{2h}^5)$. This treatment is in accord with the observed spectrum of $Hg_3(AsF_6)_2$, in which three pairs of bands are observed. The most intense band of each pair can be assigned to the symmetric A_g mode,

while the weaker can be assigned to the antisymmetric B_g mode. The band at 79 cm^{-1} in the spectrum of $Hg_3(AsF_6)_2$ might in principle arise from factor group splitting. Because there are two formula units per unit cell (Z=2) in $Hg_3(AsF_6)_2$, a factor group splitting of the Hg_3^{2+} symmetrical stretch is expected. The correlation diagram is shown in Table 4.2, and shows that splitting of the symmetrical Raman frequency into two bands is expected. However, the splitting of 61 cm^{-1} seems very large and, if correct, implies an unexpectedly strong coupling between the Hg_3^{2+} ions. Since the space group of $Hg_3(Sb_2F_{11})_2$ is not known, no prediction can be made about factor group splitting of the Hg-Hg stretching frequency. Alternatively, the low frequency band in both $Hg_3(AsF_6)_2$ and $Hg_3(Sb_2F_{11})_2$ might be due to a weak Hg...F interaction.

The crystal structure of $Hg_3(AlCl_4)_2$ shows a relatively short Hg-Cl distance of 2.54Å. The Raman spectrum of crystalline $Hg_3(AlCl_4)_2$ is very similar to that of $Hg_3(AsF_6)_2$, with two strong low frequency lines at 93 cm^{-1} and 123 cm^{-1}. These were assigned by the authors to the symmetric and antisymmetric vibrations of the Hg_3 group on the basis that the Hg_3 group is not linear but has a Hg-Hg-Hg bond angle of 174°. The authors note, however, that the antisymmetric vibration appears to be much more intense than would be expected for the slight deviation from linearity. It seems unlikely that their assignment is correct, particularly in view of the fact that the Hg_3 group in $Hg_3(AsF_6)_2$ is constrained by symmetry to be linear and centrosymmetric, and yet the Raman spectrum still shows the two bands in the low frequency region. An alternative assignment would be that the band at 93 cm^{-1} is due to the Hg-Cl-Al bending mode and the band at 123 cm^{-1} is due to the symmetric Hg-Hg stretching mode. Because

TABLE 4.2

CORRELATION DIAGRAMS FOR THE Hg_3^{2+} ION IN $Hg_3(AsF_6)_2$ AND $Hg_3(AlCl_4)_2$

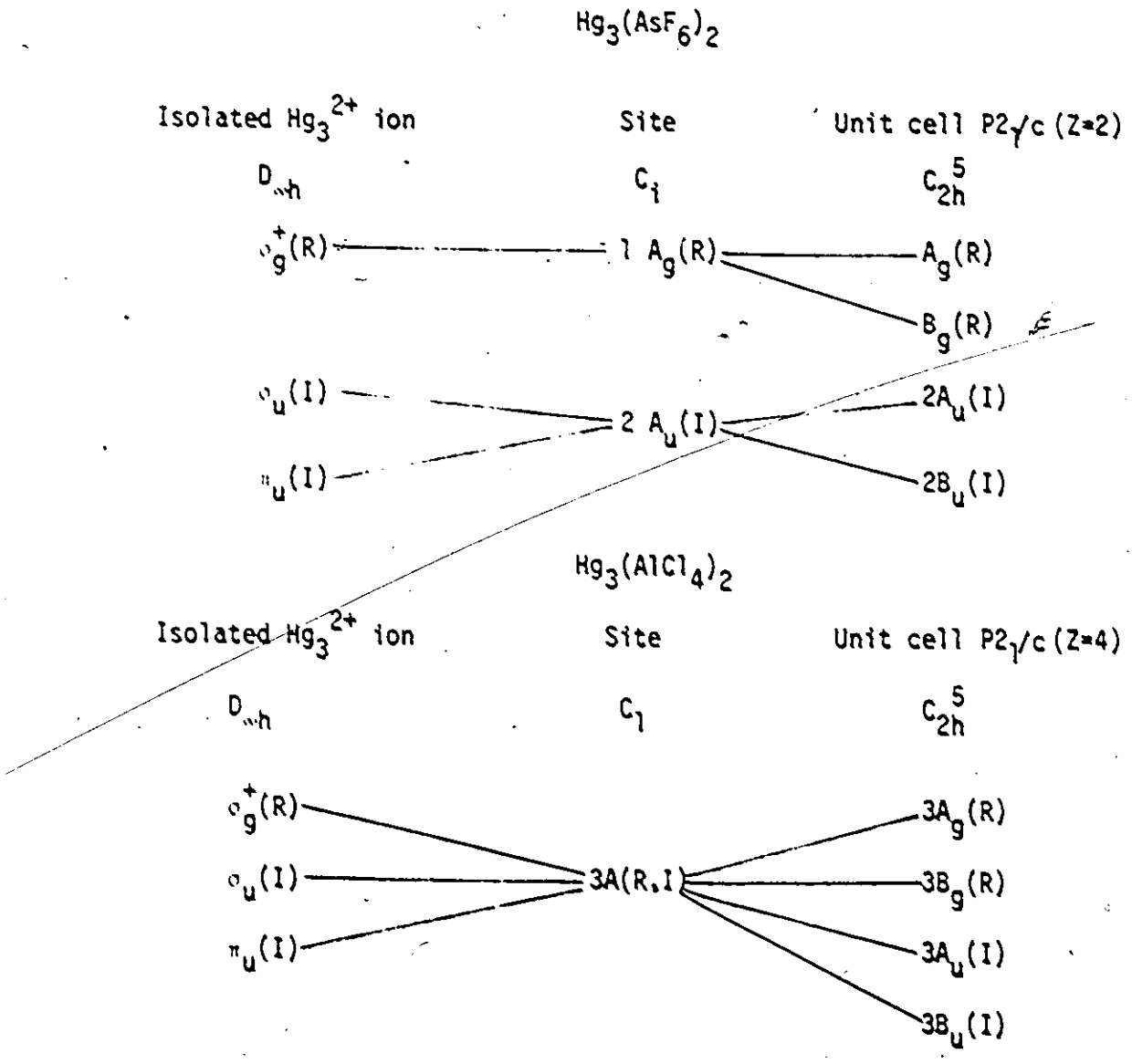

(R) = Raman active

(I) = Infrared active

the authors have assigned bands at 225 cm^{-1} and 242 cm^{-1} to the Hg-Cl stretching frequencies, the band at 93 cm^{-1} would therefore be due to the bending mode, although this band is much more intense than would be expected. One would expect factor group splitting for the Hg_3 group in $Hg_3(AlCl_4)_2$. Table 4.2 shows that the site symmetry of the Hg_3^{2+} ion in $Hg_3(AlCl_4)_2$ is C_1 and 3 Raman active frequencies are predicted, which would be split into 6 Raman active bands under the factorgroup symmetry C_{2h}. Only two bands are observed and again the splitting seems rather large. A more reasonable explanation for the observation of the two bands in $Hg_3(AlCl_4)_2$ is that under site symmetry (C_1) for the Hg_3^{2+} cation the asymmetric stretch becomes Raman active. It should be noted that although the actual symmetry of the Hg_3^{2+} ion in $Hg_3(AlCl_4)_2$ is C_{2v}, the bond lengths are equal and the angle (174°) is sufficiently close to 180° to assume $D_{\infty h}$ symmetry.

4.3 THE STRUCTURE OF $Hg_3(AsF_6)_2$

4.3.1 SOLUTION AND REFINEMENT

Precession photographs showed the characteristic absences of the space group $P2_1/c$(no. 14, C_{2h}^5). The crystal data are given in Table 4.3. The procedure used for data collection is given in Section 2.3.2. The crystal had very poorly defined faces and an irregular block (side = 0.12 mm) was used for the collection of a unique quadrant of 636 reflections ($2\theta < 50°$) with intensities greater than 3 times the standard deviation based on counting statistics.

One of the mercury atoms of the Hg_3 unit was found to lie at the origin (0,0,0). The positions of the other four mercury atoms in the unit cell were found by inspecting the three-dimensional Patterson function. Two cycles of full matrix least-squares refinement with isotropic temperature factors gave a conventional agreement index $R_1 = (\Sigma\Delta/\Sigma|F_o|$

TABLE 4.3

CRYSTAL DATA FOR $Hg_3(AsF_6)_2$

Formula Weight	979.7
System	monoclinic
Conditions limiting possible reflections	hoℓ: ℓ = 2n oko: k = 2n
Space Group	$P2_1/c$ (no. 14, C_{2h}^5)
Calculated Density	5.67 g/cm^3
Cell Constants	
a	5.981 (5)Å
b	8.551 (6)Å
c	11.282(10)Å
β	91.16 (7)°
Number of formula units/ unit cell	2
Cell Volume	577.1 Å^3
Linear absorption coefficient	497 cm^{-1}
μR	3.5

where $\Delta = ||F_o| - |F_c||$) of 0.32. The 636 reflections were used together with the phases determined from the mercury atoms to calculate a three-dimensional Fourier map which revealed the positions of the arsenic and fluorine atoms. These, when included in another four cycles of least-squares refinement, varying positional and anisotropic temperature factors for mercury and arsenic reduced R_1 to 0.111 while the weighted agreement factor R_2 ($= \Sigma w\Delta^2/\Sigma wF_o^2)^{\frac{1}{2}}$) was 0.148 with unit weights. An empirical weighting scheme of the form $\sqrt{w} = (A+BF_o + CF_o^2)^{-1}$ was calculated subject to the condition that $\Sigma w\Delta^2$ be approximately independent of $|F_o|$ and $\sin\theta/\lambda$. Least squares refinement converged at $R_1 = 0.106$ and $R_2 = 0.145$. The values of the constant A, B and C in the weighting expression were 21.11, - 0.3043 and 0.0160 respectively. A final difference Fourier showed no significant features with the largest peak height being 1.4e/Å^3. The majority of the highest peaks were concentrated within 2Å of the mercury atoms.

4.3.2 DESCRIPTION OF THE STRUCTURE

The structural parameters for $Hg_3(AsF_6)_2$ are listed in Table 4.4. The configuration of the $Hg_3(AsF_6)_2$ molecule is shown in Figure 4.3, while Table 4.5 lists the bond lengths and bond angles. The packing of the ions in the unit cell is shown in Figure 4.4. The observed and calculated structure factors are listed in Table 4.6.

To a first approximation the structure may be described as consisting of discrete linear symmetrical Hg_3^{2+} ions and octahedral AsF_6^- anions. The Hg-Hg bond length is 2.552(5)Å, which agrees well with the value of 2.56Å reported for $Hg_3(AlCl_4)_2$ (66). The central

TABLE 4.4

STRUCTURAL PARAMETERS[a] FOR $Hg_3(AsF_6)_2$

Parameter x 10^4	Hg(1)	Hg(2)	As(1)
x	0	2395(5)	2997(10)
y	0	2302(3)	6431(6)
z	0	705(3)	1722(5)
U_{11}	441(17)	567(16)	492(29)
U_{22}	514(18)	671(17)	497(31)
U_{33}	588(19)	791(18)	513(29)
U_{12}	-30(TS)	-110(12)	- 3(23)
U_{13}	62(13)	15(12)	112(22)
U_{23}	-24(13)	- 93(13)	48(22)

	x(x10^3)	y(x10^3)	z(x10^3)	B(x10^3)
F(1)	169(8)	806(6)	216(4)	98(13)
F(2)	316(7)	722(5)	34(3)	78(10)
F(3)	55(15)	551(10)	146(7)	171(28)
F(4)	306(10)	575(7)	311(4)	115(16)
F(5)	556(9)	696(6)	203(4)	98(13)
F(6)	412(9)	474(6)	114(4)	102(14)

[a] x, y, and z are fractional atomic coordinates. The isotropic temperature factor B is from the expression $\exp[-B(\sin^2\theta)/\lambda^2]$ and the form of the anisotropic thermal ellipsoid is $\exp[-2\pi^2(h^2a^{*2}U_{11} + \ldots. + 2hka^*b^*U_{12} + \ldots.)]$. Least-squares-estimated standard errors in the least significant digits are given in parentheses.

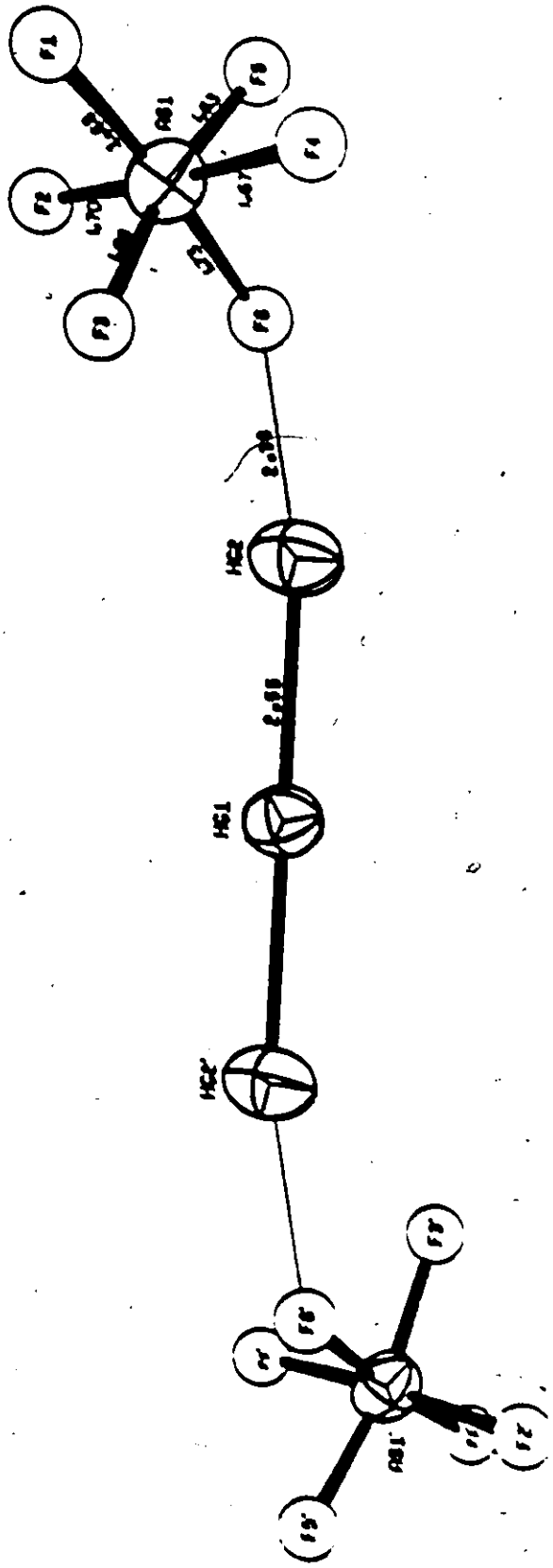

Figure 4.3 Configuration of the $Hg_3(AsF_6)_2$ molecule.

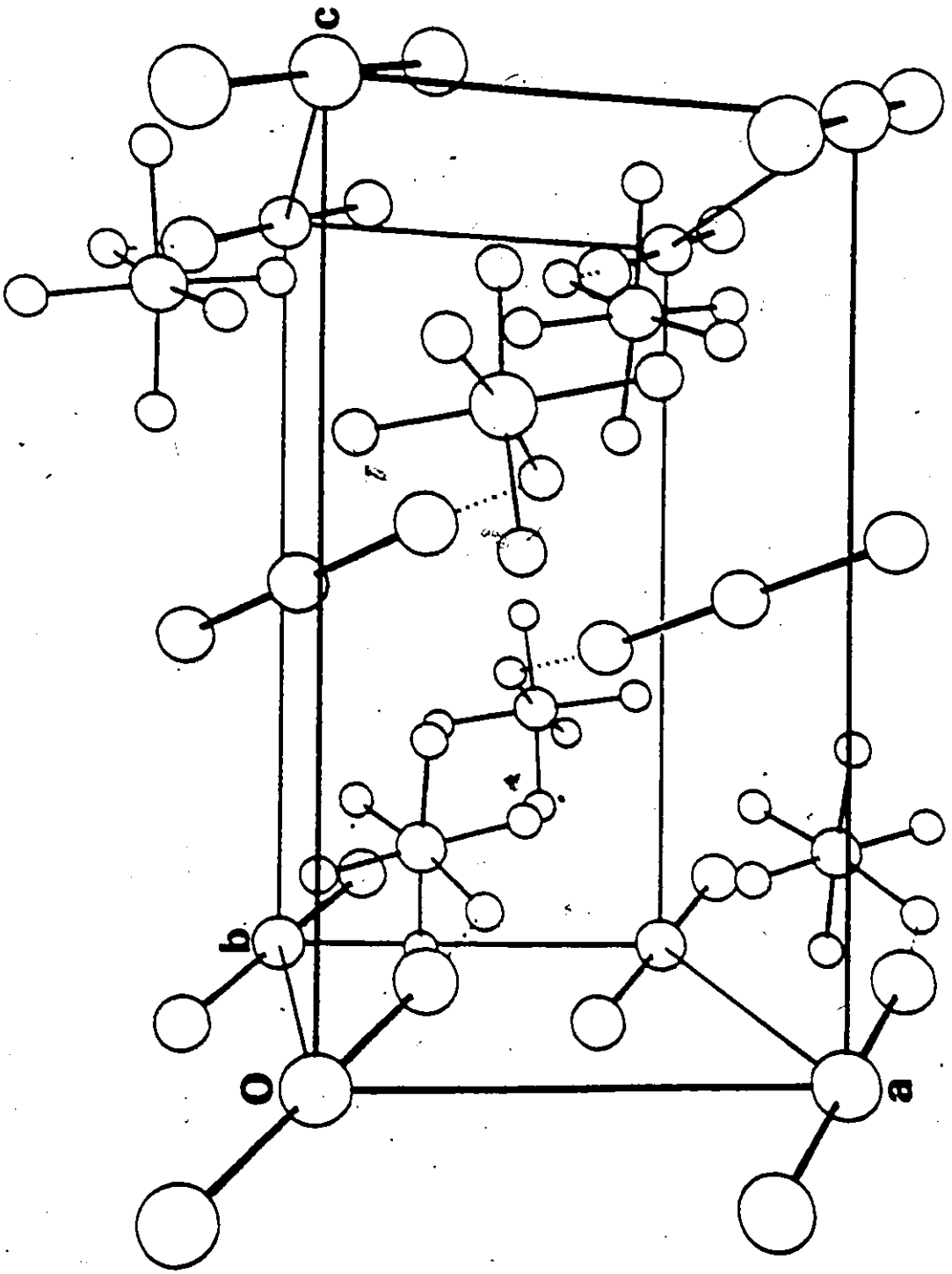

Figure 4.4 A Perspective Illustration of the Packing of Ions in $Hg_3(AsF_6)_2$.

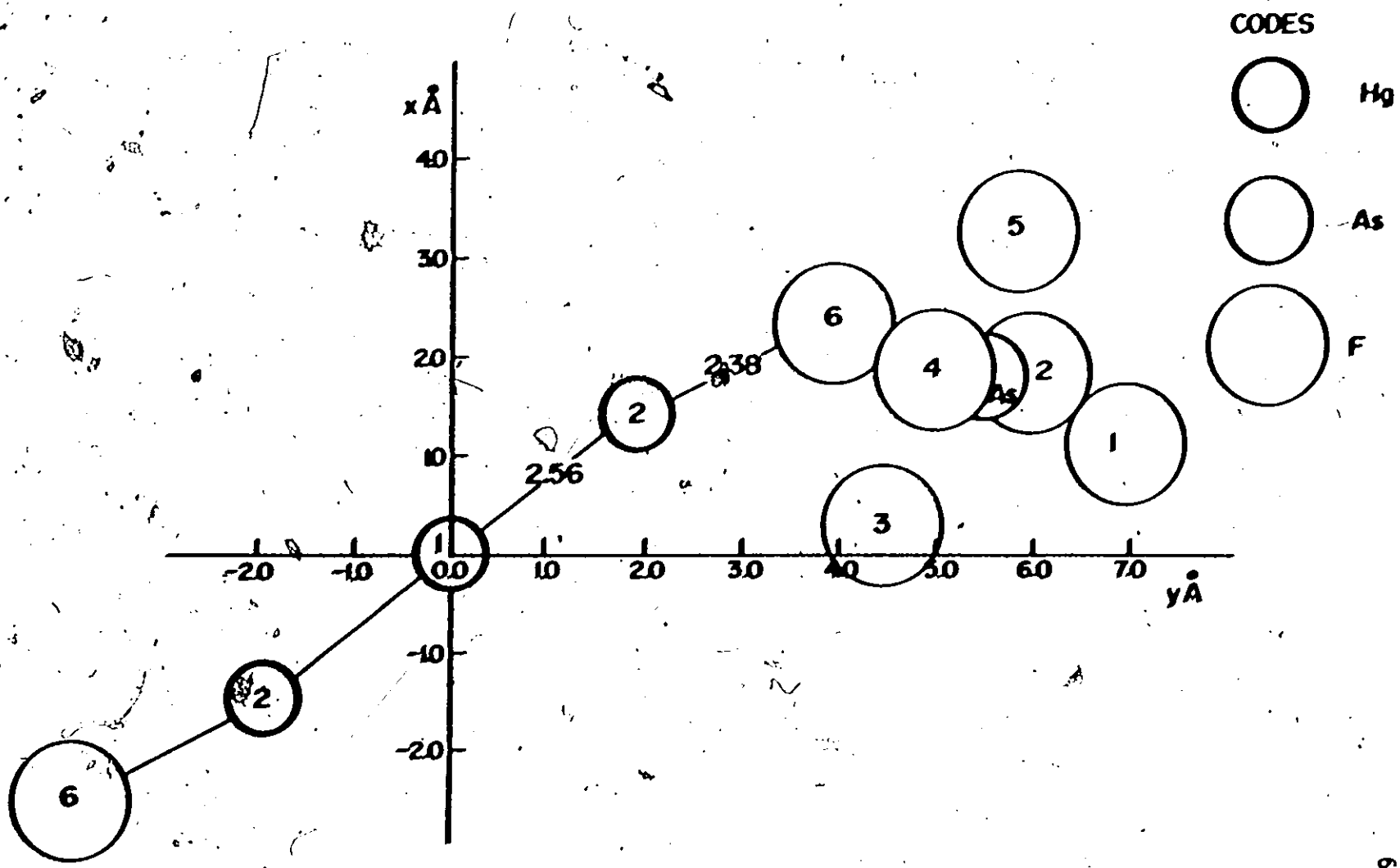

Figure 4.5 Projection of Asymmetric Unit of $Hg_3(AsF_6)_2$ Showing Hg...F Contact.

TABLE 4.5

BOND DISTANCES AND BOND ANGLES IN

$Hg_3(AsF_6)_2$

Atoms	Distance (Å)
Hg(1) - Hg(2)	2.552(5)
Hg(2) - F(6)	2.38 (5)
Hg(1) - F(4)	2.91(9)
Hg(2) - F(2)	2.96(7)
Hg(2) - F(5)	2.83(8)
As(1) - F(1)	1.68(5)
As(1) - F(2)	1.70(4)
As(1) - F(3)	1.68(8)
As(1) - F(4)	1.67(5)
As(1) - F(5)	1.63(6)
As(1) - F(6)	1.73(5)
ANGLES SUBTENDED AT Hg(2)	(DEG.)
Hg(1) - F(6)	168.9(1.2)
ANGLES SUBTENDED AT ARSENIC	(DEG.)
F(6) - F(1)	173.7(2.3)
F(6) - F(4)	93.6(2.6)
F(6) - F(2)	87.5(2.1)
F(6) - F(3)	83.5(3.4)
F(6) - F(5)	86.4(2.5)
F(1) - F(4)	90.8(2.5)
F(1) - F(2)	88.6(2.1)
F(1) - F(3)	91.8(3.4)
F(1) - F(5)	98.6(2.4)
F(4) - F(2)	174.6(2.5)
F(4) - F(3)	90.4(3.6)
F(4) - F(5)	83.9(2.6)
F(2) - F(3)	95.0(3.1)
F(2) - F(5)	90.9(2.2)
F(3) - F(5)	168.1(3.4)

mercury of the Hg_3 groups lies on a two-fold axis and the cation must therefore be linear and symmetrical. In $Hg_3(AlCl_4)_2$ the Hg_3 group deviates slightly from linearity with a bond angle of 174°, and the two Hg-Hg bond lengths are equal, although they are not required by symmetry to be so. The terminal mercury-fluorine distance is 2.38(5)Å, which is intermediate between the approximate values of 2.10Å and 2.46Å which may be estimated for covalent and ionic bonds respectively. This indicates that the mercury-fluorine interaction has some covalent character. Figure 4.5 shows a projection of the asymmetric unit of $Hg_3(AsF_6)_2$ which illustrates the Hg-F interaction. The Hg-Hg...F bond angle of 170° is also consistent with the idea that the terminal mercury atoms are forming two bonds with more or less covalent character; one to the other mercury atom and one to the fluorine atom. Such covalent bonds with mercury are expected to have an ideal bond angle of 180°. The Hg...F bridge appears to slightly distort the AsF_6^-. The As-F(6) distance is 1.73Å whereas the average of the remaining distances is 1.67Å, the same as the mean As-F distances reported previously (69) for AsF_6^-. It is noteworthy that the average bond angle between F(6) and its neighbours is 87.8° whereas the average bond angle between F(1) and its neighbours is 92.5°. It is reasonable to suppose that because a lone pair on F(6) is used to form a bond with the mercury atom, the As-F(6) bond becomes more polar, i.e., the bonding electron pair moves further away from the arsenic and the bond angles around arsenic adjust themselves so as to minimize bond-bond repulsions. This argument must be used with caution because the bond lengths and angles, when the error limits are taken into consideration, are not significantly different.

One point worthy of note is that although $Hg_3(AlCl_4)_2$ is clearly more covalent than $Hg_3(AsF_6)_2$ (AsF_6^- is a weaker base than $AlCl_4^-$), the bond lengths of the Hg_3 group in the two compounds are virtually the same. The same has been noted for the mercurous halides; the bond lengths are the same within experimental error, even though Hg_2F_2 is much more ionic than Hg_2Cl_2, Hg_2Br_2 and Hg_2I_2. The Raman frequencies vary over a wide range, however, depending on the identity of the anion.

Table 4.6

Observed and Calculated Structure Factors for $Hg_3(AsF_6)_2$

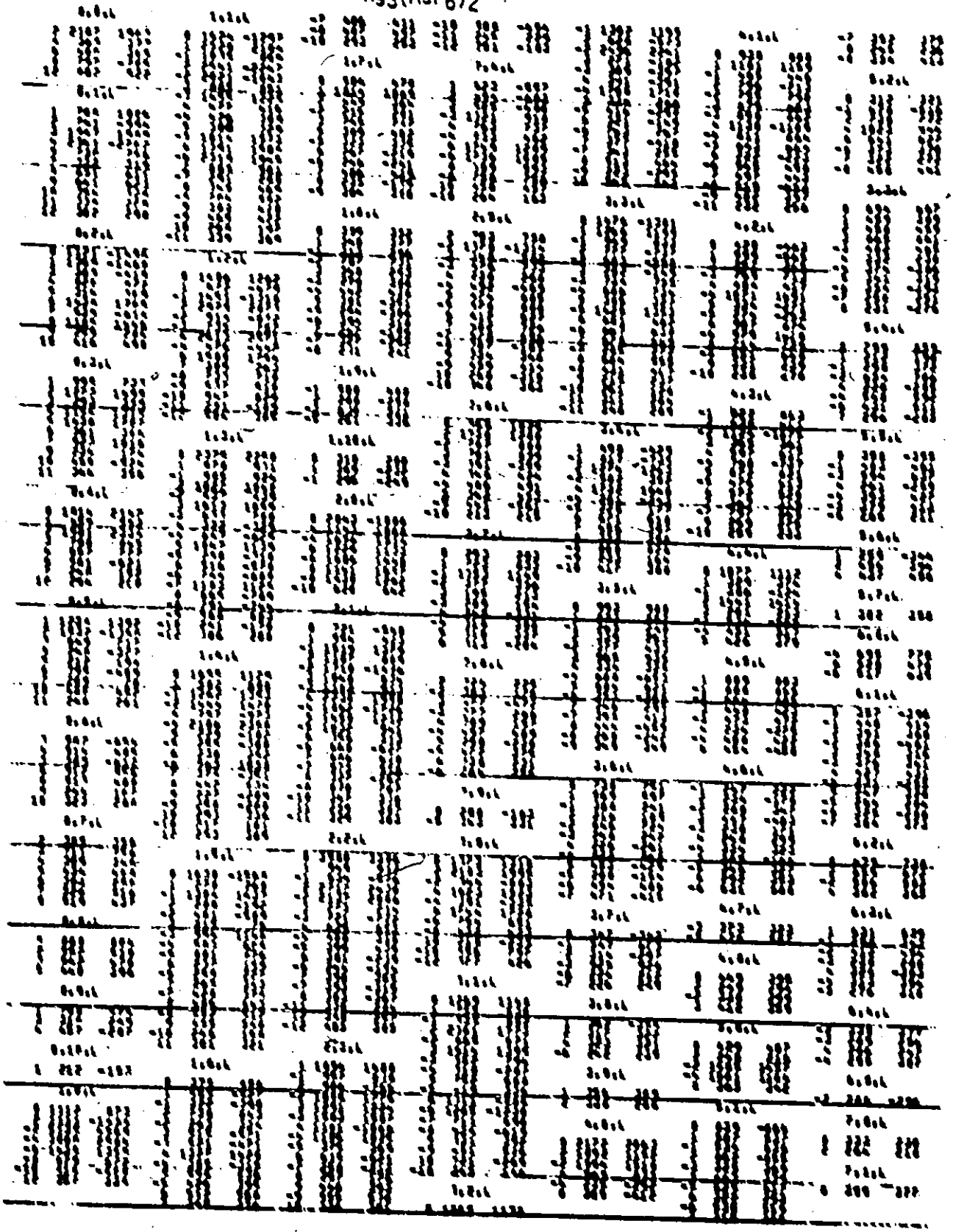

CHAPTER V

THE Hg_4^{2+} CATION

5.1 INTRODUCTION

The previous chapter reported the preparation of the Hg_3^{2+} cation in the arsenic pentafluoride/SO_2 system. It is possible to prepare polycations of mercury in still lower formal positive oxidation states and this chapter reports the preparation of the Hg_4^{2+} cation. The cation, isolated as the solid $Hg_4(AsF_6)_2$, was identified by analytical and spectral methods. An X-ray crystallographic study of $Hg_4(AsF_6)_2$ showed that the cation is very nearly linear. The equilibria in the sulphur dioxide solvent system are discussed.

5.2 THE Hg_4^{2+} CATION

5.2.1 PREPARATION AND CHARACTERIZATION OF $Hg_4(AsF_6)_2$

As described in Chapter II, oxidation of mercury by arsenic pentafluoride in the mole ratio 4:3 in liquid sulphur dioxide results in a deep red solution in equilibrium with an insoluble golden compound. Filtration, followed by rapid removal of volatiles, yielded a grey black solid, the analysis of which was consistent with a mixture of the previously identified $Hg_3(AsF_6)_2$, and a compound containing mercury in a lower formal positive oxidation state, presumably $Hg_4(AsF_6)_2$.

Very slow removal of SO_2, however, yielded two distinct types of crystals: large yellow crystals which were isolated and identified as $Hg_3(AsF_6)_2$ by Raman and UV-Visible spectra; and dark, red-black needle shaped crystals, the analysis of which was in excellent agreement with the composition $Hg_4(AsF_6)_2$. Crystals of the latter type were hand-picked from the mixture in a dry box equipped with a microscope. Contrary to the behaviour of the other mercury polycations, the Hg_4^{2+} cation cannot be prepared in the absence of the gold compound and $Hg_3(AsF_6)_2$. Upon further oxidation with AsF_5, the red colour and insoluble gold coloured crystals persist until the mole ratio $Hg:AsF_5$ of 1:1 is reached, at which point a light yellow solution is obtained. After removal of volatiles a Raman spectral analysis demonstrated that this compound was $Hg_3(AsF_6)_2$, with no detectable impurities. The reaction of mercury with AsF_5 to give $Hg_4(AsF_6)_2$ can be summarized as follows:

$$4Hg + 3AsF_5 \rightarrow Hg_4(AsF_6)_2 + AsF_3$$

$$\downarrow\uparrow$$

$$Hg_3(AsF_6)_2 + Hg_{2.86}AsF_6$$

The red solution may be filtered until it is free from the insoluble gold compound. The resultant mixture in SO_2 then showed two peaks in the UV-visible spectrum: one at 326 nm which may be assigned to Hg_3^{2+}; and the other at 380 nm, which may be assigned to the Hg_4^{2+} cation. Unfortunately the peak due to the Hg_3^{2+} cation is partially obscured by the very strong absorption of SO_2. Any attempt to use HSO_3F as a

solvent resulted in the very rapid oxidation of Hg_4^{2+} to Hg_3^{2+} and Hg_2^{2+}, as discussed in Section 4.2.1.

Although it was not possible to obtain Raman data on solid $Hg_4(AsF_6)_2$, because of the dark colour, a Raman spectrum of the red solution was obtained using the Rotating Raman cell technique described in Chapter II. It was observed that the red colour disappeared upon cooling the solution, and concurrent with the disappearance of the red colour due to the Hg_4^{2+} cation golden crystals were deposited from the solution. Clearly, the Hg_4^{2+} cation disproportionates as the temperature is lowered. The temperature dependent Raman spectrum of a solution of Hg_3^{2+}/Hg_4^{2+} is shown in Figure 5.1.

Unfortunately, the spectrum is of poor quality due to the deep red colour of the solution and the fact that the peaks fall close to the exciting frequency. At room temperature two distinct peaks are observed. The peak at 113 cm^{-1}, which appears as a weak shoulder, can be assigned to $\nu_1(\sigma_g^+)$ of the Hg_3^{2+} cation. The broad peak apparently centered at 85 cm^{-1} is shown at lower temperatures, where better resolution is possible, to consist of two peaks at 79 cm^{-1} and 95 cm^{-1}. For a linear centrosymmetric molecule of $D_{\infty h}$ symmetry, five modes are expected: $2\sigma_g^+(R) + \sigma_u^+(I) + \pi_g(R) + \pi_u(I)$ with the three symmetric modes Raman active and the two asymmetric modes infrared active. The bands at 79 cm^{-1} and 95 cm^{-1} are assigned to $\nu_1(\sigma_g^+)$ and $\nu_2(\sigma_g^+)$ respectively, the two Raman active symmetrical Hg-Hg stretching vibrations that would be expected for a linear centrosymmetric Hg_4^{2+} ion. The bending mode, $\nu_4(\pi_g)$, presumably occurs at a much lower frequency and is obscured by

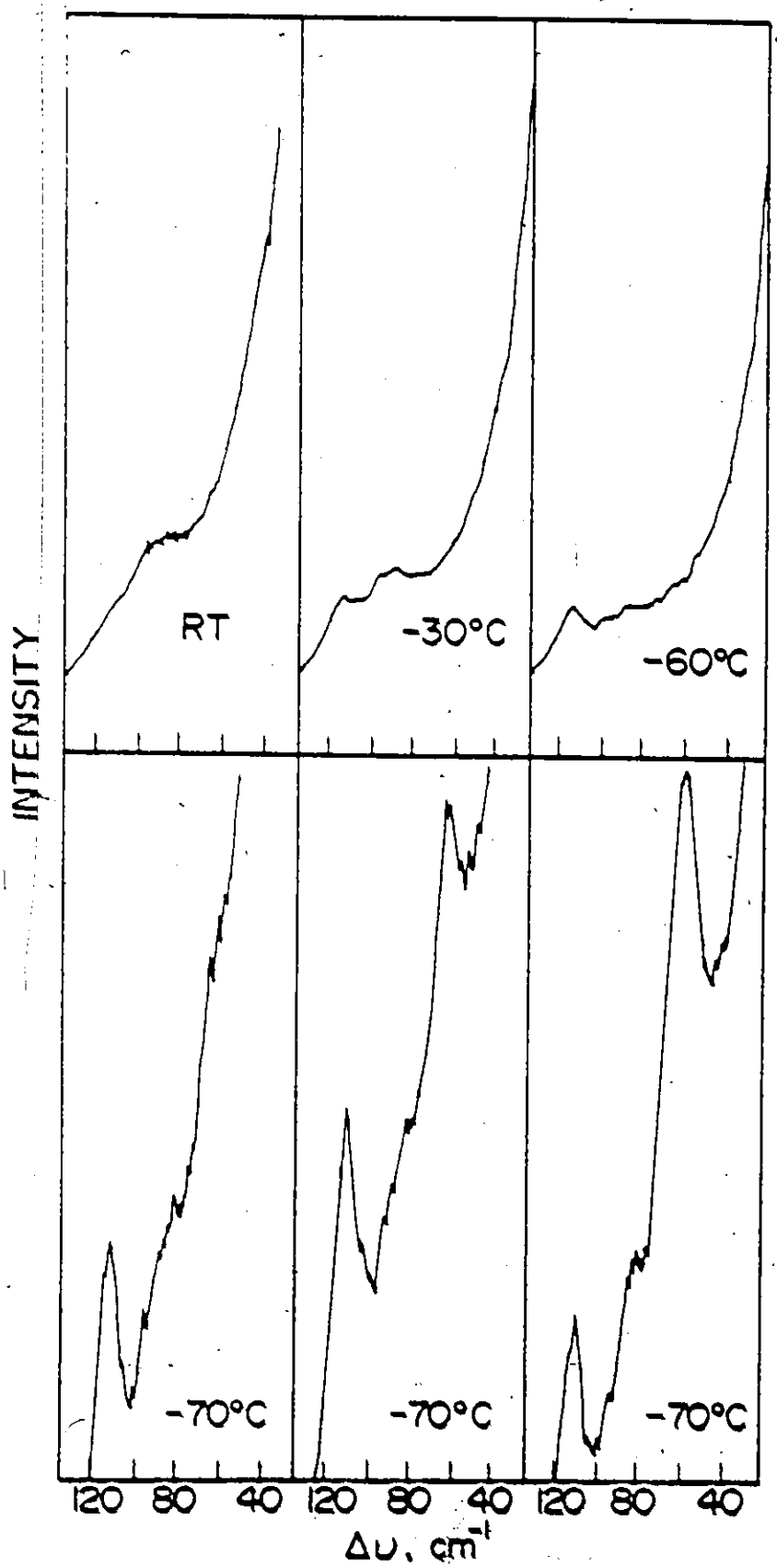

Figure 5.1 Temperature Dependent Raman Spectra of an Equilibrium Mixture of Hg_3^{2+} and Hg_4^{2+} in SO_2

the exciting line. As the temperature of the solution is lowered, the disappearance of the red colour is concomitant with a decrease in intensity of the bands at 79 cm^{-1} and 95 cm^{-1}, and an increase in intensity of the band at 113 cm^{-1} due to the Hg_3^{2+} cation. As the temperature reaches -40°C, precipitation of the insoluble golden compound can be seen. Clearly, the Hg_4^{2+} cation disproportionates at low temperatures to Hg_3^{2+} and the gold compound, which has been identified as $Hg_{2.86}AsF_6$, and is discussed in the following chapter. The disproportionation can be written in a simplified form as:

$$Hg_4^{2+} \rightarrow Hg_3^{2+} + Hg_{2.86}^{+}$$

This equation has been left unbalanced. The disproportionation of $Hg_4(AsF_6)_2$ is completely reversible, the characteristic red solution in equilibrium with $Hg_{2.86}AsF_6$ being formed as the temperature is raised. The $Hg_{2.86}AsF_6$ completely disappears over the period of an hour to yield only the red solution in the absence of any insoluble materials. The reasons for the most interesting reversible disproportionation of $Hg_4(AsF_6)_2$ can only be speculated upon. There is no doubt that the subtle differences in solvation energies of the various species in SO_2 plays an important role.

If the solution is kept at ~-72°C for 15 min. a new peak at 63 cm^{-1} appears and the solution becomes a brilliant deep blue colour as the sulphur dioxide begins to freeze. (f.p. SO_2 is -72°C). The peak, whose intensity increases with time, cannot be assigned with any

certainty but it is clear that it is due to neither Hg_3^{2+} nor Hg_4^{2+}. The blue colour cannot be due to a radical species as no esr signal was detected from the frozen solution, or indeed over the entire temperature range. The blue colour disappears very rapidly as the solution is warmed, persisting only until ~-70°C, just above the freezing point of SO_2. Therefore, it appears reasonable to consider the possibility that the peak at 63 cm^{-1} may be due to the same species that gives rise to the intense blue colour at low temperatures. It is possible, although in the absence of additional information it must be regarded as speculative, that this species is the Hg_5^{2+} cation. Clearly, the species causing the blue colour is dependent upon the presence of the Hg_4^{2+} cation; no colour change is observed when one freezes a solution of $Hg_3(AsF_6)_2$.

5.2.2 ATTEMPTED PREPARATION OF $Hg_4(Sb_2F_{11})_2$

Evidence for the Hg_4^{2+} ion has not been obtained in systems other than AsF_5/SO_2. Torsi and Mamantov's (57) study of the electrochemical reduction of $HgCl_2$ in $AlCl_3$ suggested that no species in an oxidation state lower than Hg_3^{2+} was present in this system. The preparation of $Hg_4(Sb_2F_{11})_2$ by reduction of $Hg_3(Sb_2F_{11})_2$ with elemental mercury was attempted, and although the mercury was oxidized and a very slightly soluble light yellow product precipitated from the solution, the Raman spectrum of this solid was identical with that of the starting material, $Hg_3(Sb_2F_{11})_2$ (Figure 4.2). The apparent failure to isolate any product other than $Hg_3(Sb_2F_{11})_2$ is puzzling; presumably decomposition could be taking place in the Raman beam although the

spectra were run at liquid nitrogen temperatures and no decomposition was apparent. Clearly, the system requires further study.

The presence of Hg_4^{2+}, or indeed of any species in oxidation states lower than Hg_3^{2+}, was not detected in any of the other systems studied.

5.3 THE CRYSTAL STRUCTURE OF $Hg_4(AsF_6)_2$

An x-ray crystallographic study of the compound $Hg_4(AsF_6)_2$ confirmed that the Hg_4^{2+} cation is nearly linear and centrosymmetric. The crystal used for the analysis was selected from a mixture of $Hg_3(AsF_6)_2$ and $Hg_4(AsF_6)_2$ grown by the slow crystallization of the red solution when Hg is oxidized by AsF_5 in the mole ratio 4:3. Although visually the crystals appeared to be well formed needles, precession photographs indicated that the great majority were not single. The crystal used for data collection was cut in a dry box. The crystal was an irregular cube (edge = 0.1 mm), and although not of good quality, was adequate to enable data to be collected.

5.3.1 SOLUTION AND REFINEMENT

The crystal was examined by the Precession method which showed absences characteristic to the space group $P2_1/c$ (no. 14, C_{2h}^5). The crystal data are listed in Table 5.1. Intensity data collected using a Syntex four-circle auto-diffractometer with MoK_α radiation (0.71069Å) were corrected for absorption assuming spherical geometry and used to calculate a three-dimensional Patterson function from which the coordinates

TABLE 5.1

Crystal Data for $Hg_4(AsF_6)_2$

Formula Weight	1180.2
System	Monoclinic
Conditions limiting possible reflections	hol: ℓ=2n oko: h=2n
Space Group	$P2_1/c$ (no. 14, C_{2h}^5)
Calculated Density	6.26 g/cm^3
Cell constants	
a	5.485(3)Å
b	11.623(8)Å
c	9.835(5)Å
β	92.11 (5)°
Number of formula units/ unit cell	2
Cell Volume	626.58Å^3
Linear absorption coefficient	555.4 cm^{-1}
μR	2.8

for the two mercury atoms in the asymmetric unit were found. Two cycles of least-squares refinement gave a conventional agreement index of $R_1 = 0.28$. A subsequent three-dimensional Fourier map revealed the arsenic atom. The fluorine atoms were located only after an additional two cycles of least-squares refinement with isotropic temperature factors for all heavy atoms. A further three cycles with anisotropic temperature factors for mercury and isotropic temperature factors for arsenic and fluorine converged at $R_1 = 0.138$ with a weighted agreement factor $R_2 = 0.159$. Unit weights were used as $\sum w\Delta^2$ was approximately independent of $|F_o|$ and $\sin\theta/\lambda$. The fluorine atoms are very poorly defined, with large errors on bond lengths and angles. This is due, no doubt, to the fact that only 213 unique reflections with $I>3\sigma$ were used to refine 47 variables. Because of the poor crystal quality it is doubtful that even a more accurate absorption correction would significantly improve the definition of the AsF_6^- octahedron.

5.3.2 DESCRIPTION OF THE STRUCTURE

The structural parameters for $Hg_4(AsF_6)_2$ are listed in Table 5.2. Table 5.3 lists the bond lengths and angles while Figure 5.2 shows the configuration of the Hg_4^{2+} ion. Figure 5.3 shows a projection of the molecules in the unit cell. Although not constrained by symmetry to be so, the Hg_4^{2+} ion is very nearly linear, with a Hg-Hg-Hg bond angle of 176° and a trans-configuration. Thus the expected linear configuration around mercury is maintained. The

TABLE 5.2

Structural Parameters[a] for $Hg_4(AsF_6)_2$

Parameter x 10^4	Hg(1)	Hg(2)
x	-31 (26)	-107 (30)
y	822 (9)	254 (10)
z	3868 (11)	1337 (12)
U_{11}	810(112)	687(101)
U_{22}	259 (79)	421 (86)
U_{33}	335 (73)	208 (65)
U_{12}	-20 (84)	-41 (73)
U_{13}	5 (63)	-89 (57)
U_{23}	-142 (63)	-79 (55)

	10^3x	10^3y	10^3z	$10^3B(Å^2)$
As(1)	500 (5)	289 (3)	174 (3)	22 (7)
F(1)	766(15)	311 (8)	283 (8)	1
F(2)	275(19)	277 (9)	57 (9)	16
F(3)	672(64)	286(30)	83(29)	180
F(4)	365(54)	249(20)	279(27)	141
F(5)	579(20)	134(10)	237(10)	30
F(6)	516(42)	448(16)	147(18)	103

a. x,y and z are fractional atomic coordinates. The isotropic temperature factor B is from the expression $\exp[-B(\sin^2\theta/\lambda^2)$ and the form of the anisotropic thermal ellipsoid is $\exp[-2\pi^2(h^2a^{*2}U_{11} + \ldots + 2hka^*b^*U_{12} + \ldots)]$. Least-squares estimated standard errors in the least significant figures are given in parentheses.

TABLE 5.3

Bond Distances and Angles in $Hg_4(AsF_6)_2$

Distances, Å

Hg(1) - Hg(2)	2.574(12)	As(1) - F(1)	1.80(8)
Hg(2) - Hg(2)'	2.703(12)	As(1) - F(2)	1.66(10)
Hg(1) - F(5)	2.74 (10)	As(1) - F(3)	1.32(33)
Hg(1) - F(2)	2.76 (10)	As(1) - F(4)	1.37(28)
		As(1) - F(5)	1.95(11)
		As(1) - F(6)	1.87(19)

Angles Subtended by Hg(1), Deg.

Hg(2) - F(5)	63.5 (2.2)
Hg(2) - F(2)	136.8 (2.1)

Angles Subtended by Hg(2), Deg.

Hg(1) - Hg(2)'	175.9(8)

Angles Subtended by As(1), Deg.

F(1) - F(2)	172.5(4.4)	F(2) - F(6)	91.0 (7.2)
F(1) - F(3)	79.8(13.8)	F(3) - F(4)	156.9 (18.3)
F(1) - F(4)	92.7(11.9)	F(3) - F(5)	92.3 (15.2)
F(1) - F(5)	77.2(4.5)	F(3) - F(6)	83.6 (16.5)
F(1) - F(6)	84.4(7.2)	F(4) - F(5)	64.6 (11.1)
F(2) - F(3)	93.8(13.9)	F(4) - F(6)	117.7 (12.0)
F(2) - F(4)	94.7(12.2)	F(5) - F(6)	161.5 (7.3)
F(2) - F(5)	107.3(4.7)		

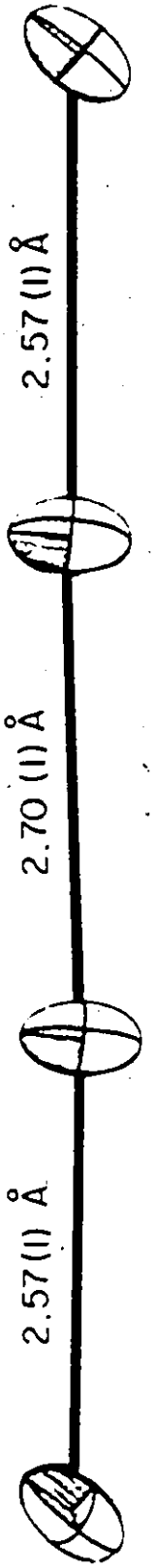

Figure 5.2 Configuration of the Hg_4^{2+} Ion

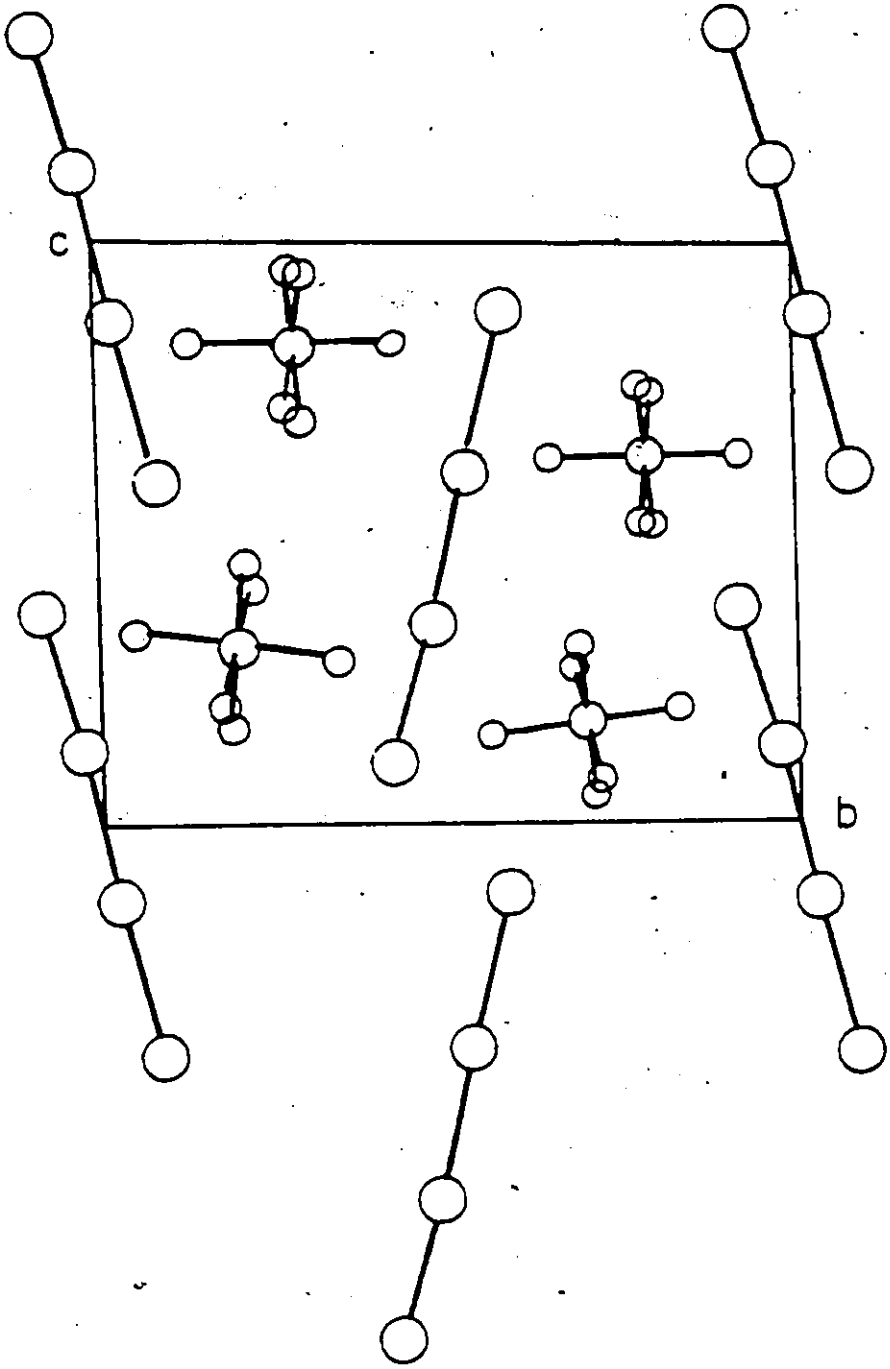

Figure 5.3 A View of the Unit Cell Contents of $Hg_4(AsF_6)_2$ (viewed down the a axis).

Table 5.4

Observed and Calculated Structure Factors for $Hg_4(AsF_6)_2$

0,3,L

2	430	-1067
4	4870	-4900
6	2051	1079

0,4,L

-2	690	-347
	661	-610
	691	266
	709	-714
-6	599	920
8	690	-361

0,5,L

0	2550	2374
1	1427	-1743
2	1122	1004
3	2232	-2003
4	1127	-1140
	790	910
-6	922	-408
7	1063	1236
8	2205	2218

0,6,L

0	1150	0
1	2000	1996
2	1004	1973
3	2002	-2070
4	710	662
5	615	-824
7	1490	1616

0,7,L

1	2127	2307
2	2349	-2331
3	1917	-2011
5	999	-1004

0,8,L

0	1071	-840
1	999	-842
2	715	-186

0,9,L

-3	2109	-2392
	703	378

1,0,L

0	878	-850
1	1452	-1453
-1	2018	2253
2	790	-832
-3	903	-1089
4	742	916
-4	773	904
-5	1153	-1288
	1287	-1060

1,1,L

1	1130	400
-1	1027	1201
2	1934	-1700
-3	1135	-2200
4	1159	-1120
-4	733	917
5	724	931
7	704	941
	777	1100

1,2,L

0	8040	-2167
1	3054	-2331
3	2441	-2500
4	3565	-3180
5	1006	1003
6	848	890
7	913	859

1,3,L

1	1350	1377
-1	1460	902
2	1283	705
-2	850	-809
3	1333	-1201
-3	1122	-1063
4	994	1063
-4	770	-1150
5	1468	-1157
-5	952	-873
6	982	-826

1,4,L

0	873	206
1	2073	-1978
-1	1862	1717
3	2452	-2362
4	846	-533
5	684	819
7	2070	2351

1,5,L

-1	2820	2456
2	3067	-2778
-3	2712	-2533
4	3110	-3099
-5	1170	-1199
6	1049	-1122
	996	991
-7	1226	1176

1,6,L

-1	770	-452
4	675	4

1,7,L

-1	1370	1240
1	1136	1132
2	1927	-2167
-2	1090	1101
3	849	-784
-5	1933	-1785
	1794	-1625

1,9,L

-1	769	-439
2	2500	-2648
-2	2725	2821

2,0,L

0	4527	5014
2	3672	-3853
-4	3290	-3440
6	760	-775
-8	811	745

2,1,L

-2	811	41
4	1350	1335
-4	984	-1440
5	941	-2357
0	603	-523
-6	1004	800
7	833	913

2,2,L

0	2992	2913
1	1453	-1430
-1	1920	1808
3	1708	-1588
-3	1191	1530
4	2240	-2420
-4	1581	-1910
6	1149	-834
7	1482	1501
-7	1324	-1349

2,3,L

1	1681	1635
-1	1396	869
2	1292	1360
-2	1102	-1026
3	2134	-2058
-3	1423	-1950
-0	779	771
-7	994	1121

2,4,L

0	877	914
1	2101	-2035
-1	1938	2139
2	941	-808
-2	1460	-1316
3	1744	1767
-3	891	-829
4	1542	1663
-5	1315	-1594
6	775	846

2,5,L

-1	1674	1665
1	1704	1484
3	747	-871
-3	702	-682
5	637	862
-5	1041	-1944
6	1870	-1902
-6	770	909
	1040	-970

2,6,L

0	983	-732
-1	861	401
2	721	-207
-3	960	-1304
4	1103	868
	860	403

2,7,L

-1	1688	1343
1	1534	1796
-2	1866	-2072
3	2047	-1989
-3	1743	-1797
4	1748	-1770
-5	712	179
-6	739	-489

2,8,L

0	806	-689
1	911	-249
-2	968	-298
3	1049	-911
-3	837	-395

3,0,L

0	1869	2218
4	2099	-2390
-4	1886	-1836
6	911	-518
-6	822	-1029

3,1,L

-1	599	-187
2	1107	1062
-2	702	-788
3	1176	-946
-4	594	-782
5	729	-860
-6	999	1000

3,2,L

0	2017	2032
-1	1094	-1064
-1	1340	1477
3	1225	-1051
-3	1011	-936
4	1943	-2182
-4	1690	-1749
5	836	996
-6	1097	772

3,3,L

0	636	-804
4	1251	716
-4	984	-1063
5	830	-997
-6	985	872

3,4,L

-1	881	869
2	708	2264
3	1599	-1687
-3	1107	1482
5	1112	885

3,5,L

-1	1780	1509
2	1549	1404
-3	1792	-1903
4	1324	-1021
	745	-305

3,6,L

1	1424	-1490
-1	1142	1258
3	76-	-843
-5	711	417

3,7,L

1	711	709
-1	875	735
2	1424	-1165
-2	1343	1290

4,0,L

0	2614	2708
-4	1663	-1484

4,1,L

-1	804	-180
-2	580	403
-3	1038	-421
-4	874	-646

4,2,L

0	866	857
-2	897	171
-3	884	830
-4	1330	-984

4,3,L

-1	925	598
2	732	870
-2	715	-698
3	1384	-913
-5	690	-974

4,4,L

1	1395	-1328
-1	1580	1384

4,5,L

0	687	342

terminal Hg-Hg distance is 2.57(1)Å while the central Hg-Hg distance is 2.70(1)Å. The significant difference in bond lengths indicates that the positive charges reside on the terminal mercury atoms. In simple valence bond terms the orbitals forming the bonds between mercury atoms are then sp hybridized. The average bond length of 2.61Å shows that as the formal positive charge on mercury is decreased in the order $Hg_2^{2+} < Hg_3^{2+} < Hg_4^{2+}$, the bond length increases. Unfortunately, because of the poor refinement of the AsF_6^- octahedron, it is difficult to say whether fluorine bridging to the terminal mercury atoms is significant. The long contact distances between Hg(1) and F(5) and F(2) of 2.74(10)Å and 2.76(10)Å respectively, indicate that fluorine bridging is not present to the extent that is in $Hg_3(AsF_6)_2$. This would be expected in view of the fact that the formal charge on each mercury atom in Hg_4^{2+} is less than that in Hg_3^{2+}. Although in the simple valence bond structure the positive charge resides exclusively on the terminal mercury atoms, there would be some delocalization of charge and Hg_4^{2+} would be less polarizing then Hg_3^{2+}. The angles subtended by the two mercury atoms and F(5) and F(2) are also far from linear. However, when the large errors in the positions of the fluorines are taken into account, it is difficult to rule out any fluorine-mercury interaction with any certainty.

The molecules in the unit cell are fairly close packed. The structure may be described as nearly linear Hg_4^{2+} cations lying in planes perpendicular to the a axis with the AsF_6^- octahedra lying in alternating planes half the unit cell edge above. It is interesting

to note that even though they are so poorly defined, the average As-F distance is 1.66Å, in good agreement with previous determinations. The observed and calculated structure factors are listed in Table 5.4.

CHAPTER VI

INFINITE CHAIN POLYMERCURY CATIONS

6.1 INTRODUCTION

As mentioned in previous chapters, mercury reacts with AsF_5 to initially yield a golden crystalline mass. If sufficient AsF_5 is added, the mixture then further reacts to give the previously identified polymercury cations, Hg_4^{2+}, Hg_3^{2+} and Hg_2^{2+}. The golden compound can, however, be prepared in the absence of other polycations by reacting Hg with AsF_5 in the approximate molar ration of 2:1. A preliminary communication from this laboratory (70) identified the substance as $Hg_6^{2+}(AsF_6)_2$. This was based on analytical results and the compound's diamagnetism. An x-ray crystallographic study (71) revealed, however, that the true composition is $Hg_{2.86}AsF_6$. The compound is unique in that it contains infinite metallically bonded polymercury cations which form part of an ionic crystal lattice. The structural results are presented and discussed in this chapter. An analogous compound has been prepared with SbF_6^- formed by the reduction of $Hg_3(Sb_2F_{11})_2$ with elemental mercury. A preliminary x-ray crystallographic study of $Hg_{2.91}SbF_6$ shows that the compound is isostructural with $Hg_{2.86}AsF_6$.

6.2 THE STRUCTURE OF $Hg_{2.86}AsF_6$

6.2.1 SOLUTION AND REFINEMENT

The compound was prepared as described in Chapter II. The crystals were washed several times in SO_2 to remove any soluble mercury impurities contaminating the surface of the crystals. A suitable crystal of approximate spherical geometry (radius = 0.08 mm) was cut with a razor blade in a dry box with the aid of a microscope. The crystal was then sealed in a thin-walled quartz capillary tube and examined by standard x-ray methods.

Precession photographs showed the absences of the space group $I4_1/amd$ (no. 141, D_{4h}^{19}). The crystal data are listed in Table 6.1. In addition to the hkl reflections characteristic to the space group, prominent sheets of diffuse intensity were observed perpendicular to (100) and (010). Two orders of these sheets were visible in each direction, which are shown diagramatically in Figure 6.1 for the hko and okl projections obtained from precession photographs. The sheets corresponded to a spacing of 2.64(1)Å and it was assumed that this distance corresponded to a Hg-Hg interaction and the mercury atoms were in some measure disordered. This was confirmed by inspection of the three-dimensional Patterson function which showed planes of high density at w = 1/4 and w = 3/4. A satisfactory solution to both the Patterson function and the diffuse sheets of intensity could be found by placing atoms in the positions given in Table 6.2. This model, refined with isotropic temperature factors and unit weights, converged at $R_1 = 0.079$. 109 symmetry independent reflections with intensities

TABLE 6.1

CRYSTAL DATA FOR $Hg_{2.86}AsF_6$

Formula Weight	573.7
System	tetragonal
Conditions limiting possible reflections	hkℓ: h+k+ℓ=2n hko: h,(k)=2n okℓ: (k+ℓ=2n) hhℓ: (ℓ=2n); 2h+l=4n
Space Group	$I4_1/amd$(no. 141, D_{4h}^{19})
Cell Constants	
a	7.538(4)Å
c	12.339(5)Å
Number of formula units/ unit cell	4
Cell Volume	701.1Å^3
Linear absorption coefficient	685.5cm^{-1}
μR	5.5

TABLE 6.2

Structural Parameters[a] for $Hg_{2.86}AsF_6$

	10^3x	10^3y	10^3z	10^3B, $Å^2$
Hg[b]	0	31	0	70(4)
	0	94	0	75(6)
	0	156	0	63(5)
	0	219	0	70(4)
As(1)	0	1/4	3/8	39(3)
F(1)	0	1/4	245(5)	96(19)
F(2)	659(7)	x+1/4	7/8	74(10)

[a] x,y and z are fractional atomic coordinates. The isotropic temperature factor B is from the expression $\exp[-B(\sin^2\theta/\lambda^2)]$. Least-squares estimated standard errors in the least significant digits are given in parentheses.

[b] For the purposes of calculation, 0.71 Hg atoms were placed at each of x = 0.03125, 0.09375, 0.15625 and 0.21875. The temp. factors of the partial weight Hg atoms used to simulate the disordered Hg chain were refined separately.

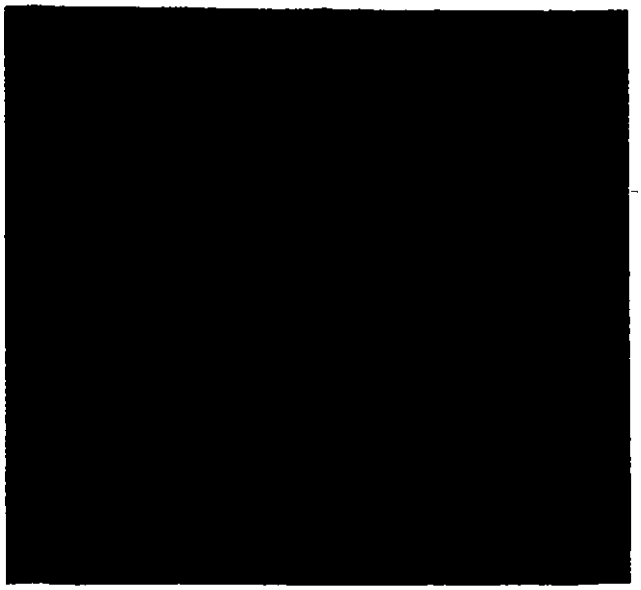

(a)

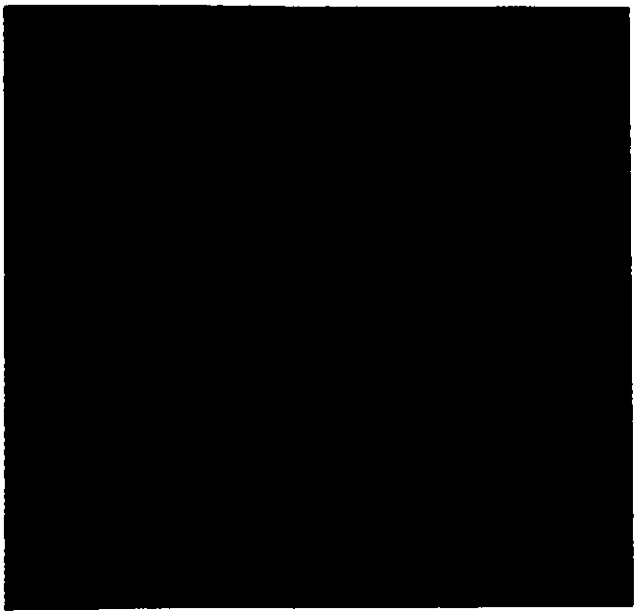

(b)

Figure 6.1 (a) hko and (b) okℓ Precession Photographs of $Hg_{2.86}AsF_6$

greater than three times the estimated standard deviation were used for the refinement after 696 reflections were corrected for absorption assuming spherical geometry and averaged to conform to the space group symmetry.

6.2.2 DESCRIPTION OF THE STRUCTURE

The structure consists of an array of octahedral hexafluoroarsenate anions conforming to the crystal symmetry, with the fluorine atoms occupying three-quarters of the points of a cubic close-packed lattice. The structure is shown in Figure 6.2. Within this lattice there is an array of non-intersecting channels running along the a and b directions. Infinite chains of mercury atoms (Hg-Hg = 2.64(1)Å) lie within these channels but the mercury-mercury distance is not commensurate with the lattice dimensions. Thus whereas a = 7.54Å, three Hg-Hg distances equal 7.92Å and therefore the empirical formula must be written as $Hg_{2.86}AsF_6$ (7.54/2.64 = 2.86). Comes et al., (72) discussing $K_2[Pt(CN)_4]Br_{0.30}3H_2O$ in their excellent paper on diffuse x-ray scattering experiments, point out that diffuse sheets of intensity perpendicular to crystallographic axes must correspond to a one-dimensional periodic structure parallel to that axis. The sheets of diffuse intensity perpendicular to the a and b axes in the present study must be due, therefore, to chains of mercury atoms parallel to the a and b axes. The mercury atoms are in different positions in adjacent unit cells and each mercury atom therefore has a different chemical environment. The positions of the mercury atoms within a given chain are also disordered with respect to the positions of the mercury atoms in adjacent chains. Because of the sharpness of the diffuse sheets of intensity, the individual

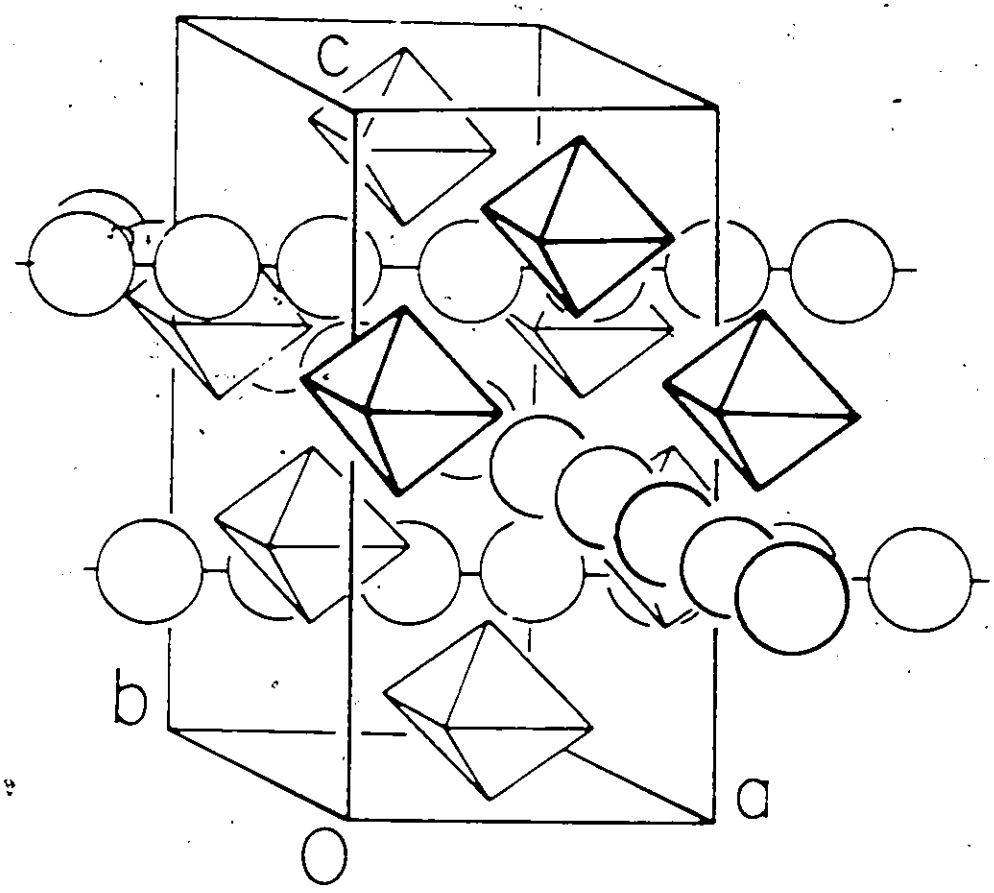

Figure 6.2 A Perspective Illustration of $Hg_{2.86}AsF_6$ (where octahedra are AsF_6^- anions and circles are mercury atoms).

mercury-mercury spacing cannot deviate significantly from the average of 2.64Å, as any distortion of the intrachain metal-metal spacing, periodic or otherwise, would be expected to broaden the sheets. In the conventional crystallographic analysis, the average unit cell can be viewed as containing continuous chains of electron density within the channels in the lattice. In order to simulate the disorder of the mercury atoms, 0.179 mercury atoms were placed at each of x(Hg) = 0.03125, 0.09371, 0.15621 and 0.21875, thus giving 16 partial atoms along each chain in the unit cell, i.e., an approximately continuous chain of mercury electron density. As only isotropic temperature factors on mercury were refined, and as the arsenic and fluorine atoms lie on special positions within the unit cell, there were only 11 variables for refinement purposes. Selected bond distances and angles are given in Table 6.3. The observed and calculated structure factors are given in Table 6.4.

The As-F distances are within the range found previously for the AsF_6^- anion, with an average As-F distance of 1.68Å. The closest contact between mercury atoms and fluorine is 2.99(4)Å, which is slightly greater than the sum of the Van der Waal's radii (2.85Å). Thus it seems reasonable to conclude that the crystal contains AsF_6^- anions and mercury chains in which the average charge per mercury atom is +0.35 (1/2.86), and that there is essentially ionic bonding between the positively charged mercury chains and the negatively charged hexafluoroarsenate anions. The Hg-Hg distance of 2.64Å is appreciably longer than those found for the mercurous halides (60) (2.49-2.54Å) or

TABLE 6.3

SELECTED BOND DISTANCES (Å) AND ANGLES (DEG)[a]

FOR $Hg_{2.86}AsF_6$

As(1) - F(1)	1.61(7)
- F(2)	1.71(4)
Hg(2) - F(2)[b]	2.99(4)
Hg-Hg	2.64(1)

[a] symmetry restricts the angles subtended by F(1)-As(1)-F(2) to 90° and angles subtended by Hg-Hg-Hg to 180°

[b] shortest distance.

0,0,L

4	5116	5257
8	5116	4777
12	1256	1035

1,0,L

1	2678	2523
3	4755	4515
5	3039	3634
7	1396	1286
9	811	904
11	1319	1197
13	695	748

1,1,L

2	1318	1411
6	1431	-1008
10	315	488
14	533	-244

2,0,L

0	4915	4851
2	3603	3453
4	2737	2723
6	2006	2208
8	2017	2154
10	955	1023
12	479	430
14	332	357

2,1,L

1	849	-804
3	413	-310
7	325	479
9	468	-324
11	378	-219

2,2,L

0	1480	-1560
4	576	617
8	724	-728

3,0,L

1	2910	2716
3	2624	2585
5	2169	2205
7	1268	1354
9	856	914
11	733	836
13	552	539

3,1,L

6	653	-459

3,2,L

1	881	914
3	515	-587
5	456	-540
7	483	523
11	240	-242

3,3,L

2	1036	-1183
6	870	849

4,0,L

0	2919	2983
2	2161	2221
4	1730	1712
6	1457	1503
8	1379	1468
10	605	732
12	276	277

4,1,L

1	531	-513
3	286	-259
5	262	275
7	306	352
9	365	-257
11	330	-159

4,2,L

0	961	-1053
4	478	543
8	539	-534

4,3,L

1	622	683
3	451	478
5	371	-428
7	404	-418

4,4,L

0	630	751
4	414	-480

5,0,L

1	1149	1128
3	1928	1954
5	1690	1655
7	619	620
9	492	472
11	603	619

5,1,L

2	561	636
6	591	-505

5,2,L

1	353	412
3	305	-303
5	306	-291
7	282	274
9	261	200

5,3,L

10	255	-211

5,4,L

1	320	-318

6,0,L

0	1957	1981
2	1132	1212
4	406	460
6	884	857
8	1029	996
10	478	441

6,1,L

1	421	-502
3	372	-305
9	306	-248

6,2,L

0	296	-413

6,4,L

8	288	272

6,5,L

1	244	-272
7	241	189

6,6,L

0	286	-257

7,0,L

1	470	478
3	1027	1038
5	958	891
7	247	268

7,1,L

2	336	400
6	382	-315

7,2,L

7	269	153

8,0,L

0	749	813
2	499	513
4	240	257
6	411	366

8,2,L

0	238	-294

8,3,L

1	248	178

Table 6.4

Observed and Calculated Structure Factors for $Hg_{2.86}AsF_6$

$Hg_3(AsF_6)_2$ (2.55Å). This, coupled with the fact that the chains are electron deficient, means that the chains can be regarded as metallic. The chains of mercury atoms are best described as having the charge delocalized over the chain, resulting from partial oxidation of a filled conduction band arising from the overlap of mercury orbitals. This is qualitatively similar to the partially oxidized band model proposed for the anisotropic tetracyanoplatinate complexes, which are discussed in some detail in Chapter VII. The Hg-Hg distance is considerably shorter than that in metallic mercury (3.005Å), but it must be remembered that the coordination number in the metal is 12 whereas in $Hg_{2.86}AsF_6$ it is only 2. The compound is unique in that it displays all types of chemical bonding: ionic, covalent, and metallic. The model proposed suggests that the compound should display anisotropic conductivity, i.e., it should be highly conducting along the a and b axes, and less so along the c axis. This has been confirmed by single crystal optical and conductivity studies, the results of which are presented in Chapter VII.

6.3 PREPARATION AND STRUCTURE OF $Hg_{2.91}SbF_6$

A golden compound identical in appearance with $Hg_{2.86}AsF_6$ can be prepared by the reaction of mercury with a solution of $Hg_3(Sb_2F_{11})_2$ in SO_2. When mercury was reacted directly with SbF_5 at room temperature, the initial product was a grey-green solid, presumably the golden compound in finely divided form. Formation of the compound by reduction of another polycation eliminated the problem of separating the insoluble product from SbF_3. Crystals suitable for x-ray analysis were

grown by reducing $Hg_3(Sb_2F_{11})_2$ with mercury in liquid SO_2 at -10°C with no stirring. The reaction can also be used to grow very large single crystals by slightly modifying the conditions. This is discussed in more detail in Chapter VII. Examination of a suitable crystal by the precession method showed that the space group was identical with that of $Hg_{2.86}AsF_6$. The crystal parameters were obtained from a full data set collected on a four-circle auto-diffractometer and are listed in Table 6.5. It may be seen that the unit cell parameters are somewhat larger than those of $Hg_{2.86}AsF_6$, as would be expected because of the larger size of the SbF_6^- anion (As-F= 1.67Å in AsF_6^-; Sb-F = 1.87Å in $XeF^+SbF_6^-$) (73). The sheets of diffuse intensity perpendicular to the a and b axes were identical in appearance with those of the analogous hexafluoroarsenate compound, and the separation between the sheets corresponded to a Hg-Hg spacing of 2.64Å. The intensity distribution was very similar and hence it may be concluded that the compound is isostructural with $Hg_{2.86}AsF_6$. In accord with the observed increase in Hg-Hg bond length with decreasing positive charge on the mercury atoms, $Hg_{2.91}SbF_6$ would be expected to have a slightly longer Hg-Hg bond than $Hg_{2.86}AsF_6$, because of the lower formal positive charge on $Hg_{2.91}SbF_6$ (+0.344 vs +0.35). However, the difference is so small that the failure to observe a slightly longer Hg-Hg bond in $Hg_{2.91}SbF_6$ is not surprising.

The ability to grow large single crystals with well-defined, identifiable crystal faces enabled the anisotropy of the compound to be established. This is discussed in Chapter VII.

TABLE 6.5

CRYSTAL DATA FOR $Hg_{2.91}SbF_6$

Formula Weight	819.47
System	tetragonal
Conditions limiting possible reflections	hkℓ: h+k+ℓ=2n hko: h,(k)=2n okℓ: (k+ℓ=2n) hhℓ: (ℓ=2n);2h+l=4n
Space Group	$I4_1/amd$ (no. 141, D_{4h}^{19})
Cell constants	
a	7.699(3)Å
c	12.610(4)Å
Number of formula units/ unit cell	4
Cell Volume	747.4Å^3
Linear absorption coefficient	645 cm^{-1}
Calculated density	7.29 gcm^{-3}

CHAPTER VII

CONDUCTIVITY AND OPTICAL STUDIES ON INFINITE CHAIN POLYMERCURY CATIONS

7.1 INTRODUCTION

In recent years the study of potential "one-dimensional" metallic systems has attracted a great deal of interest. They are interesting from both a chemical and physical viewpoint and include both organic and inorganic examples. This chapter will briefly review the field with emphasis on the inorganic complexes.

This chapter will report the results of single crystal conductivity studies which have shown that both $Hg_{2.85}AsF_6$ and $Hg_{2.91}SbF_6$ are metallic conductors. In addition, $Hg_{2.91}SbF_6$ is anisotropic. It has not yet been possible to measure the anisotropic ratio of $Hg_{2.86}AsF_6$, but preliminary optical measurements indicate that it is anisotropic.

7.2 REVIEW OF ANISOTROPIC MATERIALS

The study of one-dimensional compounds has been concentrated on three main classes of compounds: the organic charge transfer complexes involving tetracyanoquinodimethane (TCNQ), of which the best example to date is tetrathiofulvalinium tetracyanoquinodimethane (TTF)(TCNQ); the partially oxidized square-planar tetracyanoplatinate complexes such as $K_2[Pt(CN)_4]Br_{0.30}\cdot 3H_2O$; and the remarkable polythiazyl,

$(SN)_x$, the first example of a polymer composed of non-metals that displays metallic properties. The classification of a compound as "one-dimensional" is somewhat arbitrary, so it is perhaps more correct to refer to them as anisotropic materials. They are anisotropic by virtue of their electrical, magnetic and optical properties. Several of the compounds, most notably $(SN)_x$ and the infinite chain mercury cations, display some three-dimensional behaviour because of considerable interchain coupling.

The organic charge transfer complexes have been the subject of several review articles (74,75). The (TCNQ) molecule is planar (I) and, due to its strong acceptor properties, is capable of forming an anion radical by chemical reaction with a suitable donor molecule. The anion radical (II) is paramagnetic and, in the high conductivity (TCNQ) complexes, is stacked in chains with the planes of the molecules parallel to each other.

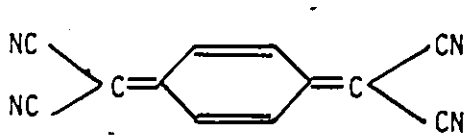

(I)

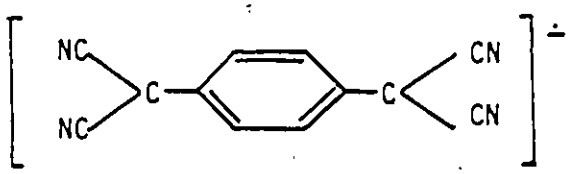

(II)

In the salt (TTF)(TCNQ), the overlap of (TCNQ) orbitals gives rise to a half-filled conduction band and one would expect the salt to exhibit metallic conduction parallel to the b axis, along which the (TCNQ) radical anions are stacked (76). Conductivity studies by Garito, Heeger et al (77) indicated that the room temperature conductivity parallel to the b axis

($\sigma_{||}^{b}$) was typically a few hundred $(\Omega cm)^{-1}$ with an anisotropy ratio ($\alpha = \sigma_{||}^{b}/\sigma_{\perp}^{a}$) of ~500 at room temperature and up to 10^4 at 58°K. Schafer et al (78) claimed a room temperature conductivity, $\sigma_{||}^{b}$, of 350 $(\Omega cm)^{-1}$ with $\alpha_{300°K} = 70$ and $\alpha_{70°K} = 600$. It is clear that (TTF)(TCNQ) is a highly anisotropic metal above 70°K, below which it undergoes a transition to a less conducting state.

The partially oxidized tetracyanoplatinate complexes have been known for many years, but only in the last ten years have they been studied from a physical viewpoint. They have been well reviewed (79,80,81). The complexes have been referred to as Mixed Valency Planar (MVP) transition metal complexes. This is somewhat misleading because it is impossible to distinguish between the metal atoms on the basis of oxidation state, and therefore they will be called "partially oxidized" in this thesis. $K_2[Pt(CN)_4].3H_2O$ crystallizes with the platinum atoms stacked to form colinear metal atom chains. It is possible to partially oxidize this compound with bromine or chlorine to obtain compounds of the composition $K_2[Pt(CN)_4]Br_{0.30}.3H_2O$. Krogmann (82) showed that the bromine atom is not incorporated in the metal atom chains, as might have been expected (bromine occupies axial positions in the complex $K_2[Pt(CN)_4Br_2]$), but rather partial oxidation reduces the Pt-Pt distance to a remarkably short 2.88Å (vs 2.77Å for Pt metal). The structure of $K_2[Pt(CN)_4]Br_{0.30}.3H_2O$, with a diagrammatic representation of the overlap of the platinum d_{z^2} orbitals, is shown in Figure 7.1. Fifty percent of the available K sites and 60% of the available Br sites are randomly occupied. The bromine content is invariant whereas the complex loses

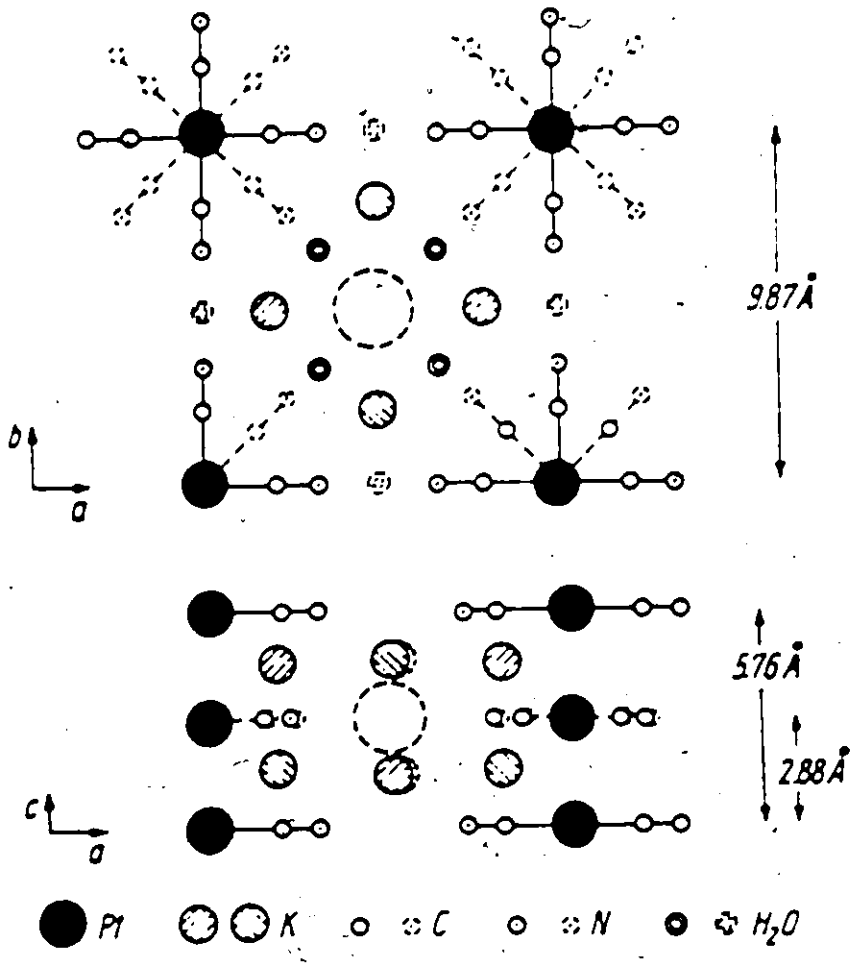

(a)

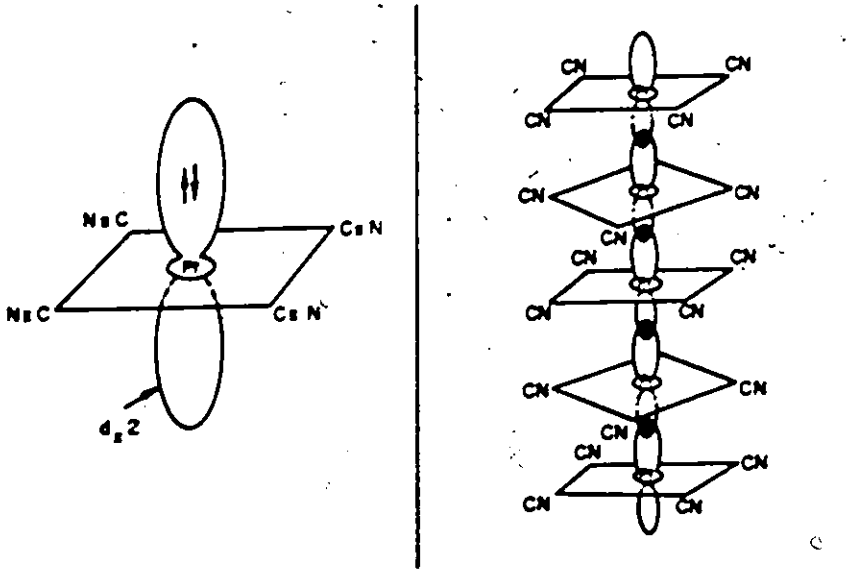

(b)

Figure 7.1 (a) The Crystal Structure of $K_2[Pt(CN)_4]Br_{0.30}\cdot 3H_2O$ (after Krogmann and Hausen (82))

(b) Overlap of the d_{z^2} Orbitals in the Platinum Chains

water easily, undergoing several phase transitions as it does. The bonding in the partially oxidized complexes can best be described by molecular orbital and band theory. In $K_2[Pt(CN)_4].3H_2O$, the overlap of the d_z2 orbitals on Pt leads to formation of a fully occupied conduction band; when partially oxidized, electrons are removed from the upper orbitals of the band, which have an antibonding effect on the Pt-Pt bond. The bond is therefore strengthened and shortened in the partially oxidized complexes, and the compounds fulfil the requirements of an anisotropic metal. These can be summarized briefly as follows: the structure must contain linear parallel rows of atoms; the interaction between the atoms must be sufficiently strong to make band formation possible; the atoms composing the chain must have an odd or fractional formal valency, leading to a partially filled conduction band; and the conducting chains must be separated from other chains to eliminate possible interchain conduction. A large number of partially oxidized tetracyanoplatinate complexes have been prepared. Electrical neutrality can be maintained by either addition of anions, or removal of cations, as in $K_{1.74}[Pt(CN)_4].1.8\ H_2O$ (83).

Conductivity studies (84) on $K_2[Pt(CN)_4]Br_{0.30}.3H_2O$ have shown that the room temperature conductivity is 300 $(\Omega cm)^{-1}$, with an anisotropy ratio ($\alpha = \sigma_{\parallel}/\sigma_{\perp}$) of 10^5. The conductivity reaches a maximum at 25°C and then decreases, with the compound becoming an insulator at low temperatures. The observed metal-insulator transiton has been predicted by Peierls (85) for one-dimensional metals. It should be noted here that conductivity in one-dimensional systems is

extremely dependent on impurities, which can interrupt the conducting strands. Many workers have reported vastly different results. For example, the dc conductivity of $K_2[Pt(CN)_4]Br_{0.30}\cdot 3H_2O$ has been reported ranging from 10^{-4} $(ohm\ cm)^{-1}$ (86) to 830 $(ohm\ cm)^{-1}$ (87). This shows that conductivity measurements on one-dimensional systems should be interpreted with caution.

Polythiazyl, $(SN)_x$, was first prepared in 1910 (88). Early measurements (89) indicated that the compound was metallic, with a dc conductivity of 10^2-10^3 $(ohm\ cm)^{-1}$. Analytically pure single crystals were first prepared by MacDiarmid and co-workers (90) by the solid state polymerization of S_2N_2. The lustrous, bronze-coloured polythiazyl crystals are composed of bundles of $(SN)_x$ fibres. An early electron diffraction study (91) showed alternating long and short S-N bond lengths. However, the structure was very poorly refined (R = 0.35) and there is no indication that the vapour is $(SN)_x$. It may be S_2N_2 or a mixture of both compounds. A single crystal x-ray diffraction study (92) showed that the bond lengths are virtually equal with an S-N-S bond angle of 119.9° and a N-S-N bond angle of 106.2°. The structure is shown in the following diagram.

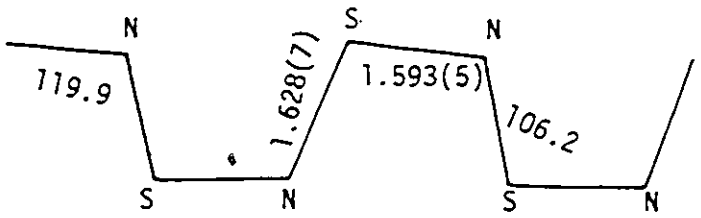

The relatively close approach of formally non-bonded atoms suggests secondary bonding interactions along the $(SN)_x$ chains. Optical studies on polycrystalline films (93) and single crystals (94) show that $(SN)_x$ is highly reflective to light polarized parallel to the fibre direction and much less so perpendicular to it. The conductivity parallel to the fibre axis was calculated as $3x10^3$ (93) or $3.4x10^4$ (94)$(\Omega cm)^{-1}$ from the reflectivity data. Both studies clearly show that $(SN)_x$ is a metallic conductor parallel to the polymeric chains, although there exists a discrepancy between the two values. It has also been possible to grow fully oriented epitaxial crystalline films of $(SN)_x$ on substrates such as Mylar, Teflon and polyethylene (95). Single crystal dc conductivity studies currently in progress by MacDiarmid and co-workers (96) indicate that there is substantial interchain coupling and, although anisotropic, $(SN)_x$ cannot be viewed as one-dimensional. The compound has been shown (97) to undergo a superconducting transition at 0.26°K.

7.3 CONDUCTIVITY STUDIES ON $Hg_{2.86}AsF_6$

7.3.1 CRYSTAL GROWTH

Single crystals of $Hg_{2.86}AsF_6$ were grown by the low temperature disproportionation of a solution of $Hg_4(AsF_6)_2$ in SO_2. As described in Section 4.2.1, $Hg_4(AsF_6)_2$ disproportionates at low temperatures to give $Hg_3(AsF_6)_2$, which is very soluble in sulphur dioxide, and $Hg_{2.86}AsF_6$, which is insoluble and precipitates from solution upon formation. A very concentrated solution of $Hg_4(AsF_6)_2$ and $Hg_3(AsF_6)_2$ was prepared directly from elemental mercury by oxidation by AsF_5 (Chapter II). The

red solution was filtered to separate the insoluble $Hg_{2.86}AsF_6$ and the solution was then cooled from room temperature to -30°C over a period of several days. Single crystals of $Hg_{2.86}AsF_6$ over two mm in size grew on the side of the Pyrex tube. If the solution was too concentrated, crystals of $Hg_3(AsF_6)_2$ and $Hg_4(AsF_6)_2$ precipitated from solution as well. When this occurred separation of the $Hg_{2.86}AsF_6$ and the contaminants was impracticable because the crystals of $Hg_{2.86}AsF_6$ reacted with the other polycations upon washing the crystals with sulphur dioxide, thereby eroding the crystal faces. When the crystals of $Hg_{2.86}AsF_6$ grew without co-precipitation of the other polycations, they were carefully washed with SO_2 to remove traces of soluble contaminants and pumped dry. Care was taken when the crystals were washed with SO_2. $Hg_{2.86}AsF_6$ undergoes a disproportionation in SO_2 at low temperatures according to the following equation:

$$2Hg_{2.86}AsF_6 \xrightarrow[\text{in } SO_2]{\text{cooling}} 2.72Hg_{(\ell)} + Hg_3(AsF_6)_2$$

The sulphur dioxide was condensed onto the Pyrex tube away from the crystals by cooling the tube with a cotton swab soaked in liquid nitrogen. When the SO_2 reached the crystals it was approximately at room temperature, and the disproportionation described above was avoided. The sample handling and techniques for measuring the resistivity have been described in Chapter II.

7.3.2 RESULTS AND DISCUSSION

The structure of $Hg_{2.86}AsF_6$ has been described in Chapter VII (Figure 6.2). The array of non-intersecting channels running along the a and b directions which contain infinite chains of mercury atoms suggests that the compound should display metallic conductivity. The mercury-mercury distance of 2.64Å is considerably shorter than that in metallic mercury (3.005Å). The interchain separation of 3.085Å, while appreciably longer than the intrachain separation, is less than the sum of metallic radii for two mercury atoms (3.14Å) (98). This suggests that although the conductivity may be anisotropic, there will be considerable interchain coupling.

Resistivity measurements were carried out without regard for crystal orientation because it was not possible to obtain crystals with sufficiently well-defined morphology to allow alignment of the contacts along the principal axes. Bismuth and antimony samples were measured to determine the absolute value of the resistivity for the contact configuration. The experimental details are given in Chapter II.

The resistivity as a function of temperature is shown in Figure 7.2. It can be seen that the compound is highly conducting, the resistivity at room temperature being of the order of 130 μΩcm. This corresponds to a conductivity of 8×10^3 $(\Omega cm)^{-1}$, a value considerably larger than that found for the partially oxidized $K_2[Pt(CN)_4]Br_{0.30} \cdot 3H_2O$ and roughly equal to that for $(SN)_x$. It must be emphasized here that the

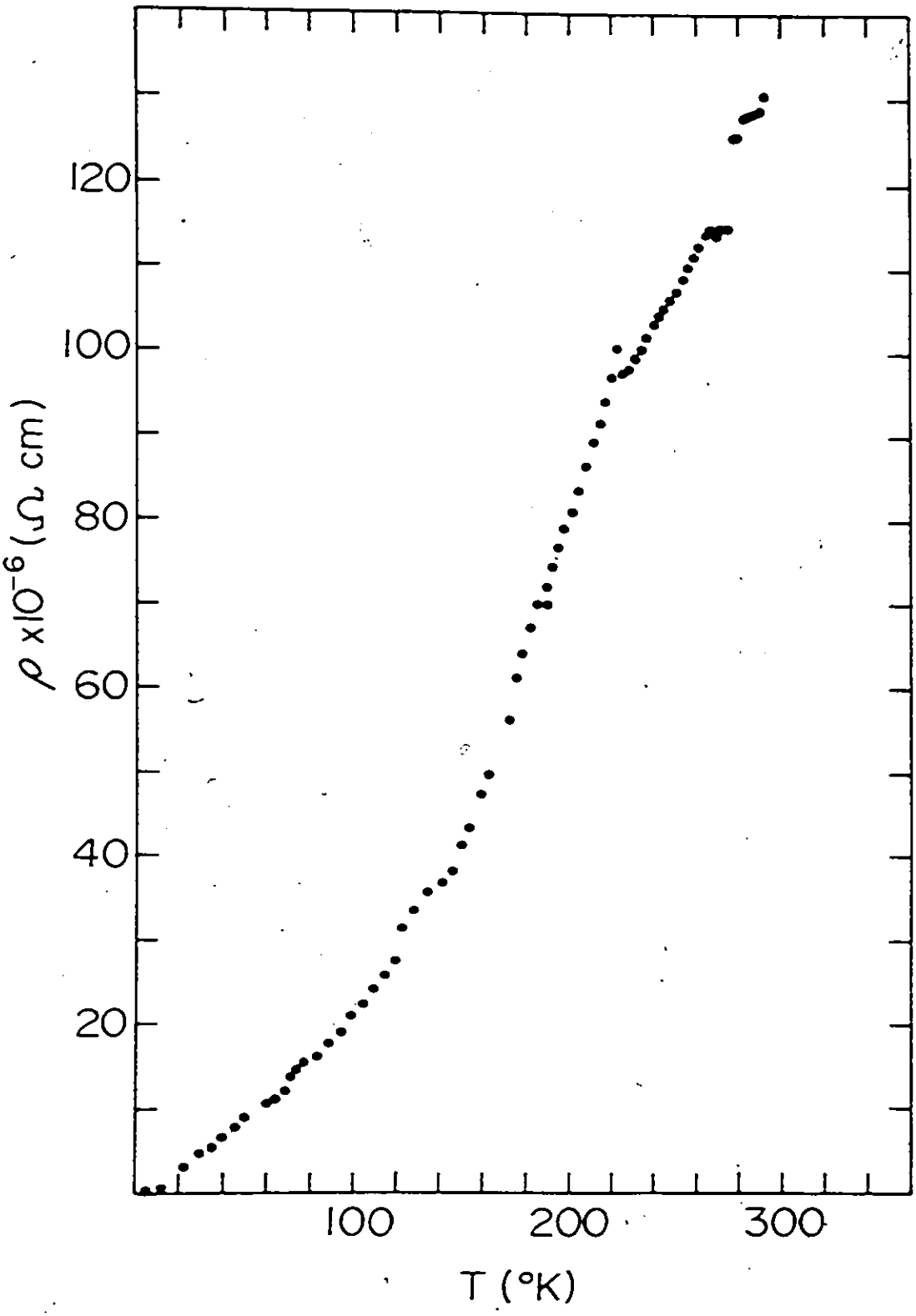

Figure 7.2 The Resistivity of $Hg_{2.86}AsF_6$ as a Function of Temperature.

calculations were based on an isotropic material. If the compound is anisotropic, as indicated by qualitative optical measurements discussed below, the use of unoriented crystals did not reveal the anisotropy because the probes were not aligned along the low and high conductivity directions. The resistivity appears to decrease dramatically with decreasing temperature. The resistivity at 4.2°K was found to be $\sim .1 \mu\Omega$ cm, which was at the lower limit of detection. Low temperature results ($\sim$ 77°K) were obtained by averaging the experimental results for several different samples. The results are shown in Figure 7.3 along with the measured temperature dependent resistivity of a bismuth sample used for calibration. The apparent decrease in resistivity by a factor of almost 10^3 over the temperature range studied is considerably larger than that observed in metals that are not highly purified, and is consistent with a metallic state arising from the interaction of mercury atoms in a chain forming a partially filled band. The increase in conductivity with decreasing temperature normalized to the room temperature conductivity is shown in Figure 7.4. The apparent large temperature dependence must be interpreted with caution. Because the contacts were not aligned a different temperature dependent resistivity in the high and low conductivity directions would lead to a spurious result.

The reflectance of $Hg_{2.86}AsF_6$ under polarized light was found to be highly anisotropic. Although it was not possible to identify the crystal axes, the results confirm the prediction that the compound is anisotropic, with two highly conducting directions (a and b) and a third (c) less so. A bright golden metallic lustre was observed with polarization parallel to, presumably, the a or b axis. Under transverse polarized light the crystals appeared blue. The crystals generally grew as

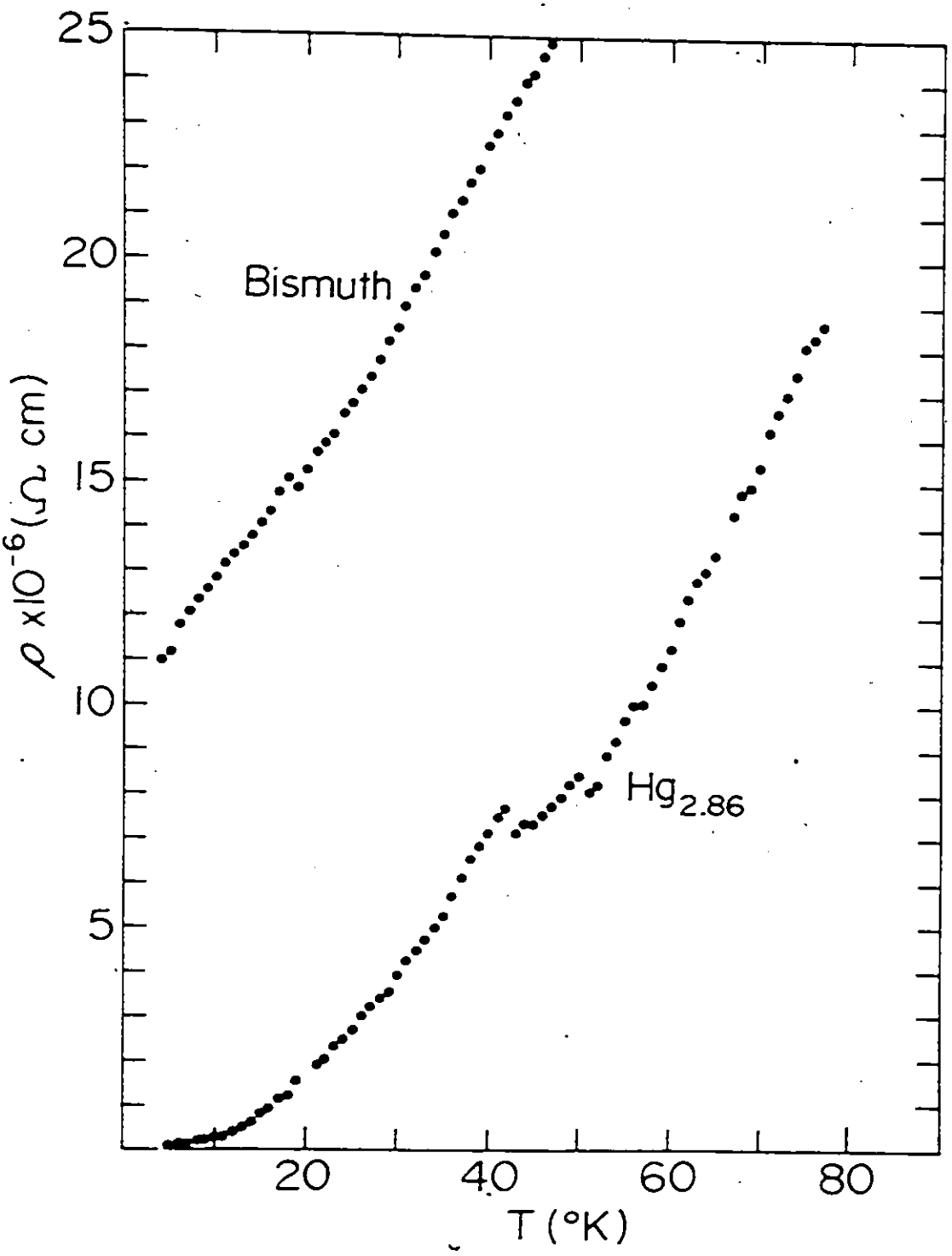

Figure 7.3 The Low Temperature Region of the Resistivity of $Hg_{2.86}AsF_6$ and Bismuth as a Function of Temperature.

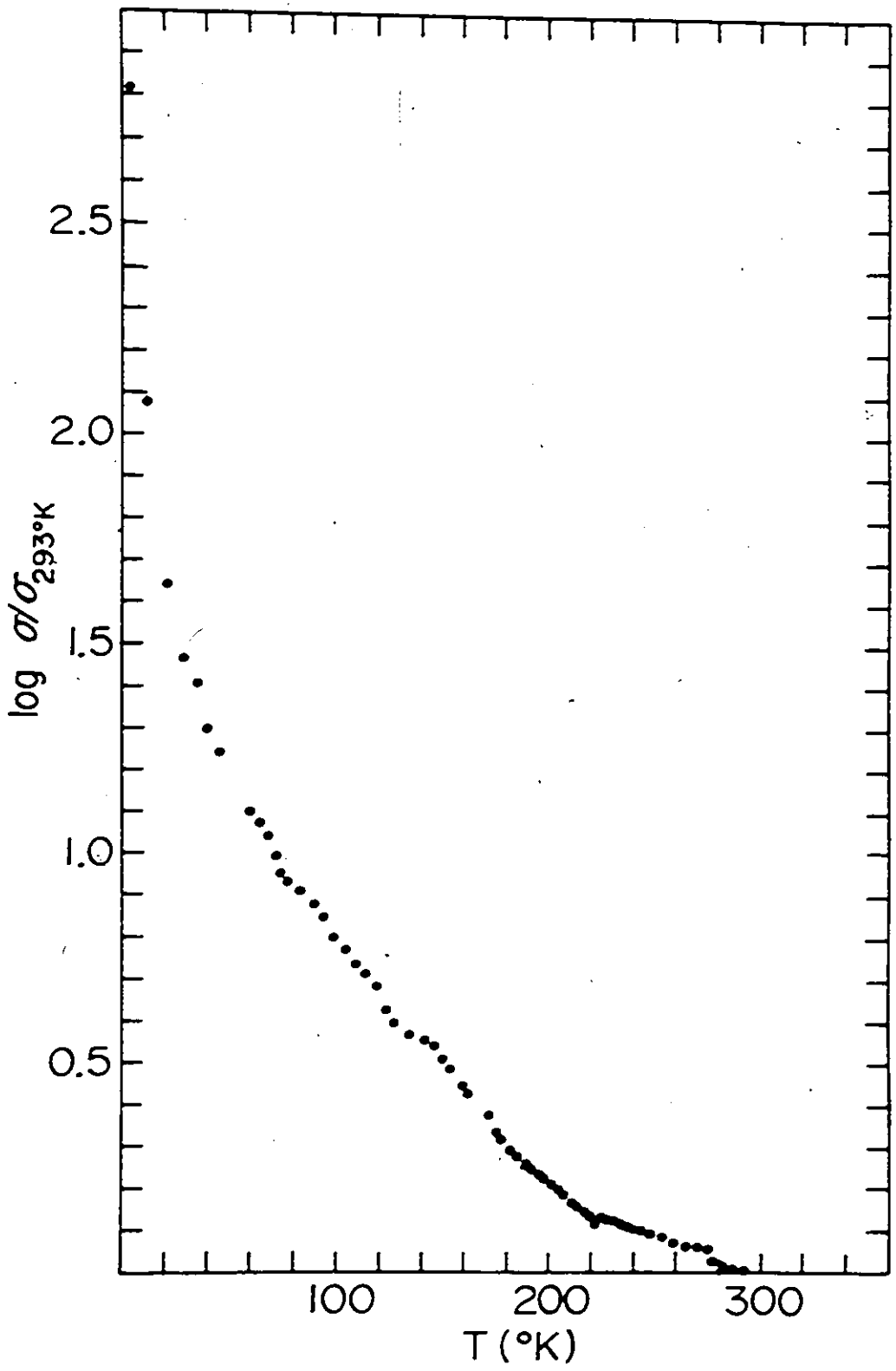

Figure 7.4 The Conductivity of $Hg_{2.86}AsF_6$ as a Function of Temperature (normalized to the room temperature conductivity).

truncated octahedra, and the reflectance of two faces on each crystal were independent of the angle of polarization, a bright golden metallic lustre being observed for all polarizing angles. Presumably these were the ab faces. All other faces showed a dramatic extinction with every 90° of rotation.

7.4 CONDUCTIVITY AND OPTICAL STUDIES ON $Hg_{2.91}SbF_6$

7.4.1 CRYSTAL GROWTH

Very large (3 mm) single crystals of $Hg_{2.91}SbF_6$ with well defined crystal faces were grown by the technique described in Section 6.3 with some modifications. Elemental mercury reacts with a sulphur dioxide solution of $Hg_3(Sb_2F_{11})_2$ to form crystals of $Hg_{2.91}SbF_6$. The reaction is very fast and to obtain large crystals it is necessary to carry out the reaction at low temperatures. A solution of $Hg_3(Sb_2F_{11})_2$ was first cooled to -35°C in an ethylene dichloride slush bath. The solution was then transferred onto the elemental mercury contained in the other side of a reaction vessel. The solution was not stirred or agitated, but simply held at -35°C. The reaction was remarkable. Large crystals of $Hg_{2.91}SbF_6$ grew on the surface of the drop of liquid mercury (f.p. of mercury is -37.5°C). Over a period of several days to a week the mercury appeared to diffuse into the crystals, which were 2-3 mm long. Upon isolation there was a clump of large crystals with a spherical hole where the mercury had been. This most interesting reaction is being studied at the present time. The crystals were washed with SO_2 to remove any insoluble impurities and pumped dry. The crystals in the clump could be conveniently separated from each other by simply tapping the container on the bench top. When prepared in this manner there were usually three

or four large crystals (2 mm) with lustrous, smooth faces suitable for conductivity experiments.

The major crystal faces were identified by x-ray photographs of a smaller crystal with the same crystal morphology. It was found that the ac (010) face, which sould show the largest anisotropy, was not formed. Rather, a face rotated about a approximately 25° diagonal to c was formed. This face showed considerable anisotropy. The major isotropic face was identified from photographs as the ab (001) face. The fact that the major anisotropic face on which conductivity experiments were conducted was not (010) has important consequences, which will be discussed later.

7.4.2 CONDUCTIVITY EXPERIMENTS

Conductivity experiments were carried out on the anisotropic and isotropic crystal faces. The Montgomery method (29) for anisotropic materials was used. This has been discussed in Chapter II. The voltages on the anisotropic face were vastly different. The voltage corresponding to the highly conducting direction (a axis) was typically of the order of 10^{-9}V, which was at the lower limit of detection, while that for the poorly conducting direction (diagonal to c axis) was of the order of 10^{-4}V. Calculations using the Mongomery method (29) gave $\sigma_L = 9\times10^{3}(\Omega cm)^{-1}$ and $\sigma_T = 6.2\times10^{2}(\Omega cm)^{-1}$ (σ_L = longitudinal conductivity, σ_T = transverse conductivity). Rotation of the crystal in the sample holder by 90° reversed the value of the voltage readings, as would be expected for an anisotropic sample. Further rotation by 90° restored the voltage readings to the original values, as expected by the Reciprocity Theorem.

Conductivity measurements on the ab (001) face confirmed that this face was isotropic. Voltages were approximately equal for both longitudinal and transverse directions, and were of the order of 3.7×10^{-6}V. (The voltages were obtained for a particular contact separation which was used in the calculations by the Montgomery method). The contact separation was typically 0.5 mm. The conductivity of the isotropic face was calculated to be 3.7×10^{3} $(\Omega cm)^{-1}$. This is in reasonably good agreement with the value of $\sigma_L = 9 \times 10^{3}$ $(\Omega\,cm)^{-1}$ obtained for the anisotropic face. No change in voltage was observed as the crystals was rotated in the sample holder. $Hg_{2.91}SbF_6$ is a good metallic conductor with a conductivity comparable to elemental mercury ($10.4 \times 10^{3} (\Omega cm)^{-1}$) (99). The anisotropy ratio is ($\alpha = \sigma_L / \sigma_T$) $\sim$ 16. It must be kept in mind that the actual anisotropy of $Hg_{2.91}SbF_6$ is bound to be considerably higher. The anisotropic face measured was not (010) and the measured conductivity of the poorly conducting direction contained a considerable component of the highly conducting b axis. Experiments are in progress which will hopefully establish the true anisotropic ratio. The interchain separation of 3.15Å in $Hg_{2.91}SbF_6$ obviously gives the material some three-dimensional character. This is confirmed by the temperature dependent resistivity of the poorly conducting direction shown in Figure 7.5. Caution should be exercized when interpreting such a result. The apparent decrease in resistivity by a factor of 2.5×10^{2} could be caused by a slightly misaligned contact configuration, discussed by Schafer et al (78) for (TTF)(TCNQ) measurements. Even if the contacts are aligned correctly a different temperature dependence for the highly conducting direction would tend to give a spurious temperature dependence for the poorly conducting direction.

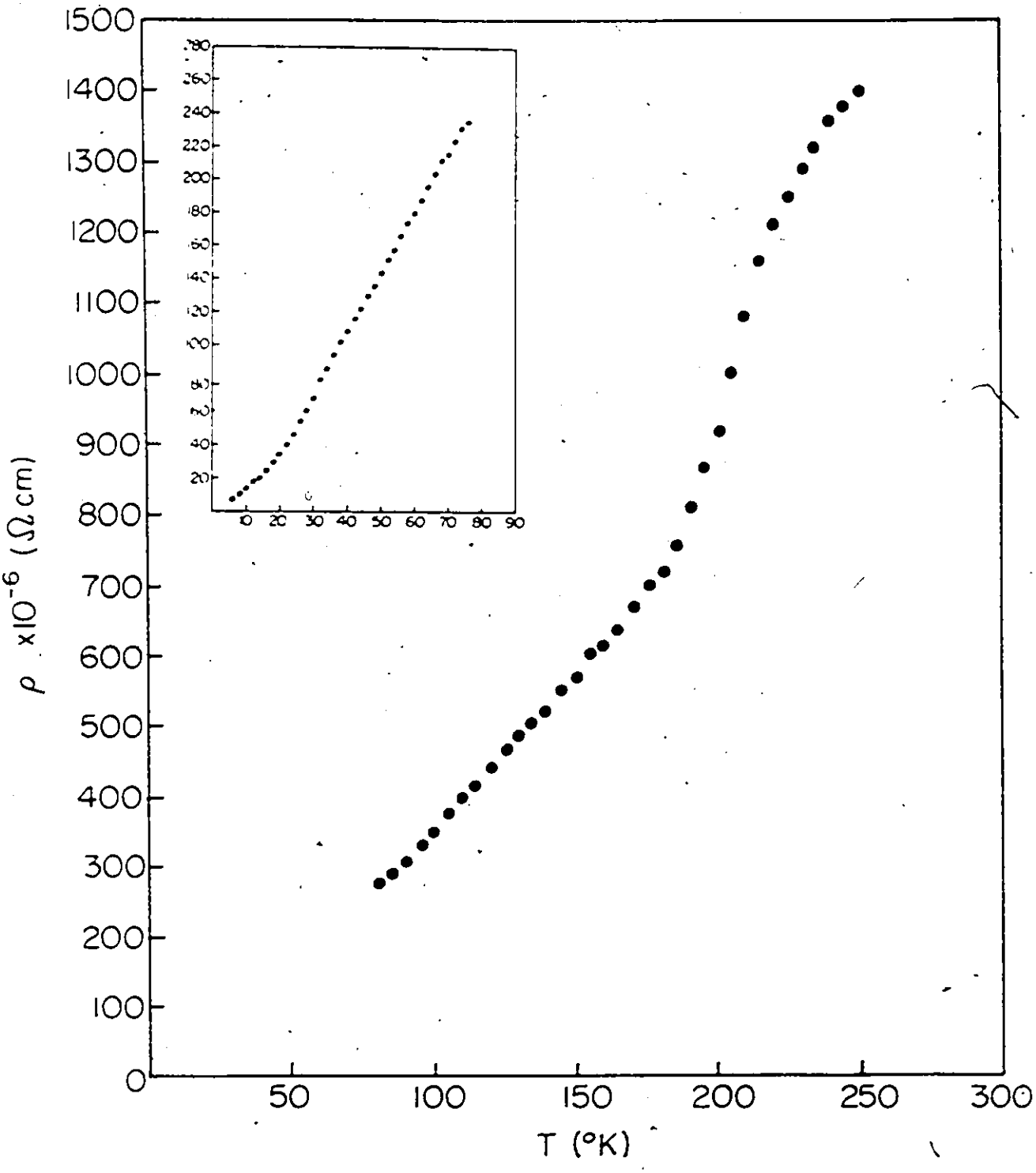

Figure 7.5 Temperature Dependent Resistivity of $Hg_{2.91}SbF_6$

Unfortunately, it was not possible to obtain meaningful temperature dependent data for the highly conducting direction because the voltage (lnV) was at the lower limit of detection at room temperature. The conductivity of the ab face was confirmed by measurements using four in-line contacts. A large number of different crystals were examined and the conductivity results were in reasonable agreement. Several voltage readings for the same contact configuration are shown below.

Typical Voltages Obtained for High and Low Conductivity Directions

Crystal	V_1(V)	V_2(V)
1	10^{-9}	1.08×10^{-4}
2	10^{-9}	1.54×10^{-4}
3	10^{-9}	$.73 \times 10^{-4}$

7.4.3 OPTICAL STUDIES

Qualitative optical studies were similar to those carried out on $Hg_{2.86}AsF_6$. Under light polarized parallel to the a axis on the anisotropic face the crystals were highly reflective, with a golden metallic lustre. Under transverse polarization, the crystals appeared greenish-yellow. On the isotropic face, which was identified by x-ray experiments as the ab (001) face, the crystals were reflective and metallic at all polarizing angles. This is in complete agreement with the structural model and the conductivity experiments.

Quantitative experiments were kindly done by Dr. Emil Koteles of the Department of Physics. The sample was mounted in a quartz tube, with the highly reflecting faces approximately parallel to the side of

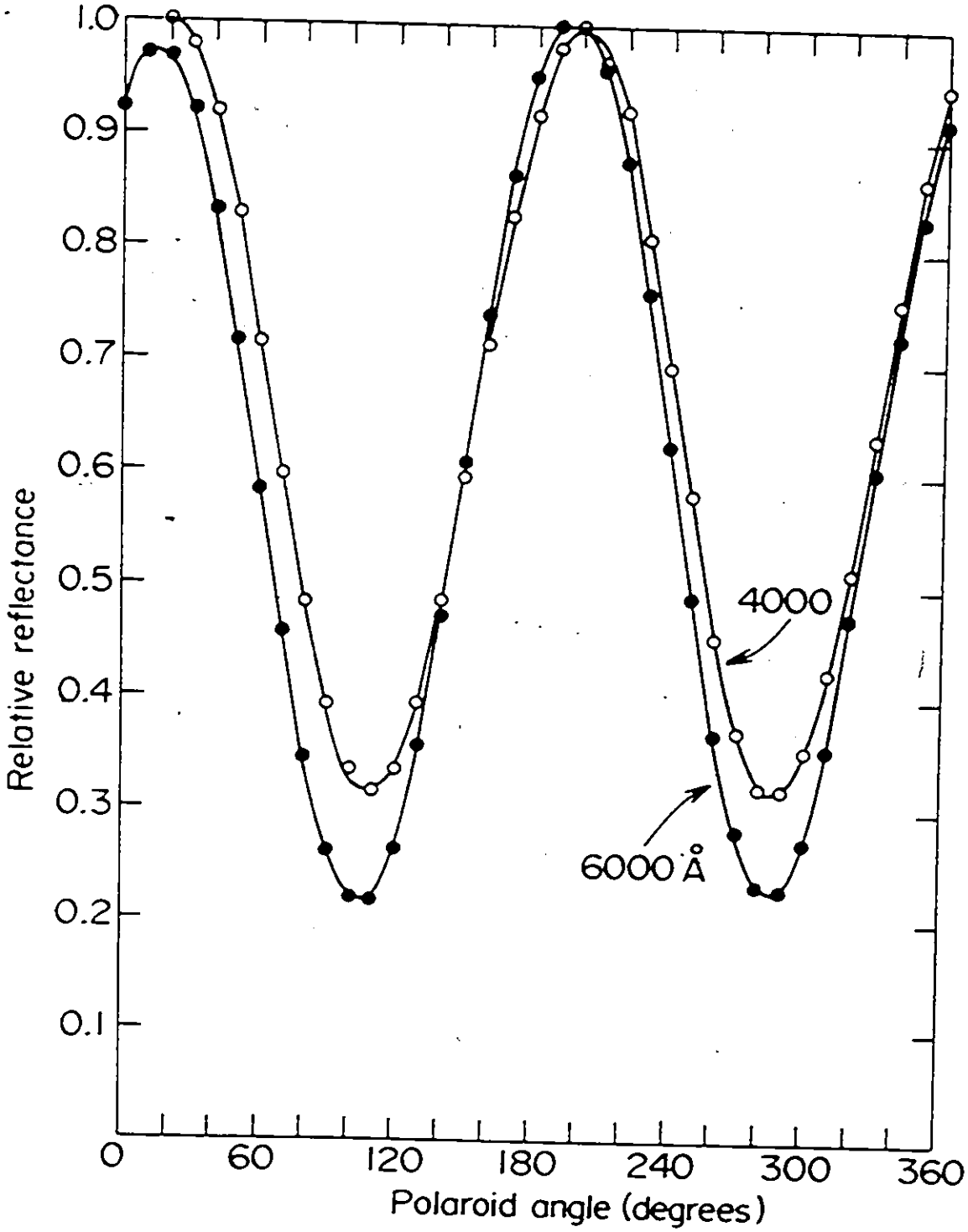

Figure 7.6 Relative Reflectivity of $Hg_{2.91}SbF_6$ as a Function of Polaroid Angle.

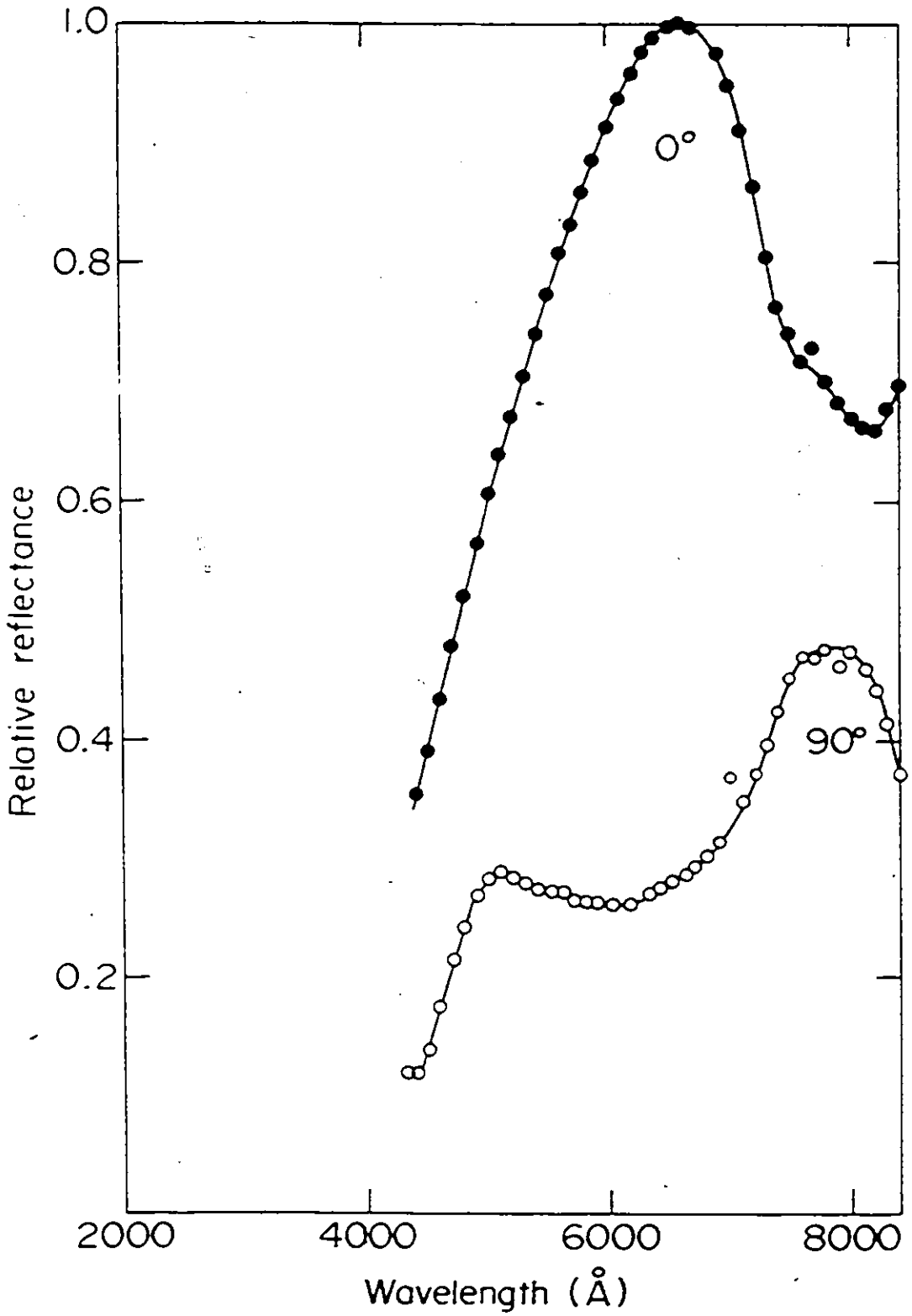

Figure 7.7 Reflectivity of $Hg_{2.91}SbF_6$ as a Function of Wavelength (4000-8000 Å)

glass. The crystal was held in place with glass wool. The relative reflectivy as a function of polaroid angle is shown in Figure 7.6. It can be seen that the reflectivity is drastically reduced every 90°, the curve being a function of $\cos^2\theta$. The absolute reflectivity has not yet been determined, but thecurve confirms the anisotropy. The maximum reflectivity corresponds to light polarized parallel to the a axis. The curve is displaced 20° because the crystal was only approximately aligned in the quartz tube.

The reflectivity as a function of wavelength is shown in Fig. 7.7. Again the reflectivity is relative with the highest reading being assigned a value of 1.0 and it has been corrected for reflection caused by the quartz tube. It may be seen that the reflectivity is much greater for light polarized parallel to the a axis. The characteristic plasma edge associated with a metal has not been observed. Experiments are being conducted with wavelengths longer than 3000Å and it is hoped that the plasma frequency will be observed in the infrared.

CHAPTER VIII

CONCLUSIONS

8.1 INTRODUCTION

This thesis has reported the preparation of mercury polyatomic cations in formal oxidation states of (+1) and lower. Hg_2^{2+} has been known for many years and, before the intensive study of metal-metal bonds in Transition Metal chemistry that has occurred in the last decade, provided the only example of a direct metal-metal bond. Other workers have prepared Cd_2^{2+} (20) and Zn_2^{2+} (22), both of which are much less stable than the analogous mercury dication. The Hg_3^{2+} cation has been reported in two preliminary communications(23,65).

In addition to several new compounds containing the mercurous cation, compounds containing the Hg_3^{2+} and Hg_4^{2+} cations have been prepared and characterized by Raman spectroscopy and x-ray crystallography. These cations are stable only with relatively non-polarizable anions (AsF_6^-, SbF_6^- and SO_3F^-) in weakly basic media (SO_2,HSO_3F).

Two compounds containing infinite, linear, non-intersecting chains of mercury atoms in two mutually perpendicular directions have been prepared and characterized by x-ray crystallography. A reliable experimental technique was developed to measure the electrical conductivity of these extremely hygroscopic compounds, and both have been shown to be highly metallic, anisotropic conductors. As such, they constitute a completely new class of anisotropic materials, a field of considerable interest at the present time.

8.2 STRUCTURES OF MERCURY POLYCATIONS

The polymercury cations that have been prepared to date are listed in Table 8.1.. The mercury-mercury bond length in $Hg_3(AsF_6)_2$ is 2.552 (5) Å (100) and the cation is linear and centrosymmetric. The bond length is in good agreement with the value of 2.56 Å in $Hg_3(AlCl_4)_2$ (66). The Hg_3 group in the tetrachloroaluminate salt is nearly linear (∠ Hg-Hg-Hg 174°). The compound $Hg_4(AsF_6)_2$ contains nearly linear Hg_4^{2+} ions (∠ Hg-Hg-Hg 176°) with terminal Hg-Hg bond lengths of 2.57 (1) Å and a central Hg-Hg bond length of 2.70 (1) Å (101). All structures show the expected linear two-coordination about mercury. In simple valence bond terms the bonding between mercury atoms can be described as arising from the overlap of sp hybridized orbitals on each atom. The short terminal bond lengths in the Hg_4^{2+} cation indicate that the positive charges are localized on the terminal Hg atoms. In $Hg_3(AsF_6)_2$, there are relatively short terminal Hg-F bond lengths of 2.38 Å, although there are no fluorine atoms within bonding distance of the central Hg atom. This indicates again that the positive charges are primarily located on the terminal Hg atoms.

There is a correlation between formal oxidation state and bond length in the mercury polycations, shown in Table 8.2. The Hg_2^{2+} ion, which has a formal positive charge on each Hg atom of (+1), has the shortest bond. $Hg_{2.86}AsF_6$ and $Hg_{2.91}SbF_6$, which have formal positive charges on each Hg atom of + 0.35 and + 0.34 respectively have the longest Hg-Hg bond (2.64 Å). The bond lengths of the other mercury polycations in the + 2/3 (Hg_3^{2+}) and + 1/2 (Hg_4^{2+}) formal oxidation states have intermediate bond lengths.

The Raman stretching frequencies of mercury polycations vary over a wide range (Table 8.2). Even though the bond lengths in mercurous halides do not vary significantly with the electronegativity of the

TABLE 8.1

Polyatomic Cations of Mercury

Hg_2^{2+}	Hg_3^{2+}	Hg_4^{2+}	Hg_n^{+}
$Hg_2(AsF_6)_2 \cdot SO_2$	$Hg_3(AlCl_4)_2$[b]		
$Hg_2(AsF_6)_2$	$Hg_3(AsF_6)_2$	$Hg_4(AsF_6)_2$	$Hg_{2.86}AsF_6$
$Hg_2(SbF_6)_2 \cdot SO_2$			
$Hg_2(SbF_6)_2$			$Hg_{2.91}SbF_6$
$Hg_2(Sb_2F_{11})_2 \cdot SO_2$	$Hg_3(Sb_2F_{11})_2$		
$Hg_2(SO_3F)_2$	$Hg_3(SO_3F)_2$[a]		
$Hg_2(TaF_6)_2$			

a. in solution in HSO_3F

b. reference (67)

TABLE 8.2

Bond Lengths and Hg-Hg Stretching Frequencies

For Mercury Polycations

Compound	Formal Oxidation State	Bond Length Å	ν(Hg-Hg)cm^{-1}
Hg_2F_2	+1	2.507 (1)[a]	186[b]
Hg_2Cl_2	+1	2.526 (6)[a]	169[c]
Hg_2Br_2	+1	2.49 (1)[a]	136[c]
Hg_2I_2	+1		113[c]
$Hg_2(AsF_6)_2.SO_2$	+1	2.45 (1)	180
$Hg_2(AsF_6)_2$	+1		188
$Hg_2(SbF_6)_2.SO_2$	+1		197 172
$Hg_2(SbF_6)_2$	+1		194
$Hg_2(SO_3F)_2$	+1		162
$Hg_3(AlCl_4)_2$	+2/3	2.56[d]	123[e]
$Hg_3(AsF_6)_2$	+2/3	2.552 (5)	140
$Hg_3(Sb_2F_{11})_2$	+2/3		133
$Hg_4(AsF_6)_2$	+1/2	2.57(1)(terminal) 2.70(1)(central)	95 79
$Hg_{2.86}AsF_6$	+0.35	2.64	
$Hg_{2.91}SbF_6$	+0.34	2.64	

a. reference (60)
b. reference (33)
c. reference (61)
d. reference (66)
e. reference (67)

All other values are from this work

anion (60), the Raman active stretching frequency is strongly dependent on the nature of the anion. Many previous workers have mistakenly used the Raman active Hg-Hg stretching frequency as an indication of the strength of the metal-metal bond. In the mercurous halides considerable coupling would be expected between the Hg-Hg stretching frequency and the Hg-X stretching frequency. As the mass of the ligand is varied from fluoride to iodide, the mercurous halides become more covalent and coupling becomes increasingly important. Clearly, the Hg-Hg stretch is no longer a "pure" Hg-Hg mode. In the homologous series $Hg_n^{2+}(AsF_6)_2$, the Hg-Hg frequency does give an indication of the metal-metal bond strength.

8.3 INFINITE CHAIN CATIONS

Experiments have shown that $Hg_{2.91}SbF_6$ is an anisotropic conductor. While the anisotropy of $Hg_{2.86}AsF_6$ has not yet been measured, it is a good conductor and optical measurements indicate that it is anisotropic as well. The bonding between the mercury atoms in the infinite chains is best described by band theory. Overlap of atomic orbitals on the mercury atoms leads to a filled conduction band, which is then partially oxidized by the removal of 0.35 electrons per mercury atom (for $Hg_{2.86}AsF_6$). This model suggests complete delocalization of charge along the mercury atom chains. This is similar to the model proposed for the partially oxidized $K_2[Pt(CN)_4]Br_{0.30}\cdot 3H_2O$. A partially filled conduction band leads to high conductivity along the mercury atoms chains. The interchain conductivity of $Hg_{2.91}SbF_6$ is still

metallic, because of the relatively short interchain spacing (3.15 Å). These compounds can best be described as anisotropic materials with considerable three-dimensional properties. In this respect they are similar to $(SN)_x$.

8.4 SUGGESTIONS FOR FUTURE WORK

The reaction of mercury with other Lewis acids such as NbF_5 and TaF_5 is currently being studied in this laboratory. There is a possibility that the Hg_5^{2+} cation, which has not yet been prepared, can be isolated as a solid compound in these or other systems. There would seem to be no reason why this species should not be stable.

It is clearly of interest to investigate further the electrical and optical properties of the infinite chain mercury cations. It is hoped that optical measurements will allow the anisotropic ratio of $Hg_{2.86}AsF_6$ to be determined, which so far has been impossible using the conductivity methods described in this thesis because of the crystal morphology. A theoretical treatment of these compounds would be desirable. It might be possible to incorporate heteroatoms, such as zinc and cadmium, into the mercury atom chains. The effect of this on the solid state properties would be of interest.

Preliminary experiments in these laboratories indicate that it may be possible to prepare polyatomic cations with Zn and Cd, such as Cd_3^{2+} and Cd_4^{2+}. Polyatomic cations of the GpIIB elements are interesting because they provide simple examples of metal-metal bonds in the absence of other ligands.

REFERENCES

1. R.J. Gillespie and J.B. Milne, Inorg. Chem., 5, 1577 (1966).
2. R.J. Gillespie and M.J. Morton, Quart. Rev. Chem. Soc., 25, 533 (1971).
3. N. Bartlett and D.H. Lohman, Proc. Chem. Soc., 115 (1962).
4. J. Barr, R.J. Gillespie, R. Kapoor and G.P. Pez, J. Amer. Chem. Soc., 90, 1081 (1970).
5. R.J. Gillespie, J. Passmore, P.K. Unmat and O.C. Vaidya, Inorg. Chem., 10, 1327 (1971).
6. R.J. Gillespie and J. Passmore, Accounts Chem. Res., 4, 413 (1971).
7. F.A. Cotton, ibid., 2, 240 (1969).
8. M.C. Baird, Progress Inorg. Chem., 9, 1 (1968).
9. A. Hershaft and J.D. Corbett, Inorg. Chem., 2, 979 (1963).
10. N.J. Bjerrum, C.R. Boston and G.P. Smith, ibid., 6, 1162 (1967).
11. N.J. Bjerrum and G.P. Smith, ibid, 6, 1968 (1967).
12. J.D. Corbett, ibid, 7, 198 (1968).
13. J.D. Corbett and R.E. Rundle, ibid., 3, 1408 (1964).
14. R.J. Gillespie, "Molecular Geometry", Van Nostrand Reinhold, London (1972).
15. L.A. Woodward, Phil. Mag., 18, 823 (1934).
16. P. Krishnamurty, I.J. Phys., 5, 1 (1930).
17. P. Krishnamurty, ibid., 5, 113 (1930).
18. G. von Hevesy and E. Lowenstein, Z. Anorg. Allgem. Chem., 187 266 (1930).

19. J.D. Corbett, S. von Winbush and F.C. Albers, J. Amer. Chem. Soc., 79, 3020 (1957).

20. J.D. Corbett, W.J. Burkhard and L.F. Druding, ibid., 83, 76 (1961).

21. J.D. Corbett, Inorg. Chem., 1, 700 (1962).

22. D.H. Kerridge and S.A. Tariq, J. Chem. Soc. (A), 1122 (1967).

23. C.G. Davies, P.A.W. Dean, R.J. Gillespie and P.K. Ummat, J. Chem. Soc. Chem. Commun., 782 (1971).

24. B. Landa, Ph.D. Thesis, McMaster University (1974).

25. W. Kiefer and H.J. Bernstein, Appl. Spect., 25, 500 (1971).

26. M.M. Woolfson, "An Introduction to X-ray Crystallography", Cambridge University Press, London (1970).
G.H. Stout and L.H. Jensen, "X-ray Structure Determination, a Practical Guide", Macmillan, New York (1968).

27. "International Tables for X-ray Crystallography", Kynoch Press, Birmingham (1962).

28. J.M. Stewart, F.A. Kundell and J.C. Baldwin, "X-RAY 71 System of Crystallographic Programs", Technical Report, University of Maryland (1971).

29. H.C. Montgomery, J. Appl. Phys., 42, 2971 (1971).

30. P.K. Ummat, Ph.D. Thesis, McMaster University (1971).

31. A. Ogg, Z. Phys. Chem., 27, 285 (1898).

32. E. Abel, Z. Anorg. Allgem. Chem., 26, 376 (1901).

33. H. Stammreich and T.T. Sans, J. Mol. Struct., 1, 55 (1967).

34. W.C.E. Higginson, J. Chem. Soc., 1438 (1951).

35. R.D. Shelton, A.H. Nielsen and W.H. Fletcher, J. Chem. Phys., 21, 2178 (1953).

36. R.J. Gillespie and K.C. Moss, J. Chem. Soc. (A), 1170 (1966).

37. P.A.W. Dean and R.J. Gillespie, J. Amer. Chem. Soc., 91, 7260 (1969).

38. V.L. Kolditz, D. Weisz and V. Calov, Z. Anorg. Allgem. Chem., 316, 261 (1962).

39. R.J. Gillespie and G.J. Schrobilgen, to be published in Inorg. Chem.

40. A.M. Qureshi and F. Aubke, Can. J. Chem., 48, 3117 (1970).

41. A.M. Qureshi, L.E. Levchuk and F. Aubke, ibid., 49, 2544 (1971).

42. R.J. Gillespie and B. Landa, Inorg. Chem., 12, 1383 (1973).

43. J. Goubeau and J.B. Milne, Can. J. Chem., 45, 2321(1967).

44. H. Grdenic, J. Chem. Soc., 1312 (1956).

45. H. Grdenic and C. Dgordjevic, ibid., 1316 (1956).

46. S. Hietanen and L.G. Sillen, Arkiv Kemi, 10, 103 (1956).

47. G. Infeldt and L.G. Sillen, Svensk, Kem. Tidskr., 58, 104 (1946).

48. G. Anderegg, Helv. Chim. Acta, 42, 344 (1959).

49. T.H. Wirth and N. Davidson, J. Amer. Chem. Soc., 86, 4314 (1964).

50. R.A. Potts and A.L. Allred, Inorg. Chem., 5, 1066 (1966).

51. P.A.W. Dean and D.G. Ibbott, Inorg. Nuc. Chem. Lett., 11, 119 (1975).

52. P.A.W. Dean and D.G. Ibbott, Private Communication.

53. B.J. Aylett, in "Comprehensive Inorganic Chemistry", Pergamon Press, Oxford, 1973; vol. 3, p.187.

54. F.A. Cotton and G. Wilkinson, "Advanced Inorganic Chemistry", Interscience, New York, 3rd. Ed., 1972; p.508.

55. H.L. Roberts, Adv. Inorg. Chem. Radiochem., 11, 309 (1968).

56. A. Van Arkel, Research, 2, 307 (1949).

57. R.J. Havighurst, J. Amer. Chem. Soc., 48, 2113 (1926).

58. J. Lewis, Pure Appl. Chem., 10, 11 (1965).

59. D. Grdenic, Quart. Rev. Chem. Soc., 19, 303 (1965).

60. E. Dorm, J. Chem. Soc. Chem. Commun., 466 (1971).

61. J.R. Durig, K.K. Lau, G. Nagarajan, M. Walker and J. Bragin, J. Chem. Phys., 50, 2130 (1969).

62. J. Meyer and G. Schram, Z. Anorg. Allgem. Chem., 206, 24 (1932).

63. R. Gut. Helv. Chim. Acta, 43, 830 (1960).

64. C.S.G. Phillips and R.J.P. Williams, "Inorganic Chemistry", Oxford University Press, New York, 1966; p.530.

65. G. Torsi and G. Mamantov, Inorg. Nuc. Chem. Lett., 6, 843 (1970).

66. R.D. Ellison, H.A. Levy and K.W. Fung, Inorg. Chem., 11, 833 (1972).

67. G. Torsi, K.W. Fung, G.H. Begun and G. Mamantov, Inorg. Chem., 10, 2285 (1971).

68. Handbook of Chemistry and Physics, Chemical Rubber Co., Cleveland, 48th ed., 1968; p.F-155.

69. F.O. Sladky, P.A. Bulliner, N. Bartlett, D.G. DeBoer and A. Zalkin, J. Chem. Soc. Chem. Commun., 1048 (1968).

70. R.J. Gillespie and P.K. Ummat, J. Chem. Soc. Chem. Commun., 1168 (1971).

71. I.D. Brown, B.D. Cutforth, C.G. Davies, R.J. Gillespie, P.R. Ireland and J.E. Vekris, Can. J. Chem., 52, 791 (1974).

72. R. Comes, M. Lambert, H. Launois and H.R. Zeller, Phys. Rev. B, 571 (1973).

73. P. Boldrini, R.J. Gillespie, P.R. Ireland and G.J. Schrobilgen, Inorg. Chem., 13, 1690 (1974).

74. I.F. Shchegolev, Phys. Stat. Sol. (a), 12, 9 (1972).

75. A.F. Garito and A.J. Heeger, Accounts Chem. Res., 7, 232 (1974).

76. T.E. Phillips, T.J. Kistenmacher, J.P. Ferraris and D.O. Cowan, J. Chem. Soc. Chem. Commun., 471 (1973).

77. M.J. Cohen, L.B. Coleman, A.F. Garito and A.J. Heeger, Phys. Rev. B, 10, 1298 (1974).

78. D.E. Schafer, F. Wude, G.A. Thomas, J.P. Ferraris and D.O. Cowan, Sol. State Commun., 14, 347 (1974).

79. K. Krogmann, Angew. Chem. Internat. Edit., 8, 35 (1969).

80. H.R. Zeller, Festkorperprobleme, Adv. Sol. Stat. Phys., 13, 31 (1973).

81. J. S. Miller and A.J. Epstein, Progr. Inorg. Chem., 20,(1975).

82. K. Krogmann and H.D. Hausen, Z. Anorg. Allgem. Chem., 67, 358 (1968).

83. K. Krogmann and H.D. Hausen, Z. Naturforsch, 23B, 1111 (1968).

84. H.R. Zeller and A. Beck, J. Phys. Chem. Solids, 35, 77 (1974).

85. R.E. Peierls, "Quantum Theory of Solids", Oxford University Press, London, 1955; p.108.

86. P.S. Goom and A.E. Underhill, J. Chem. Soc. Dalton, 334 (1972).

87. M.J. Minot, J.H. Perlstein and T.J. Kistenmacher, Sol. State Commun., 13, 1319 (1973).

88. F.P. Burt, J. Chem. Soc., 1171 (1910).

89, V.V. Walatka, Jr., M.M. Labes and J.H. Perlstein, Phys. Rev. Lett., 31, 1139 (1973).

90. C.M. Mikulski, D.J. Russo, M.S. Saran, A.G. MacDiarmid, A.F. Garito and A.J. Heeger, to be published in J. Amer. Chem. Soc. (1975).

91. M. Boudelle, Ph.D. Thesis, University Claude-Bernard De Lyon (1974).

92. A.G. MacDiarmid, C.M. Mikulski, P.J. Russo, M.S. Saran, A.F. Garito and A.J. Heeger, J. Chem. Soc. Chem. Commun., 476 (1975).

93. A.A. Bright, M.J. Cohen, A.F. Garito, A.J. Heeger, C.M. Mikulski, P.J. Russo and A.G. MacDiarmid, Phys. Rev. Lett., 34, 206 (1975).

94. L. Pintschovius, H.P. Geserich and W. Moller, Sol. State Commun., 17, 477 (1975).

95. A.A. Bright, M.J. Cohen, A.F. Garito, A.J. Heeger, C.M. Mikulski and A.G. MacDiarmid, Appl. Phys. Lett., 26, 612 (1975).

96. A.G. MacDiarmid, Private Communication.

97. R.L. Greene, G.B. Street and L.J. Suter, Phys. Rev. Lett., 34, 577 (1975).

98. from reference (53), p.278

99. from reference (68), p.E-80

100. B.D. Cutforth, C.G. Davies, P.A.W. Dean, R.J. Gillespie, P.R. Ireland and P.K. Unmat, Inorg. Chem., 12, 1343 (1973).

101. B.D. Cutforth, R.J. Gillespie and P.R. Ireland, J. Chem. Soc. Chem. Commun., 723 (1973).